NUMERICAL AND EXPERIMENTAL INVESTIGATION OF MECHANICAL PROPERTIES OF PARTS MANUFACTURED VIA CARBON FIBER REINFORCED MATERIAL EXTRUSION

A THESIS SUBMITTED TO
THE GRADUATE SCHOOL OF NATURAL AND APPLIED SCIENCES
OF
MIDDLE EAST TECHNICAL UNIVERSITY

BY

AKINCAN SÜRE

IN PARTIAL FULFILLMENT OF THE REQUIREMENTS
FOR
THE DEGREE OF MASTER OF SCIENCE
IN
MECHANICAL ENGINEERING

AUGUST 2024

Approval of the thesis:

NUMERICAL AND EXPERIMENTAL INVESTIGATION OF MECHANICAL PROPERTIES OF PARTS MANUFACTURED VIA CARBON FIBER REINFORCED MATERIAL EXTRUSION

submitted by **AKINCAN SÜRE** in partial fulfillment of the requirements for the degree of **Master of Science in Mechanical Engineering Department, Middle East Technical University** by,

Prof. Dr. Naci Emre Altun
Dean, Graduate School of **Natural and Applied Sciences** ______________

Prof. Dr. Serkan Dağ
Head of Department, **Mechanical Engineering** ______________

Assoc. Prof. Dr. Ulaş Yaman
Supervisor, **Mechanical Engineering, METU** ______________

Prof. Dr. Mehmet Ali Sahir Arıkan
Co-supervisor, **Mechanical Engineering, METU** ______________

Examining Committee Members:

Prof. Dr. Hüsnü Dal
Mechanical Engineering, METU ______________

Assoc. Prof. Dr. Ulaş Yaman
Mechanical Engineering, METU ______________

Assoc. Prof. Dr. Kıvanç Azgın
Mechanical Engineering, METU ______________

Assist. Prof. Dr. Hakan Çalışkan
Mechanical Engineering, METU ______________

Assoc. Prof. Dr. Recep Muhammet Görgülüarslan
Mechanical Engineering, TOBB ETU ______________

Date:13.08.2024

I hereby declare that all information in this document has been obtained and presented in accordance with academic rules and ethical conduct. I also declare that, as required by these rules and conduct, I have fully cited and referenced all material and results that are not original to this work.

Name, Surname: Akıncan Süre

Signature :

ABSTRACT

NUMERICAL AND EXPERIMENTAL INVESTIGATION OF MECHANICAL PROPERTIES OF PARTS MANUFACTURED VIA CARBON FIBER REINFORCED MATERIAL EXTRUSION

Süre, Akıncan
M.S., Department of Mechanical Engineering
Supervisor: Assoc. Prof. Dr. Ulaş Yaman
Co-Supervisor: Prof. Dr. Mehmet Ali Sahir Arıkan

August 2024, 102 pages

With the improvements in manufacturing technology, it is possible to produce light parts with complex geometries with additive manufacturing today. This brings critical advances in many industrial fields, such as aerospace, defense, and automotive, where the weight of the parts is crucial. A new material extrusion process, continuous fiber fabrication (CFF), has been developed by an industrial company, namely Markforged, which enables the design of composites with fiber reinforcement in the material extrusion process. CFF process includes two types of reinforcements: isotropic and concentric. In isotropic reinforcement, the parts' interior is reinforced continuously with fibers, while concentric reinforcement allows the strengthening of the design locally, such as reinforcement of outer shells or regions around the holes where high stresses are usually encountered. The latter one, concentric reinforcement, is investigated in the scope of this thesis. One of the challenging problems regarding CFF is the mechanical performance measurement of the parts under certain loading cases. Although testing is usually the preferred way of evaluating mechanical performance, it is not always possible or feasible. Hence, finite element analysis (FEA) should be considered as an alternative way of measuring the mechanical responses of the parts. However, one should be meticulous about the accuracy and validity of numerical analysis. Even though there are many studies in the literature about the evaluation of the mechanical performance of CFF parts with FEA, there are many discrepancies between research. Hence, in this thesis, a finite element modeling strategy for parts manufactured with CFF is developed, and the modeling technique is verified with tests.

First, required material characterizations are performed in order to obtain material properties for selected materials. Then, three specimens having different loading conditions, tensile, bending, and eccentric loads, are designed and manufactured. Later, specific load cases are created, and tests are performed. Finally, corresponding numerical models for tests are prepared, and FEA simulations are run to validate the numerical modeling approach. The validation criterion is based on the force and displacement of the parts for their elastic behavior. The results of the numerical models and tests are in good agreement with each other for lower displacement values since FE analyses are done with linear and elastic material properties. For higher displacements, where the mechanical response of the parts is plastic, there are discrepancies between numerical analysis and test results. The sources of errors are discussed in the thesis in order to develop better mathematical modeling techniques in the future.

Keywords: Additive Manufacturing, Continuous Filament Fabrication, Composite Materials, Finite Element Analysis, Material Characterization

ÖZ

KARBON FIBER ILE GÜÇLENDİRİLMİŞ MALZEME EKSTRÜZYON YÖNTEMİ İLE ÜRETİLMİŞ PARÇALARIN MEKANİK ÖZELLİKLERİNİN NUMERİK VE DENEYSEL OLARAK İNCELENMESİ

Süre, Akıncan
Yüksek Lisans, Makina Mühendisliği Bölümü
Tez Yöneticisi: Doç. Dr. Ulaş Yaman
Ortak Tez Yöneticisi: Prof. Dr. Mehmet Ali Sahir Arıkan

Ağustos 2024 , 102 sayfa

İmalat teknolojisindeki gelişmelerle birlikte, günümüzde eklemeli imalat ile karmaşık geometrilere sahip ve hafif parçalar üretmek mümkündür. Bu teknoloji, parça ağırlığının hayati önem taşıdığı havacılık, savunma ve otomotiv gibi birçok endüstriyel alanda kritik ilerlemeler sağlamaktadır. Markforged isimli bir endüstriyel şirket tarafından malzeme ekstrüzyon prosesinde fiber takviyeli kompozitlerin tasarlanmasını mümkün kılan yeni bir malzeme ekstrüzyon prosesi olan sürekli fiber imalatı (SFİ) geliştirilmiştir. SFİ süreci iki tür güçlendirme içerir: izotropik ve eşmerkezli takviye. İzotropik takviyede, parçaların iç kısmı sürekli fiberlerle güçlendirilirken; eşmerkezli takviye ile parçaların dış kabuklarının veya gerilmelerin yüksek olduğu delik etrafı bölgelerin lokal olarak güçlendirilmesine olanak tanınır. Bu tez kapsamında eşmerkezli güçlendirme yöntemi incelenmiştir. SFİ ile ilgili zorlu problemlerden biri de parçaların mekanik performansının ölçülmesidir. Her ne kadar mekanik performansı değerlendirmenin genellikle tercih edilen yolu test olsa da, parçaların test edilmesi her zaman mümkün veya uygulanabilir değildir. Bu nedenle sonlu elemanlar analizi

(SEA), parçaların mekanik cevaplarını ölçmenin alternatif bir yolu olarak düşünülmelidir. Ancak sayısal analizin doğruluğu ve geçerliliği konusunda titiz davranılmalıdır. Literatürde SFİ parçalarının mekanik performansının sonlu elemanlar analizleri ile değerlendirilmesi konusunda çok sayıda çalışma bulunmasına rağmen araştırmalar arasında birçok farklılık bulunmaktadır.Bu nedenle bu tezde, SFİ ile üretilen parçalar için sonlu elemanlar modelleme stratejisi geliştirilmiş ve modelleme tekniği testlerle doğrulanmıştır.

İlk olarak malzeme karakterizasyon testleri ile seçilen malzemeler için gerekli malzeme özellikleri elde edilmiştir. Çekme, eğme ve eksantrik yükleme gibi 3 farklı yükleme koşullarına numuneler tasarlanıp tasarlanıp üretilmiştir. Ardından belirli yük durumları oluşturularak testler gerçekleştirilmiştir. Nihayetinde, testlere tekabül eden sayısal modeller hazırlanıp, sayısal modelleme yaklaşımını doğrulamak için SEA simülasyonları koşulmuştur. Bu tezde kullanılan doğrulama kriteri, parçaların elastik davrandığı bölgedeki deformasyonlara karşılık gelen kuvvetlerin kıyasına dayanmaktadır. Sonlu elemanlar analizleri doğrusal ve elastik malzeme özellikleriyle yapıldığından, daha düşük deplasman değerleri için sayısal model ve testlerin sonuçları birbiriyle iyi uyum göstermektedir. Parçaların mekanik tepkisinin plastik olduğu, yani daha yüksek deformasyonlara sahip bölgelerde sayısal analiz ve test sonuçları arasında farklılıklar bulunmaktadır. Gelecekte daha iyi matematiksel modelleme tekniklerinin geliştirilmesi amacıyla tezde hataların kaynakları tartışılmıştır.

Anahtar Kelimeler: Eklemeli İmalat, Sürekli Fiber İmalatı, Kompozit Malzemeler, Sonlu Elemanlar Analizi, Malzeme Karakterizasyonu

For those who died alone...

ACKNOWLEDGMENTS

The author would like to express his sincere gratitude to his supervisor Assoc. Prof. Dr. Ulaş Yaman and his co-supervisor Prof. Dr. M.A. Sahir Arıkan, for their guidance and encouragement throughout the thesis. Moreover, the author would like to thank Prof. Dr. Hüsnü Dal, Assoc. Prof. Dr. Kıvanç Azgın, Assist. Prof. Dr. Hakan Çalışkan, and Assoc. Prof. Dr. Recep Muhammet Görgülüarslan for being on the thesis committee and for their valuable feedback.

The author is deeply grateful to his company, ASELSAN A.Ş. for letting and supporting him to conduct this research.

The author is immensely thankful to his manager Oğuz Doğan, his team leader Serap Aykan, and his colleagues Canberk Bacıkoğlu and Rahman Uncu for their stimulating advice.

The author is thankful to Dr. Murat Tolga Ertürk, Volkan Kandemir, Tolga Bolol, and METU ROMER for their assistance during manufacturing and testing.

The author extends heartfelt thanks to his incredible friends Levent Güner, Kerem Genelioğlu, Hasan Hüseyin Yüksel, and Sercan Emir, whose warmth and unwavering support have made this journey so much brighter.

The author sincerely appreciates Dicle Naz Toker for always being there for him.

The author would like to express his deepest love to his father, Halil Süre, mother, Hayriye Süre, and sisters, Sevcan Süre İlhan and Duygu Süre Pirhan for trusting, loving and supporting him throughout his life.

Finally, special thanks are given to Ibrahim Maalouf for inspiring the author with his elegant and unique music.

TABLE OF CONTENTS

LIST OF TABLES

TABLES

LIST OF FIGURES

FIGURES

LIST OF ABBREVIATIONS

2D	2 Dimensional
3D	3 Dimensional
AM	Additive Manufacturing
ASTM	American Society for Testing and Materials
CAD	Computer Aided Drawing
CFR	Carbon Fiber Reinforced
CFF	Continuous Fiber Fabrication
EE	Embedded Elements
E	Young's Modulus
ν	Poisson's Ratio
FE	Finite Element
FEA	Finite Element Analysis
FDM	Fused Deposition Modeling
FFF	Fused Filament Fabrication
Hz	Hertz
PLA	Polylactic Acid
SLA	Stereolithography
SLS	Selective Laser Sintering
STL	Standard Tessellation Language
UV	Ultraviolet

CHAPTER 1

INTRODUCTION

1.1 Motivation and Problem Definition

Many engineering applications require high strength and low-weight products. Composite parts are usually preferred in the defense, aerospace, and automotive industries where low-weight and high strength are needed. Although stress-critical components are generally manufactured using traditional methods, AM may provide efficient solutions. Traditional manufacturing techniques bring numerous disadvantages for engineers, which can be listed as design limitations considering the part's manufacturability, the requirement of special molds, well-trained technicians, etc. All these disadvantages create a need for more efficient manufacturing methods. At this point, AM may be considered as an option. Since it particularly gives design flexibility to engineers in designing lighter products with high mechanical performance, eliminates the requirement for molds, and offers faster and cheaper solutions for prototyping purposes, AM is considered as an alternative manufacturing technique for composites. Many specialized AM techniques have been developed and commercialized to manufacture composites using AM. However, AM brings some limitations also. It is unsuitable for mass production, and the mechanical performance of parts is still questionable. The need to measure the mechanical performance of any part is satisfied in two ways: Testing and Finite Element Analysis (FEA). Even though testing always gives more reliable results than simulations, testing every part for any loading conditions is not always possible. Moreover, testing requires special fixtures and equipment, which brings extra cost and time consumption. However, FEA is faster, and the behavior of mechanical parts can be calculated under any loading condition. For composite materials manufactured with traditional techniques, FEA approaches are verified with tests and there are many studies in the literature for performance evaluation, hence, the modeling methodology is well-defined. However, for the composite parts that are manufactured using AM, there are still questions about numerical modeling. Stated approaches are mostly part-specific, and there are discrepancies between results in the literature. Therefore, this thesis study about numerical modeling and experimental validation of carbon fiber reinforced material extrusion has been conducted to develop an FEA approach for the CFF parts.

1.2 Proposed Methods and Models

Additive Manufacturing (AM) is a brand-new technology for manufacturing lighter parts with high mechanical performance and complex geometries. Continuous Fiber Fabrication (CFF) is an AM process capable of manufacturing composites made of thermoplastics (as matrix) with fiber reinforcements. In this thesis, the numerical modeling approach of parts manufactured with CFF is researched. Three different types of specimens, namely tensile, bending, and eccentric, were manufactured using the CFF method for different loading scenarios. Finite Element Analysis (FEA) of loading cases are prepared and solved, then results are compared with experiments in order to verify the accuracy of modelling technique.

1.3 Contributions and Novelties

The contributions of this thesis are as follows:

- Tensile specimens with different fiber orientations (0,45,90 degrees) are manufactured and tested to determine the material properties of carbon fiber reinforcement.
- Tensile specimens made of white nylon with solid infill are manufactured and tested to determine material properties of matrix material white nylon.
- Tensile specimens having triangular infill with carbon fiber reinforcement are designed, numerically modeled, and tested to evaluate the accuracy of the modeling technique under tensile loading.

- Bending specimens having triangular infill with carbon fiber reinforcement are designed, numerically modeled, and tested to evaluate the accuracy of the modeling technique under bending loading.
- Eccentric specimens having triangular infill with carbon fiber reinforcement are designed, numerically modeled, and tested to evaluate the accuracy of the modeling technique under combined bending and tensile loading.
- The results of tests and analyses for three specimens are compared. Possible sources of errors between numerical solutions and tests are discussed.

1.4 Limitations of the Thesis

The modeling technique developed in this thesis is only valid for the loading in the elastic regime since the plastic behavior of white nylon and carbon fiber is highly complex and requires numerous tests. Moreover, the validation of the numerical model is based on displacements and corresponding forces because strains cannot be measured inside the part where cracks start to propagate.

1.5 The Outline of the Thesis

- In Chapter 2, related works in the literature are reviewed, and the inaccuracies in the state of the art for this topic are discussed.
- In Chapter 3, material characterization procedures and results for carbon fiber and white nylon are provided.
- In Chapter 4, the design and fabrication of CFF test specimens are presented.
- In Chapter 5, first, the numerical modeling approach for CFF parts and stages of numerical modeling for test specimens are covered.
- In Chapter 6, tests of specimens are shared. Then, the test results are compared with numerical analysis results and possible causes of errors are discussed.
- In Chapter 7, results and findings are brought to a conclusion.

CHAPTER 2

BACKGROUND AND LITERATURE REVİEW

In this chapter of the thesis, related literature reviews and the state of the art of the topic are given in four sections, namely Fundamentals of Additive Manufacturing 2.1, Additive Manufacturing of Composite Parts 2.2, Material Characterization of Additively Manufactured Composite Part 2.3, and Numerical Modelling of Additively Manufactured Composite Parts 2.4.

2.1 Fundamentals of Additive Manufacturing

AM is one of the most popular topics in the field of manufacturing. The main difference from conventional manufacturing technologies is that parts are created layer by layer in AM, and, as the name implies, the process is additive. In contrast, parts are made from the raw material in a subtractive manner in conventional machining. This technology was found in 1986 by Charles Hull[1]. However, since 2010, many patents have expired, and many people have started using and developing the technology. Compared to conventional manufacturing technologies, AM has numerous advantages, including the capability of manufacturing more complex geometries, mass and cost reduction, the requirement for fewer process steps, post-machining, assembly, etc. However, it also has plenty of drawbacks to conventional machining, such as surface finish quality, allowable materials, size limitations, and anisotropy in mechanical properties.

Although various types of AM processes exist, the basic procedure to make the final product is the same for all, as shown in Figure 2.1.

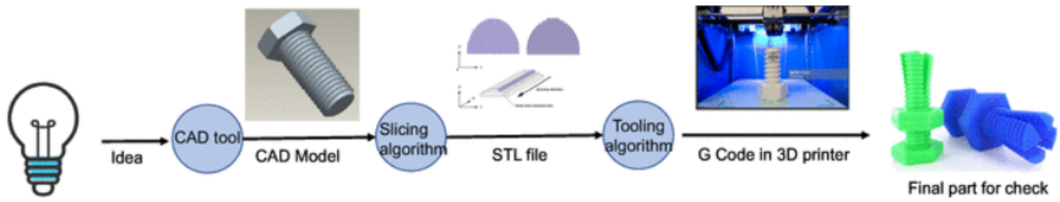

Figure 2.1: Additive Manufacturing Process Chain[2]

First, a 3D model of the object should be designed. Then, the part should be converted into Standard Tessellation Language File (STL) format to tessellate and slice the part to create multiple layers. The next step is uploading the STL file to the printer. The machine is set up with printing parameters, and the model is ready to be printed layer by layer. Finally, post-processing operations, such as extra polishing, cleaning, and coating, may be applied if needed [3]. According to ASTM 52900, [4], additive manufacturing can be divided into seven main types, considering the production method:

- Material Jetting
- Binder Jetting
- Material Extrusion
- Powder Bed Fusion
- Sheet Lamination
- Directed Energy Deposition
- Vat Photopolymerization

This chapter will discuss only the material extrusion process in detail since this method is preferred for manufacturing the parts in this thesis.

2.1.1 Material Extrusion

Material extrusion technique, also called Fused Filament Fabrication (FFF) or Fused Deposition Modelling (FDM), is one of the most widely used and researched additive

manufacturing technology because of its simplicity, versatility, and cost-effectiveness [5]. It works by extruding the filament, which is liquidized with supplied heat and becomes semi-solid, to create a layer. After extrusion, the material solidifies in order to have the desired shape and bound to the previous layer.
Material Extrusion is frequently used when functional prototypes are needed. Moreover, it enables designers to change and customize their designs freely since the process allows manufacturing complex geometries. Compared with the conventional methods, the cost could be lower, and manufacturing time could be drastically decreased. These benefits make the material extrusion process suitable for rapid prototyping and small-batch production.

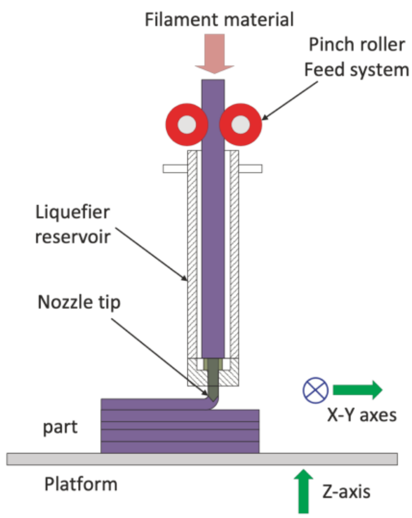

Figure 2.2: Material Extrusion System Working Principle [6]

The part should first be designed using a CAD software in FFF processes. Then, the proper software, which should be capable of communicating and transferring the model to the printer, slices the part. The term slicing is obtaining 2D layers from the 3D model and creating tool paths (G-code) to manufacture the whole part layer by layer. Tool paths must be created for each layer; then, the G-code should be transferred to a 3D printer. Once the printer receives the tool path, it prints the part. As seen in Figure 2.2, the filament is placed into a filament holder. Using a pinch-roller system, the solid filament is pushed through to a liquefier reservoir section, where heat is given to liquidize the material. After liquidizing, the material is pressurized, and extrusion from the nozzle starts. The nozzle can move in x-y (horizontal plane), and it follows the path provided in the G-code. Once the nozzle finishes printing a layer, it goes down in the z-axis, and the same procedure applies to the next layer. This process continues until all the layers are printed.

2.2 Additive Manufacturing of Composite Parts

Composite materials generally consist of two or more different materials combined to obtain better properties such as lower weight, higher strength, etc. In general, a composite part includes a matrix material, which is generally a thermoplastic, thermoset, or elastomer, and is responsible for bonding the reinforcement material, transferring the load to reinforcement, providing chemical resistance, and giving the desired shape to the mechanical part; and reinforcement material, which is better in terms of mechanical properties, stiffer, having higher elastic and shear modulus, and strength [7]. For many applications where lightweight and high strength is needed, such as defense, aerospace, biomedical, etc., composites are mostly preferred [8]. However, the production of composite parts is highly challenging. When a part is used repeatedly, a mold is usually used to produce composites. However, manufacturing a mold is highly pricey and time-consuming for prototyping purposes. Also, the manufacturing of composites is highly labor-dependent; generally, it is done manually. Since AM offers design flexibility and requires no mold, etc., using it to fabricate composites is very efficient and handy. Moreover, AM is a multi-directional manufacturing process, enabling the enforcement of the part for a specific direction where the load case is critical. While the designer has less concern about the manufacturability of the part with AM, mechanical parts with lighter weight and higher strengths are possible.

Although, for producing 3D printed composites, Selective Laser Sintering and Direct Energy Deposition are used, Fused Filament Fabrication is the most preferred additive manufacturing method [8].
Composite AM varies considerably in terms of production technique, matrix material, reinforcement type, etc. In this thesis, different types of 3D printed composites are classified considering the type of reinforcement such that: [9]

- Particle Reinforcement
- Nanofiller
- Fiber Reinforcement

In the next section, particle reinforcement and reinforcement with nanofillers will be mentioned briefly. Fiber reinforcement will be explained in detail in the following sections.

2.2.1 Particle Reinforcement

Particle reinforced composites are very popular because the filament is easily mixed and reinforced, has fewer voids than other techniques, and has better surface properties [10]. In particle reinforced composites, particles carry the load, and the matrix transports the load.[11]
Chung et al. [12] used glass beads as a filler material with varying volume fractions of 0-30% in a functionally graded material to enhance tensile modulus and strength. Reinforced composites are used to increase load carrying capacity and in many other applications. Kalssom et al. [13] added micro diamond particles in composite materials to obtain higher thermal conductivity to transfer heat better in a heat sink printed with SLA 3D printing. Moreover, Hwang et al. [14] benefited metal particle reinforcement in order to obtain better dimensional properties. Their work aimed to reduce the coefficient of thermal expansion to reduce the thermal strains induced in additive manufacturing. In short, particle reinforced composites are used in many applications and have the potential to be used in various fields because they eliminate many disadvantages of 3D printing, such as warping, distortion, mechanical and thermal performance, etc.

2.2.2 Nanofiller

Nanofiller reinforced composite materials also offer many improvements in different material properties, such as high strength, good thermal and electrical conductivity, and good optical properties [15]. Various types of AM processes may be utilized to manufacture Nanofiller composites. SLS and FDM are the most common types, and SLA is also used when the material is not opaque so that UV lights can be passed through the material to be activated with energy [16]. Figure 2.3 summarizes nanofiller reinforcement in the FDM process. Research in this area mainly focuses

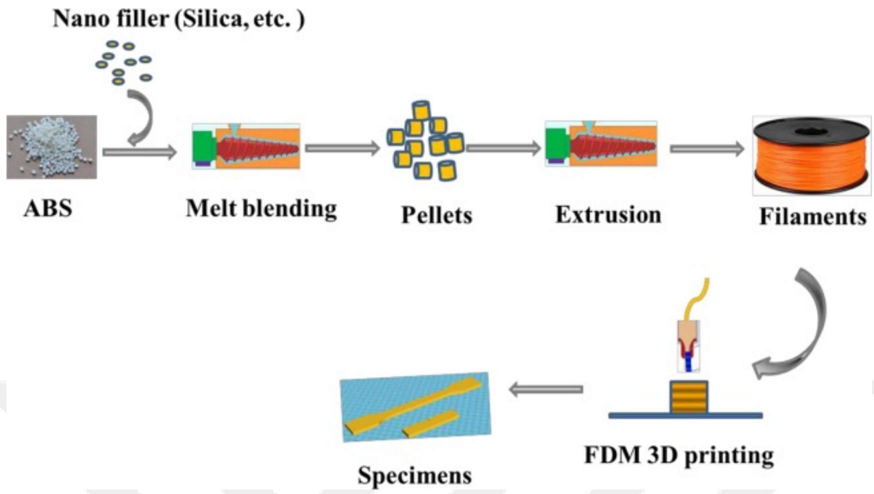

Figure 2.3: Nanofiller Reinforced FDM Process Principles [17]

on carbon-based materials like graphene, carbon nanotubes, etc., as nanofiller reinforcement. Nadernezhad et al.[18] investigated the effects of different process parameters like layer thickness, infill pattern, and orientation for the additive manufacturing of nanotube reinforced PLA material in terms of mechanical and thermal aspects and showed the improvement in properties. Plymill et al. [19] is researched for carbon nanotube reinforced PLA extrusion in terms of mechanical and thermal aspects. They showed that reinforcement increased ultimate tensile strength and Young's modulus, about 40% increase in Young's modulus for only 1% weight percentage reinforced material. Bai et al. [20] examined the effect of nanotubes on the mechanical performance of the parts manufactured with the selective laser sintering (SLS) method. They obtained a result that, for 0.2% weight percentage of carbon nanotube reinforcement, resulted in a 17% enhancement in Young's modulus.

2.2.3 Continuous Fiber Reinforcement

Material extrusion is the most common technology for continuous fiber reinforcement [21]. Hence, Continuous Fiber Reinforcement (CFR) is not only a way of reinforcing

3D printed composites but also a unique FFF technique called Continuous Filament Fabrication (CFF) that is commercialized. This technology has been developed in order to enhance the mechanical performance of plastic parts by utilizing different reinforcement materials in various forms such as Carbon Fiber, fiberglass, kevlar, etc. The part's strength considerably relies on the fiber orientation and volume fraction of fiber to plastic material [22]. In this technology, the basic principle of creating an object is similar to the FDM process, first creating a 3D design, slicing it into layers, and 3D printing of the part.

However, unlike the traditional and usual FDM techniques, in CFF, two separate pools are used to supply different materials; one is responsible for matrix material and plastic, and the other is responsible for reinforcement filament supply. Two different approaches are commonly used in this technology. One and the older one is that both materials meet in one extrusion head. Since the melting point of the plastic part is lower than the reinforcement material, when the nozzle is heated, the plastic part becomes molten and deposits along the reinforcement material to create a layer that solidifies rapidly to stick to the previous layer [23]. The representative process schematic is given in Figure 2.4.

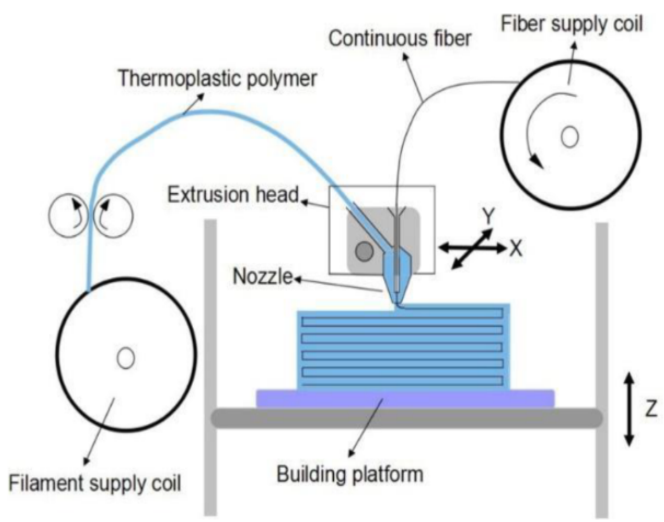

Figure 2.4: CFF with One Extrusion Head [23]

The other, and the newest technology, is commercialized by the company Markforged in 2014, in which two separate nozzles are used to deposit material; one is responsible for plastic extrusion, and the other is for reinforcement material. This technique is more specialized than the one with a single nozzle because, with two separate nozzles, one has the opportunity to reinforce any layer and oppositely not reinforce any layer; in this way, overall material cost can be reduced. Although there are two separate nozzles in Markforged systems, they do not work simultaneously, bringing a slower process. The schematic of the Markforged printer is given in Figure 2.5

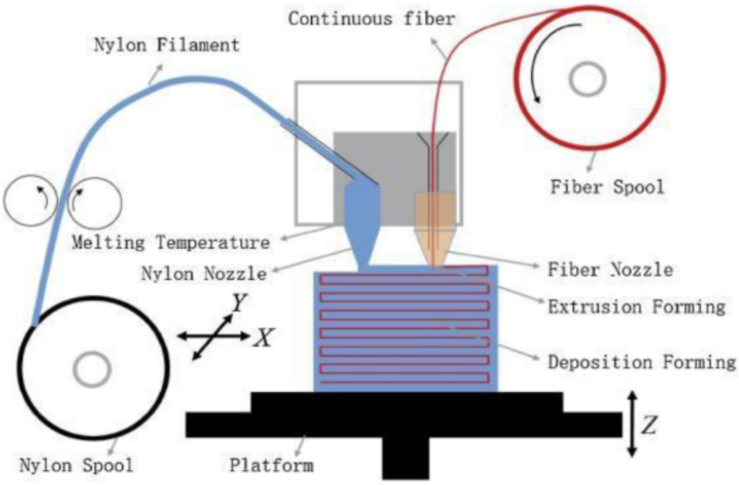

Figure 2.5: CFF with Two Extrusion Head [24]

In CFF, matrix and reinforcement materials behave like traditional composites. Matrix is the base material responsible for sticking reinforcement and protecting it from exterior effects like corrosion, degradation, etc. On the other hand, reinforcement fiber enhances mechanical properties like load capacity, stiffness, etc. Markforged offers two types of reinforcements. One is concentric fill reinforcement, which can reinforce the plastic outer walls and the regions around the holes with reinforcement material. The rest of the part consists of infill as a usual FFF part. This technique is proper when the part is under bending and impact loads. Concentric fiber reinforcement enables designers to reinforce the part locally so that the overall weight can be minimized and regions having more stress can be reinforced. The other type is isotropic reinforcement, where the part is reinforced with directional fibers having different fiber angle orientations. Fiber angles can be changed in every layer so that one can achieve the unidirectional strength [25]. A comparison of the two reinforcement types is given in Figure 2.6. Moreover, a detailed view of a tensile specimen reinforced concentrically by kevlar material is presented in Figure 2.7.

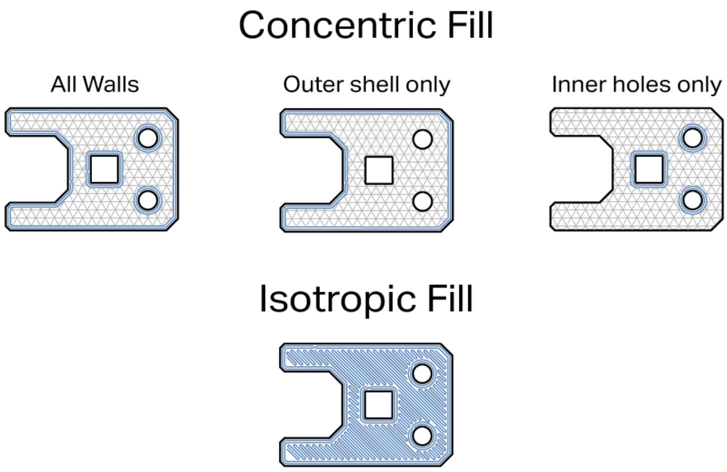

Figure 2.6: Concentric vs isotropic reinforcement [25]

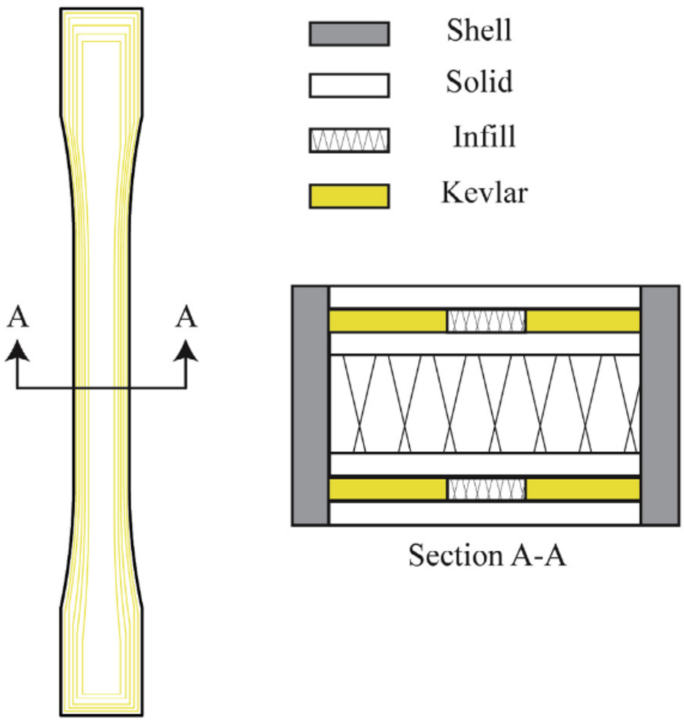

Figure 2.7: Concentric fiber reinforcement [26]

Markforged offers many CFF materials to be used for matrix and reinforcement purposes. Some offered materials are White Nylon, Onyx (nylon with chopped Carbon Fibers) for matrix (base) material, and kevlar, Carbon Fiber, and fiberglass for reinforcement materials. Regarding mechanical performance, the most critical parameter is selected materials, and according to Markforged, Carbon Fiber is as strong as Aluminum 6xxx series materials. They claim Carbon Fiber has 60 GPa of Young's modulus and 800 MPa tensile strength [27]. The mechanical performance comparison for different materials is given in the datasheet provided by Markforged and shown in Figure 2.8a and 2.8b for matrix and reinforcement materials, respectively.

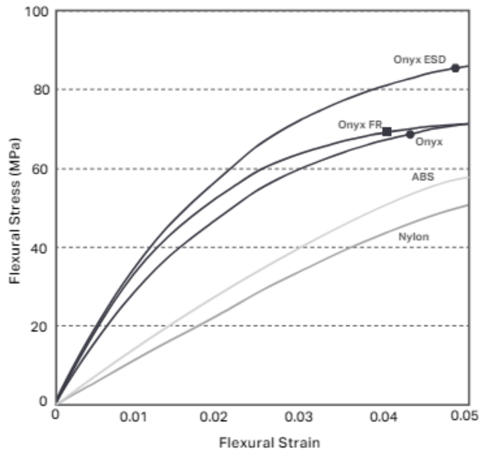

(a) Comparison of matrix materials

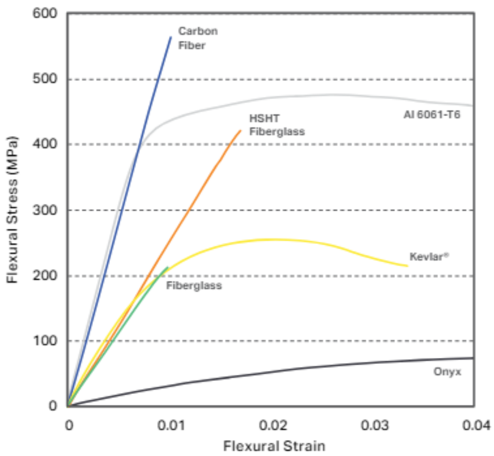

(b) Comparison of reinforcement materials

Figure 2.8: Comparisons of materials provided by Markforged data sheet [27]

In addition to the used material, process parameters like nozzle temperature, nozzle diameter, layer thickness, geometry of the part, building orientation, and environmental conditions (since, in general, matrix materials are made of polymers and sensitive to moisture and UV lights) affect the mechanical performance of the printed part [28].

According to Ning et al., [29], printing speed has a low influence on the tensile strength of the printed part, but for better inter-laminar bonding and finer surface finish, low-speed rates should be used — however, a deficient printing speed results in a longer process time. Qiao et al. [30] discussed the effect of infill pattern and percentage on mechanical properties for PLA material in their work, and they concluded that maximum bending force before failure increases with increasing infill percentage. They compared three different infill patterns, namely grid, honeycomb, and gyroid, depicted in Figure 2.9, and obtained that honeycomb and gyroid infill patterns have better mechanical properties than simple grid patterns.

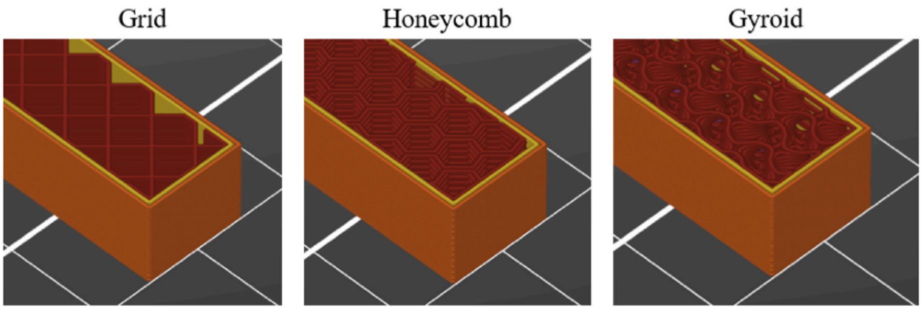

Figure 2.9: Different infill patterns [30]

Atatreh et al. [31] compared the tensile properties of 17-4 PH steel with triangular and solid infill. They proposed that tensile strength drops 42 % when triangular infill is used, but the total mass also reduces to 34 %. Their samples are provided in Figure 2.10.

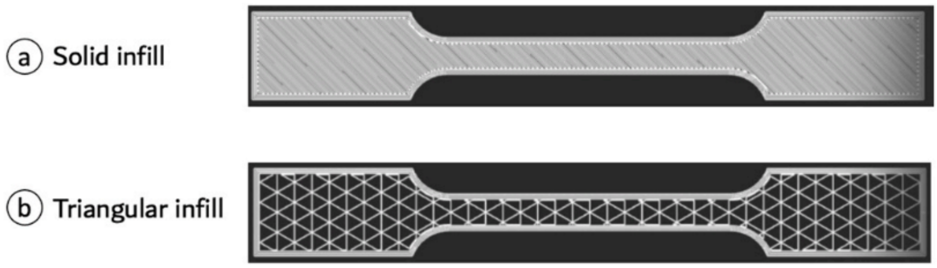

Figure 2.10: Solid vs triangular [31]

Moreover, Huit et al. [32] did tedious work about how different infill types affect the elastic modulus and tensile strength of White Nylon parts reinforced by fiberglass, Carbon Fiber, and Kevlar. For all types of infill, Carbon Fiber has the highest elastic modulus and tensile strength compared to others when tested with the same infill ratios and patterns. Also, the conclusion of this work suggests that rectangular infill has a higher elastic modulus and tensile strength than hexagonal infill, followed by triangular infill. In another study, Naranjo et al. [33] also investigated the same subject, the effect of infill pattern on continuous and chopped Carbon Fiber reinforced White Nylon. They concluded that triangular infill performs better mechanical performance (better elastic modulus and tensile strength). Hence, different results are present in the literature on this field.

Chacon et al. investigated the effect of printing parameters on mechanical properties in their work [34]. They examined the impact of three build orientations, namely flat, on edge, and upright, given in Figure 2.11, layer thickness, and feed rate, on the mechanical properties of PLA material.

For the same layer thickness and feed rate, they obtained similar results for elastic modulus for on-edge and flat orientations but lower elastic modulus for upright orientation. Upright specimens show inter-layer failure with lower strength and elastic modulus, while on-edge and flat specimens exhibit trans-layer failure with higher tensile strength and elastic modulus. For the same feed rate, layer thickness affects changes with build orientation. For upright specimens, tensile strength increases with layer thickness; however, layer thickness has almost no significant effect on mechanical performance for on-edge and flat build orientations. The impact of the feed rate also depends on the orientation of the part. For the upright samples, tensile properties improve with the increasing feed rate, while flat and on-edge orientations have minor significance.

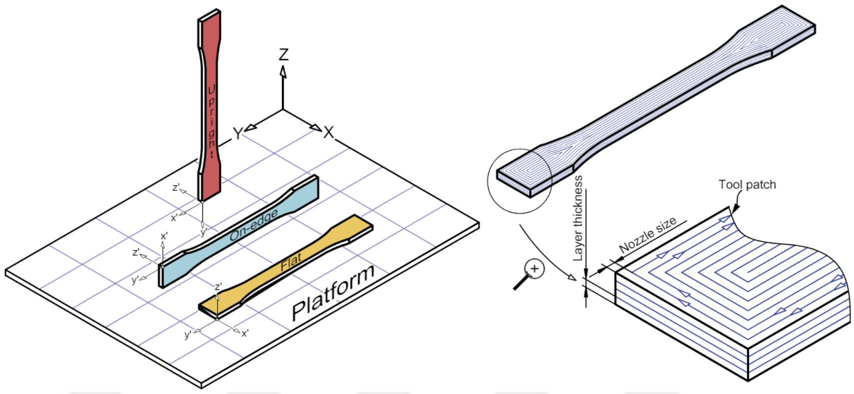

Figure 2.11: Build orientation and layer thickness [34]

As mentioned in the previous paragraphs, many factors affect the mechanical properties. In conventional FFF printers, slicers (the software that slices the part into layers) require some printing parameters as user input. However, Markforged has its own slicing software as an online website (eiger.io). The slicer does not allow the manipulation of many printing parameters. It only allows a few settings that are independent of material, such as required roof and top layers, number of wall layers, and layer height. The nozzle temperature, feed rate, and layer thickness parameters are not changeable by users.

The required roof and top layers settings are the number of layers of the solid plastic to be used in the top and bottom layers of the part to ensure the hold the part on the printer bad [35].

The number of wall layers is the number of pure plastic shells that enclose the part entirely. More walls make it easier to stick the reinforcement material, but they also reduce the area that can be reinforced [35].

The layer thickness is nothing but the thickness of a single layer. It depends on the material to be extruded [35].

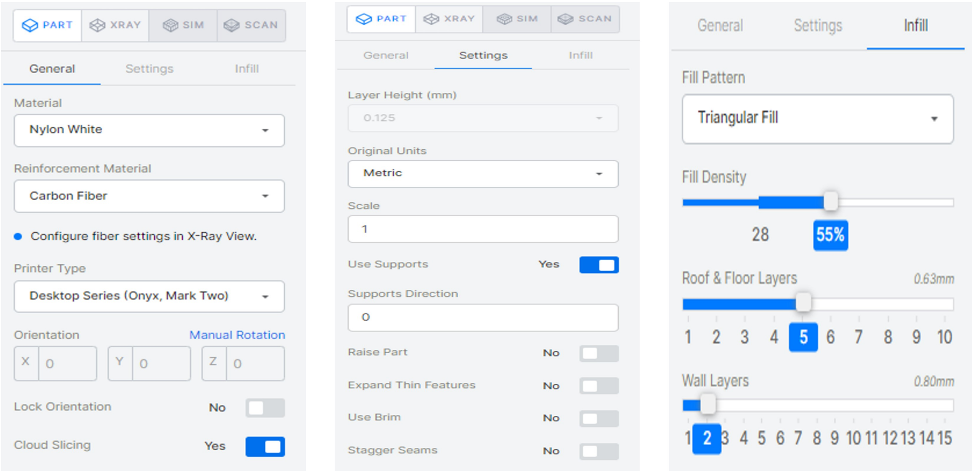

Figure 2.12: Eiger software settings

2.3 Material Characterization of Additively Manufactured Composite Parts

In order to understand the mechanical behavior of a material, required material characterization tests must be done for any type of material (metal, composite, polymer, etc.). However, required tests are changeable and should be determined according to specific material models. For instance, for isotropic materials like aluminum and steel alloys, having Young's Modulus and Poisson's ratio is enough to characterize the elastic stress-strain law for the particular material since it is assumed the material obeys Hooke's law; however, for hyperelastic materials, which do not obey Hooke's law, required tests change with the selected materials. Hence, the types of characterization tests vary depending on the material model used. As the number of terms to define the stiffness matrix of the material increases, the number of tests increases. In this section, only characterization tests of CFR are investigated.

Hence, first, one should decide which material model best reflects the mechanical behavior of a part. There is a lot of research in the literature on the material modeling of CFR parts. A research done by Galati et al. [36] to characterize the CFR composite part where the matrix material is White Nylon and reinforcement material is kevlar and Carbon Fiber. To emulate the mechanical behavior of the part, they decided to model the reinforcement material as a transversely isotropic material. A transversely isotropic material has the same elastic modulus in two directions, and the other direction has a different elastic modulus, so it has a plane of symmetry about an axis that is perpendicular to the plane of isotropy. Therefore, they calculated longitudinal elastic modulus E_1, transverse elastic modulus E_2, and in-plane shear modulus G_{12} for Kevlar. For the matrix material White Nylon, they just chose isotropic material model since the overall stiffness of the part is dominated by Carbon Fiber. For the characterization of reinforcement materials, they manufactured tensile specimens having different fiber orientations 0, 45, and 90 degrees for kevlar and Carbon Fiber as given in Figure 2.13 and zig-zag 45-degree orientation for White Nylon since it is decided to modeled as isotropic material.

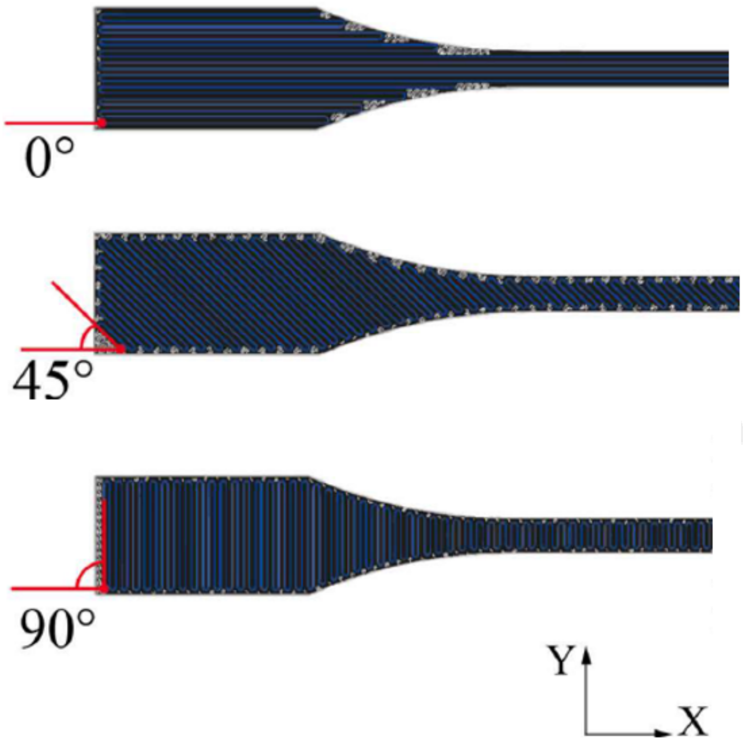

Figure 2.13: Fiber orientations for tensile testing [36]

The test is done according to ASTM D638 tensile testing standard. Results of the tests suggest that White Nylon has an elastic modulus of 0.69 GPa, Poisson's ratio of 0.39, and a shear modulus of 0.25 GPa. For the Carbon Fiber, 35 GPa of elastic modulus in longitudinal direction E_1, 7.5 GPa of elastic modulus in transverse direction E_2, 4 GPa of shear modulus G_{12}, and 0.15 of Poisson's ratio are found. Klift et al. also tested White Nylon [37] for its elastic properties and found the elastic modulus as

2.8 GPa. Abadi et al. tested tensile specimens with different volume fractions (ratio to volume of matrix material to reinforcement material) to find the volume averaged stiffness of the reinforced composites using lamination theory. Their test specimens are similar to ones that Galati et al. used [36], where fibers are printed along 0,45,90 degrees. However, the results of the two studies [36] and [38] are conflicting since Abadi et al. [38] found the elastic modulus of White Nylon as 0.38 GPa, elastic modulus of the Carbon Fiber in the longitudinal direction as 85 GPA and in the transverse direction 26 GPa. Hence, for the elastic properties, although there are many studies in the literature, the results have a lack of agreement with each other.

2.4 Numerical Modelling of Additively Manufactured Composite Parts

To evaluate the mechanical performance, which can be deflection under a specific loading case, yield stress or fracture, etc., of a mechanical part, two options are generally preferred: testing and finite element analysis. Testing a part under desired load conditions is not always feasible because it could be too expensive, fixtures and testing machines could be needed, and load cases can vary. Because of all these disadvantages, engineers usually benefit from finite element simulations. However, setting up a correct and realistic finite element model requires many input parameters to be predetermined by material characterization tests. A fine mathematical model in terms of accuracy, solution time, and physics should be reflected as it is in actual load conditions. Due to all these facts, one should be very careful when constructing the finite element model of a mechanical part.

For the 3D printed composites, there are numerous studies in the literature about their finite element analysis. However, there are many techniques to model this kind of part, and all of them have their own advantages and disadvantages. One technique is called as embedded elements. It is a homogenization technique where two independent mesh elements of bodies, called as embedded and hosts, are overlapped. The term embedding implies constraining nodes of embedded part to host elements kinematically, that is, the displacement of embedded parts will be calculated according to displacements of host parts with some weighting functions [39]. This technique can be applied to model composites in an FEA environment. It allows model reinforcement by means of long fibers (embedded parts) separately from the matrix (host); the schematic is given in Figure 2.14. In the end, a unit volume is obtained with homogenized elastic material properties, using the input material data for reinforcement and matrix, as well as geometries.

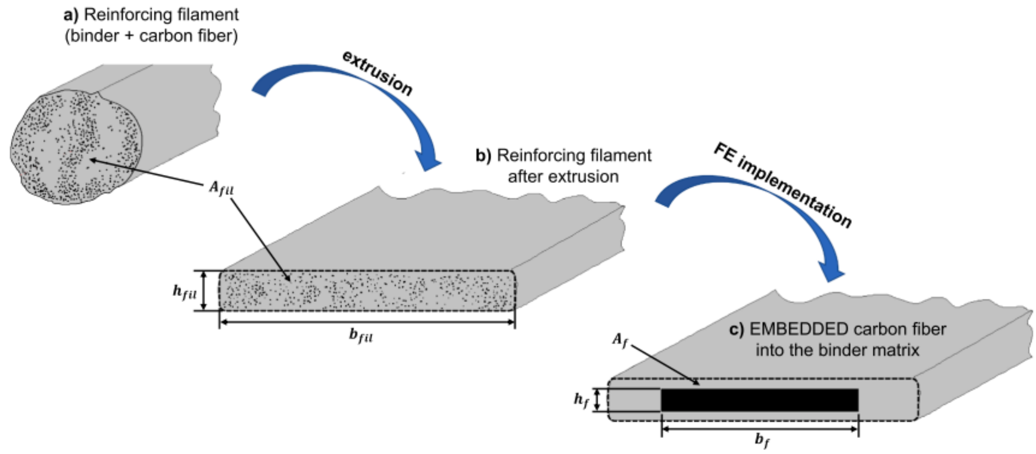

Figure 2.14: Modelling composites with EE technique [40]

Avanzini et al. [40] conducted a study using the EE technique. They used material properties from literature to model a tensile specimen that is concentric reinforced with notches, given in Figure 2.15a. They made tensile tests and FEA simulations to compare the load-displacement behavior of the specimens and claim a slight overestimation in stiffness compared to tests as given in Figure 2.15b.

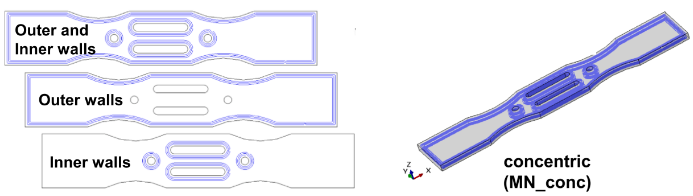

(a) Design of notched tensile specimen

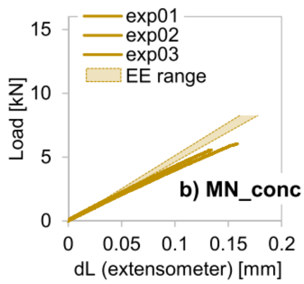

(b) Test-analysis comparison

Figure 2.15: Design and test-analysis comparison of notched tensile specimen [40]

The discrepancy in results is due to the nature of the EE technique. According to the Abaqus User's Guide, the EE technique brings some drawbacks and limitations, such that this technique adds model artificial stiffness and rotational degrees of freedom at a host node, which is unconstrained [41].

Another approach is followed by Zmindak et al. [42] to model CFR parts. They used shell elements to model the rectangular tensile specimens consisting of materials Onyx (as matrix) and Carbon Fiber (reinforcement) with 0,45,90 degree orientations. The assumptions are linear elastic and orthotropic material properties with no air gaps or cracks. The layers are modeled as perfectly bonded, which neglects the inter-layer shear strengths. The material properties are directly taken from the data sheet provided by Markforged. The results of tests and simulations are in good agreement, the difference in deformation is less than 1 percent. Ghebret et al. [43] used a similar approach to model flexural and tensile test simulations of specimens made of Onyx and Carbon Fiber. The material properties are taken from the literature to model orthotropic lamina; however, the results are not correlated with the tests. Galati et al. [36] also use a similar approach to model the tensile specimens concentrically reinforced by kevlar, using shell elements and bonded contacts. They compared force-displacement curves of numerical analysis and experiments as given in Figure 2.16 and results are matching.

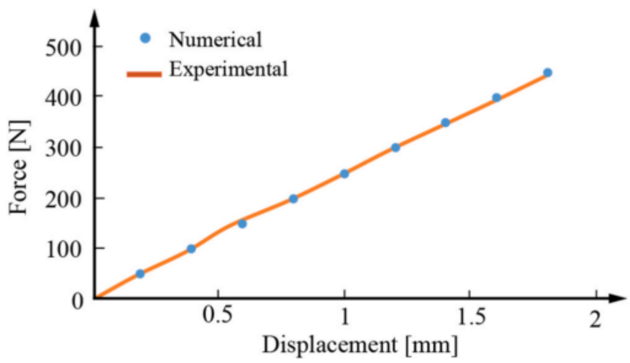

Figure 2.16: Comparison of numerical and experimental results [36]

2.5 Closure

AM enables engineers to design and produce parts with complex geometries and reduced weights compared to traditional methods. However, challenges remain regarding the mechanical performance of these parts. A commercially available solution involves designing parts with continuous fibers, where thermoplastics are reinforced with various fibers. FEA is a useful tool for evaluating the performance of continuous fiber-reinforced composites. Although numerous studies have explored FEA for such parts, most have focused on simple loading scenarios, such as tensile loading, revealing limitations in the current state of the art. Additionally, there are numerous material modeling approaches, but no well-defined or universally accepted technique has been established. In terms of numerical modeling, while many approaches exist, only a few studies have been validated with experimental tests, and their results often raise questions about accuracy. Therefore, developing a robust finite element strategy for continuous fiber-reinforced composites could significantly enhance the literature and provide valuable insights for future advancements in continuous fiber reinforcement technology.

In the Table 2.1 all the mentioned state of the art on fiber-reinforced composite parts are summarized.

Table 2.1: Summary of the state of the art

Effects of Process Parameters on Mechanical Properties		
Process Parameter	Description	Reference
Printing Speed	Printing speed has a low influence on the tensile strength of the printed part, but for better inter-laminar bonding and finer surface finish, low-speed rates should be used.	[29]
Effect of Infill Pattern	Maximum force before failure increases with increasing infill percentage. The honeycomb infill pattern provides highest stiffness to the part. Triangular infill performs better mechanical performance than gyroid and simple infill patterns.	[30] -[33]
Building Orientation	For the same layer thickness and feed rate, elastic modulus is similar for on-edge and flat orientations but it is lower for upright orientation.	[34]
Layer Thickness	For upright specimens, tensile strength increases with layer thickness; however, layer thickness has almost no significant effect on mechanical performance for on-edge and flat build orientations.	[34]
Feed Rate	For the upright samples, tensile properties improve with the increasing feed rate, while flat and on-edge orientations have minor significance.	[34]

Table 2.2: Material characterization of AM composites

Material Characterization of AM Composites		
Materials	Description	Reference
White Nylon, Kevlar and Carbon Fiber	Transversely Isotropic for Kevlar and Carbon Fiber. Isotropic for White Nylon.	[36]
White Nylon	Isotropic Material.	[37]
White Nylon Carbon Fiber	Orthotropic for Carbon Fiber, isotropic for White Nylon.	[38]

Table 2.3: Numerical modeling of AM composites

Numerical Modeling of AM Composites		
Modeling Technique	Description	Reference
Embedded Elements	Material properties are taken from literature. Tensile specimen is modeled with embedded elements. Force-displacement curves are obtained and compared with experiments. Results of numerical model are stiffer than the experiments.	[40]
Shell Elements	Onyx and Carbon Fiber materials are used. Linear elastic and orthotropic material model is utilized. Rectangular tensile specimens are modeled and tested. Results of FEA are in agreement with tests.	[42]
Shell Elements	3-point bending and tensile test simulations are performed; however, tests are not performed.	[43]
Shell Elements	Tensile specimens are modeled and numerical results are compared with tests. Tests and simulations are correlated.	[36]

CHAPTER 3

MATERIAL CHARACTERIZATION OF CONTINUOUS FILAMENT FABRICATED PARTS

In this chapter, the steps for material characterization are explained. Material modeling, testing, and results of the tests are given.

The main purpose of CFF is to achieve parts with a high strength-to-weight ratio while making use of the flexibility of AM in design. However, mechanical parts should be verified before they are used in real applications. As discussed in Chapter2, verification can be done in two ways: testing and numerical simulation. To get reliable results in a numerical model, the correct material model and properties are a must. Hence, this chapter is devoted to explaining material characterization stages.
The scope of the thesis is the modeling of CFF parts in FEA for the elastic regime. Generally, these parts are made from two materials, a matrix material, and a reinforcement material, just like traditional composites. Hence, a matrix and a reinforcement material are chosen as White Nylon (as matrix) and Carbon Fiber (as reinforcement). These materials are selected because although they are investigated in the literature, there is no well-accepted material model and properties for these materials. Moreover, they are relatively cheaper and reachable than alternatives.

According to Markforged, one of the pioneer companies of CFF technology, White Nylon is a thermoplastic that is smooth, non-abrasive, and easily painted. Moreover, it is compatible with various reinforcement materials such as Fiber glass, Carbon Fiber, Kevlar, etc. It builds the skin of the specimen by enclosing the part. White Nylon constitutes most of the volume of the designed part since it is not only the skin but the infill material [44].

Carbon Fiber is highly used in many applications, including automotive, defense, aerospace, etc. However, the so-called Carbon Fiber used in continuous fiber printing differs from that used in classical composite material technologies. Its physical and mechanical properties are distinct both from the traditional Carbon Fiber and ordinary FDM materials. Carbon Fiber used in CFF process is not actually melted or extruded like plastics. However, instead, it is laid down intact through the nozzle. According to Markforged, Continuous Carbon Fiber filaments are coated with thin plastic coating, which melts during process in order to adhere to the matrix [45]. The most remarkable feature of continuous Carbon Fiber is its strength, heat resistance, and durability. While short fibers create discontinuities, which result in transferring load to matrix material and limit the part's strength, long continuous fibers are good at carrying loads and minimizing the load transfer to the matrix material. As a result, the part is capable of carrying higher loads than the parts with short fibers.
Although many filament manufacturers, including Markforged, share the technical data sheets for the filaments, material properties are found to be different when real parts are tested as discussed in Chapter2. These changes arise from numerous reasons in additive manufacturing, such as:

- Applied heat and pressure during the process
- Inter-layer adhesion
- Process parameters like nozzle temperature, number of layers etc.

In general, technical data sheets do not include the effect of the above parameters when they share material properties. Hence, to understand the behavior of the materials, characterization tests are a must for White Nylon and Carbon Fiber.
White Nylon and Carbon Fiber material properties should be carefully obtained to set a realistic FE model. Therefore, material characterization tests should be carefully chosen. After the literature review, it is concluded that reinforcement materials show highly orthotropic material behavior in the elastic region. Moreover, White Nylon is modeled as an isotropic material in many papers for simplicity since its stiffness is relatively low compared to Carbon Fiber. On the other hand, Carbon Fiber is modeled as an elastic lamina, and material directions are given in Figure 3.1.

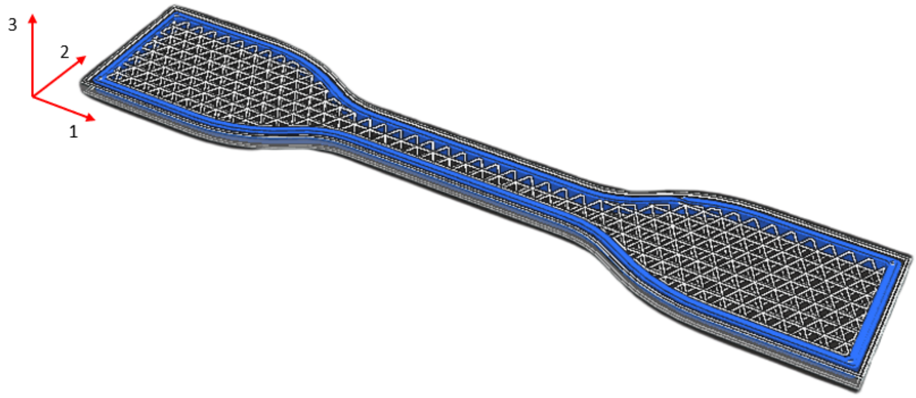

Figure 3.1: Material directions

Direction 1 is the printing direction (fiber direction), and the material behaves much stiffer in this direction than in directions 2 and 3. Direction 2 is the transverse direction according to direction 1, and direction 3 is the out-of-plane direction. Since the analysis has been decided to be set up with shell elements, out-of-plane material properties are not of interest.

For the decided material models, isotropic for White Nylon and orthotropic for Carbon Fiber, the required material parameters and tests to obtain those parameters are listed in Table 3.1

Table 3.1: Summary of material characterization tests

Property	Description	Test Type
E_1	Young's modulus in direction 1	Tensile test of $0°$ CFF
E_2	Young's modulus in direction 2	Tensile test of $90°$ CFF
G_{12}	Shear modulus in 1-2 plane	Off-axis tensile test of $45°$ CFF
ν_{12}	Poisson's ratio in 1-2 plane	Tensile test of $0°$ CFF
$E_{\text{White Nylon}}$	Young's modulus for White Nylon	Tensile test
$\nu_{\text{White Nylon}}$	Poisson's ratio for White Nylon	Tensile test

In the following sections, characterization tests will be discussed.

3.1 Characterization of White Nylon

As mentioned in the previous section, White Nylon is modeled as an isotropic elastic material. Hence, Young's Modulus $E_{\text{White Nylon}}$ and Poisson's Ratio ν_{nylon} should be determined from tensile tests. For tensile tests, rectangle specimens having dimensions of 250 mm x 15 mm x 1 mm are used. In this test the purpose is not to measure the yield and ultimate tensile strengths but to measure Young's Modulus and Poisson's ratio.

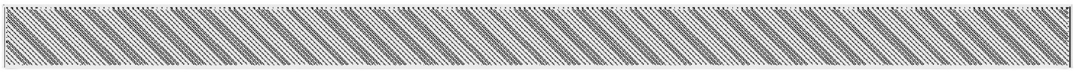

Figure 3.2: Cross-section view of White Nylon tensile specimen

Four rectangular tensile specimens manufactured from pure White Nylon with solid infill are tested. The cross-section of one specimen is given in Figure 3.2.

A video extensometer, which tracks the distance between the pre-defined points to calculate strains, is used to measure the strains both in tensile and transverse directions simultaneously, and a build-in load-cell of the universal testing machine, capable of measuring 200 kN of load is used for force measurements. A photo taken during the tests is given in Figure 3.3

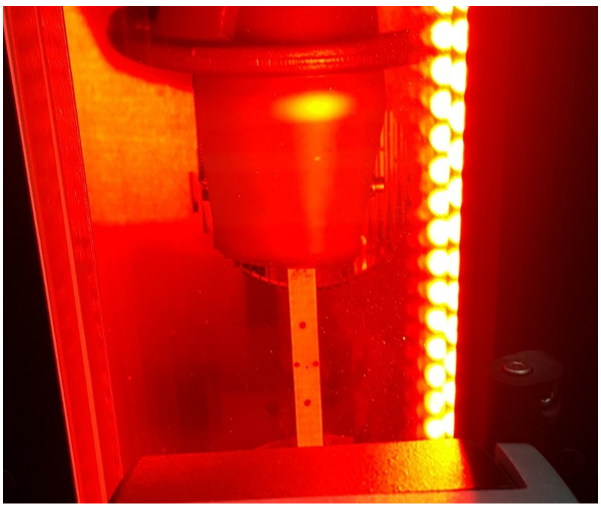

Figure 3.3: Video dot tracking system

Material properties Young's Modulus and Poisson's Ratio are calculated using Hooke's law. The related equation for Poisson's Ratio is given in equation 3.1

$$\nu = -\frac{\epsilon_1}{\epsilon_2} \tag{3.1}$$

For the calculation of Young's modulus, first tensile stress is calculated by dividing instantaneous force F by initial area A as given in equation 3.2, then using the related Hooke's law equation 3.3 Young's Modulus is calculated.

$$\sigma = \frac{F}{A} \tag{3.2}$$

$$E = \frac{\sigma}{\epsilon_1} \tag{3.3}$$

Note that White Nylon behaves as almost a linear elastic material since the stress-strain relation is linear in the elastic region. Hence, normal stress increases linearly with axial strain. As a result, Young's Modulus could be obtained from Hooke's law using the least squares method to fit a linear curve to the linear portion of the stress-strain diagram in which the slope of the curve is Young's Modulus. For four different specimens, Young's Modulus values derived from least squares fit given in Table 3.2

Table 3.2: Results of curve fitting for Young's Modulus of White Nylon specimens

Specimen	**Young's Modulus (MPa)**
1	996
2	1005
3	932
4	905

Since the purpose of the tests is to understand the linear elastic behavior of the White Nylon, only the linear elastic region is of interest (up to 3.5 percent axial strain) and marked in Figure 3.4. After applying the least square curve to fit the linear region for four separate tests, Young's Modulus of White Nylon is found to be 960 MPa by averaging the results of four tests.

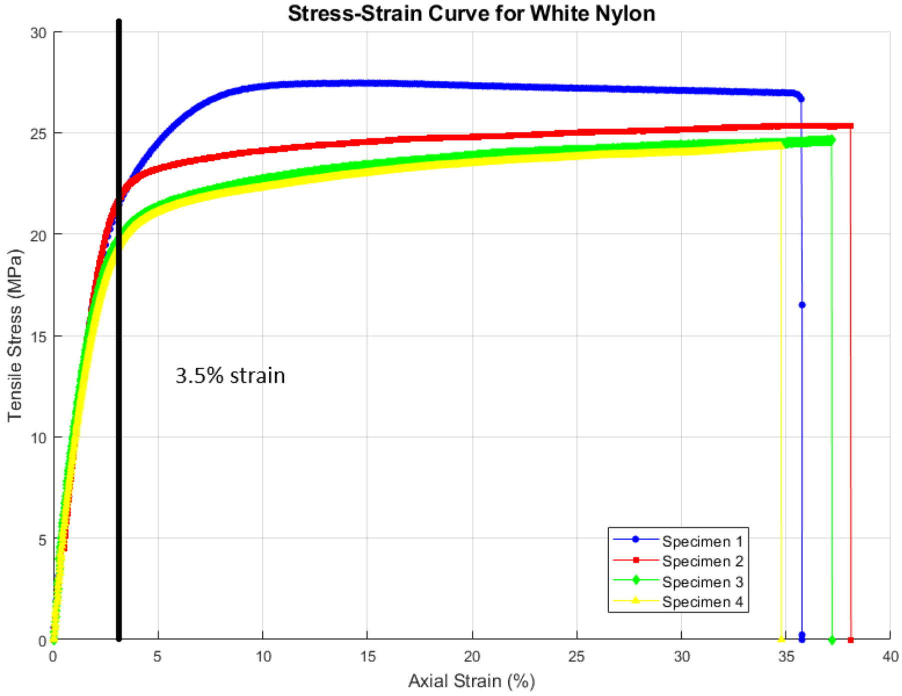

Figure 3.4: White Nylon's stress-strain diagram

A similar procedure is followed to determine Poisson's ratio for White Nylon. As stated previously, axial and transverse strains are measured simultaneously during the tensile tests. One can calculate the Poisson's ratio by using the equation 3.1. In Figure 3.5, measured axial and transverse strains are given for four specimens.

As mentioned before, only the linear elastic region is of interest, and the least squares curve fit is performed for this region separately for four specimens, then averaged to determine Poisson's ratio. As a result, Poisson's ratio of 0.41 is calculated by averaging test results, as given in Table 3.3.

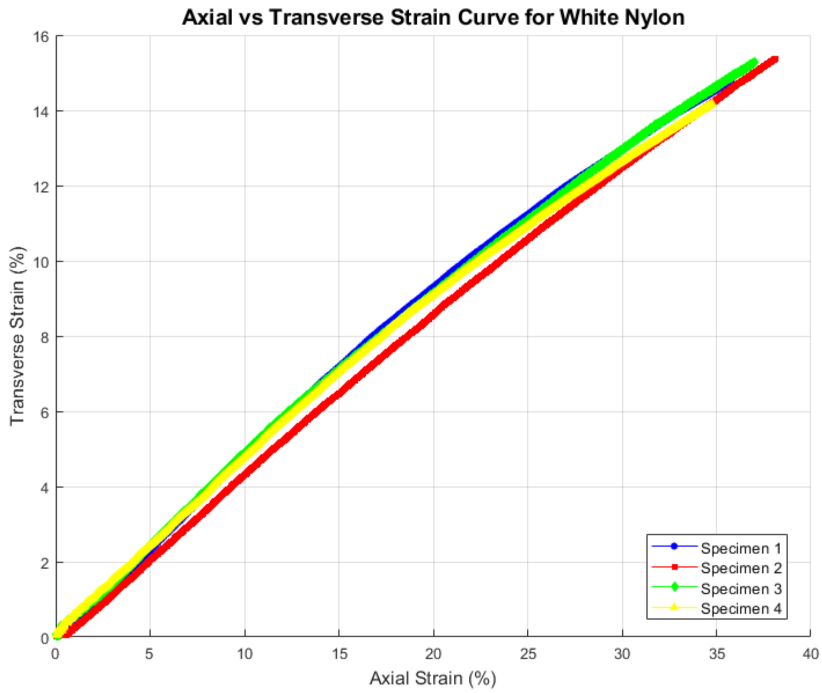

Figure 3.5: White Nylon axial vs transverse strain

Table 3.3: Results of Poisson's Ratio for White Nylon specimens

Specimen	**Poisson's ratio**
1	0.42
2	0.41
3	0.41
4	0.40

In short, linear elastic material properties of White Nylon are given in Table 3.4

Table 3.4: Material properties of White Nylon

Property	Value
Young's Modulus	960 MPa
Poisson's Ratio	0.41

3.2 Characterization of Continuous Carbon Fiber

As discussed in Chapter 2, Continuous Carbon Fiber shows orthotropic material properties. It has been decided that, in finite element models, continuous Carbon Fiber should be modeled as an elastic lamina. Table 3.1 lists the tests and parameters for White Nylon and Carbon Fiber.

Note that since finite element analyses are planned as 2D, only planar material properties of the elastic lamina are determined. These properties are E_1, E_2, G_{12} and ν_{12} where E_1 represents elastic modulus of lamina in direction 1, i.e printing direction, E_2 stands for elastic modulus in transverse direction, G_{12} is shear modulus in 1-2 plane and ν_{12} is the Poisson's ratio for the same plane. Tension tests were conducted on all these material properties.

3.2.1 0 Degree Carbon Fiber Characterization

For direction 1, five specimens with dimensions of 250 mm x 15 mm 1 mm and only fibers of $0°$ are designed and manufactured. Interior of a specimen can be seen in Figure 3.6.

Figure 3.6: Direction 1 specimen's interior

Moreover, force and displacement are measured simultaneously to obtain tensile stress and axial strain, which are used to calculate Young's modulus. Figure 3.7 gives the stress-strain diagram of five specimens.

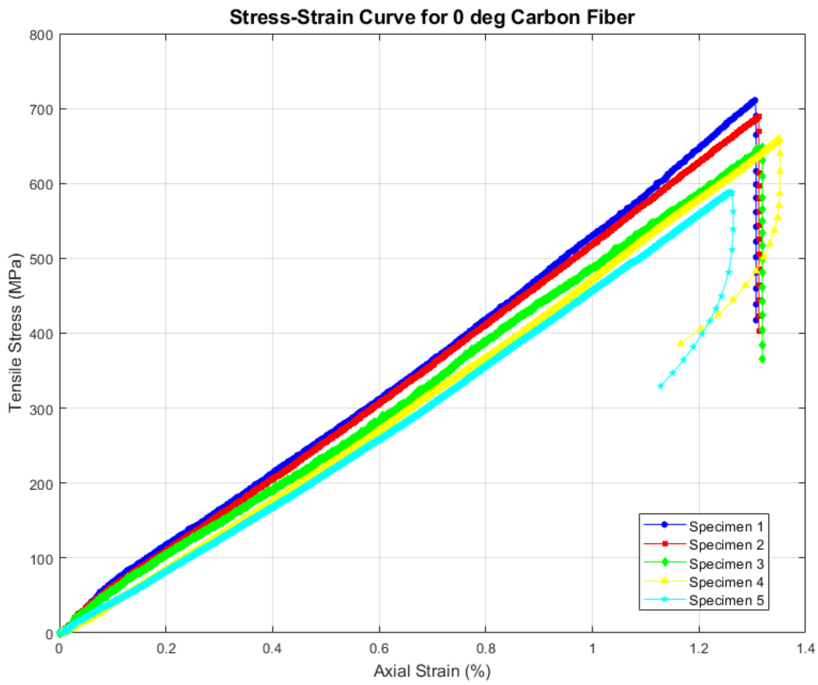

Figure 3.7: Direction 1 specimen's stress-strain relation

Young's modulus is obtained using the least squares method by fitting a linear curve to a stress-strain diagram. Results of least squares curve fit for $0°$ Carbon Fiber specimen are given in Table 3.5.

Table 3.5: Results of Young's Modulus for $0°$ Carbon Fiber specimens

Specimen	**Young's Modulus**
1	53.0 GPa
2	51.9 GPa
3	48.6 GPa
4	47.1 GPa
5	45.0 GPa

By averaging the Young's Modulus values for five specimens, Young's modulus in direction 1, E_1, is obtained as 49.1 GPa.

For specimen 5, transverse strain is also measured during the tensile tests to calculate Poissons's ratio ν_{12} from equation 3.1.

In Figure 3.7, axial stress and transverse strain of the specimen are given. The slope of the curve is found by least squares curve fit, and the resulting Poisson's ratio is 0.34.

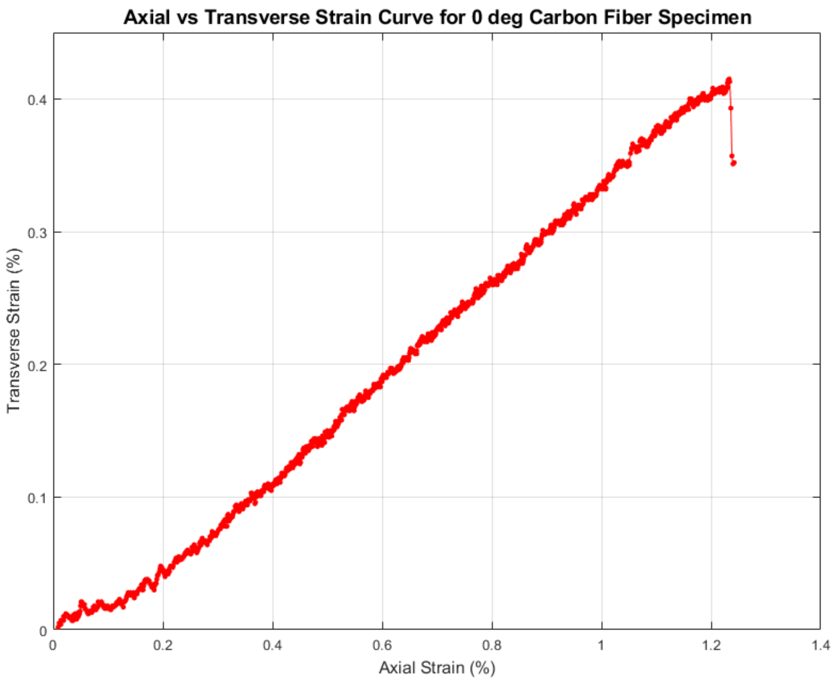

Figure 3.8: Direction 1 specimen-axial vs transverse strain

3.2.2 90 Degree Carbon Fiber Characterization

For direction 2, five specimens having dimensions of 250 mm x 15 mm 1 mm and having only fibers of 90° are designed and manufactured. Interior of a specimen can be seen in Figure 3.9. In characterization tests, a video dot tracking system is used to measure strains in direction 1 (axial direction).

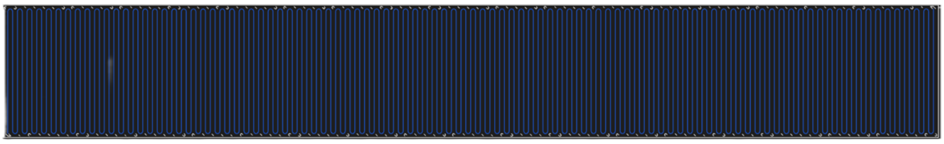

Figure 3.9: Direction 2 specimen’s interior

The stress-strain diagrams of the direction 2 specimens are given in Figure 3.10.

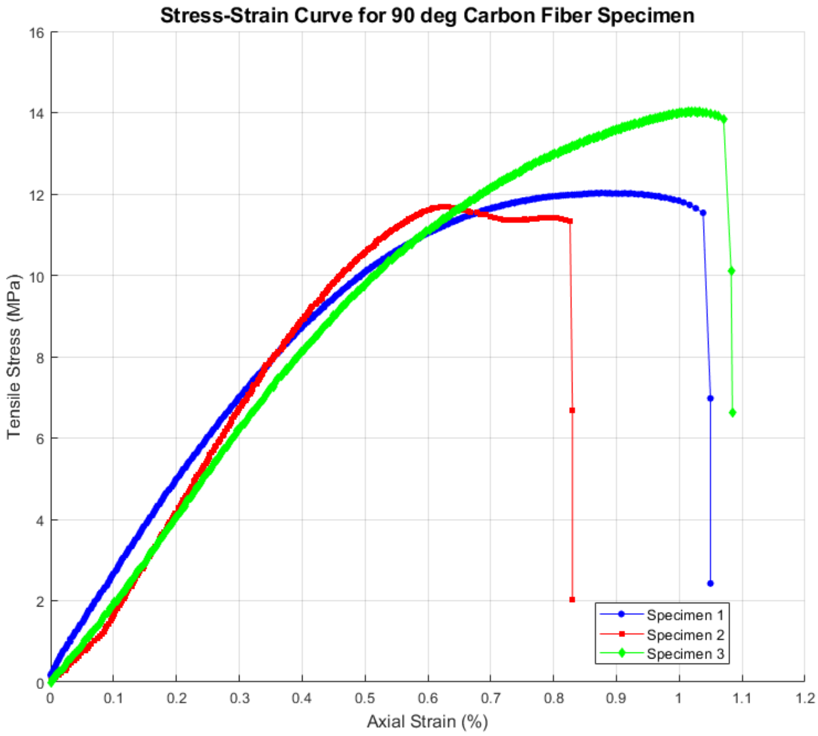

Figure 3.10: Direction 2 specimen’s stress-strain relation

Curve fitting with the least squares method is applied to each specimen separately in the linear elastic region, and results are provided in Table 3.6. The mean of each result is obtained, and E_2 is found as 2.17 GPa.

Table 3.6: Results of Young's Modulus for 90° Carbon Fiber specimens

Specimen	Young's Modulus
1	2.3 GPa
2	2.2 GPa
3	2.0 GPa

3.2.3 45 Degree Carbon Fiber Characterization

In order to estimate the shear modulus G_{12}, off-axis tension tests are done for four specimens having dimensions of 200 mm x 25 mm x 1.25 mm. The off-axis tension test is one of the easiest tests to determine the shear properties of an orthotropic material by a tensile test [46]. It evaluates shear strain and stress values from tensile stress and axial and transverse strains, respectively. 4 specimens having a stack-up $\pm 45^{\circ}$ are designed and manufactured as shown in Figure 3.11.

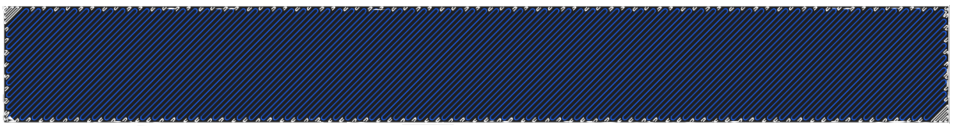

Figure 3.11: Shear specimen's interior

Strains both in axial and transverse directions are measured by a video dot tracking system, in addition to measuring instantaneous force to obtain strain-stress relation. However, for the off-axis test, the measured engineering tensile stresses could not be directly used in Hooke's law to find the in-plane shear modulus G_{12}. The following relations are used:

$$\tau_{12} = \frac{P}{2A} = \frac{\sigma_{\text{tensile}}}{2} \tag{3.4}$$

$$\gamma_{12} = \epsilon_x - \epsilon_y \tag{3.5}$$

$$G_{12} = \frac{\sigma_{\text{tensile}}}{2(\varepsilon_x - \varepsilon_y)} \tag{3.6}$$

Hence, the relation of G_{12} vs γ_{12} is obtained and given in Figure 3.12. The results of the least square analysis of the linear elastic region of the stress-strain diagrams are given in Table 3.7, and it provides an average shear modulus G_{12} as 1.3 GPa.

Table 3.7: Results of Shear Modulus for $45°$ Carbon Fiber specimens

Specimen	Shear Modulus
1	1.35 GPa
2	1.23 GPa
3	1.30 GPa
4	1.31 GPa

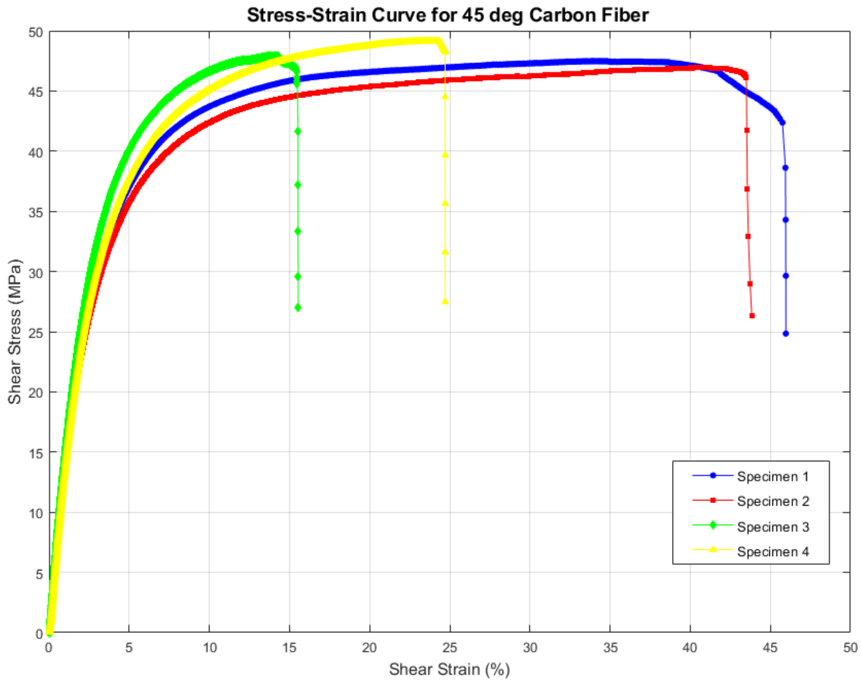

Figure 3.12: 45 degree specimen's stress-strain relation

In short, all material properties needed for finite element analyses are obtained and listed in Table 3.8

Table 3.8: Summary of Material Properties

Material	Property	Value
White Nylon	$E_{\text{White Nylon}}$	$960\,\mathrm{MPa}$
	$\nu_{\text{White Nylon}}$	0.41
Continuous Carbon Fiber	E_1	$49.1\,\mathrm{GPa}$
	E_2	$2.17\,\mathrm{GPa}$
	G_{12}	$1.36\,\mathrm{GPa}$
	ν_{12}	0.34

Definitions: White Nylon is a linear isotropic material with uniform properties in all material directions. Continuous Carbon Fiber is a linear elastic lamina with orthotropic properties that vary with fiber orientation.

3.3 Closure

In this Chapter, the material characterization procedure for White Nylon and Carbon Fiber is explained. Simple tension tests are performed to measure force and displacements, and then required stresses and strains are obtained via Hooke's law. Finally, least squares are applied to each test, and the results are averaged to obtain material properties, summarized in Table 3.8.

CHAPTER 4

DESIGN AND FABRICATION OF CONTINUOUS FILAMENT FABRICATED TEST SPECIMENS

This chapter will discuss the design and fabrication stages of three specimens, tensile, bending, and eccentric, in detail.

This thesis aims to develop a mathematical modeling technique for the parts manufactured with CFF. In order to validate the accuracy of the mathematical model, experiments with three different loading cases were conducted to compare the results of numerical models with tests.
The first specimen is called as the tensile specimen. In this case, a classical dog-bone-shaped tensile specimen was planned to be designed, manufactured, and tested to validate that the numerical model works well under tensile load.
The second specimen is the bending specimen. The purpose of manufacturing and testing bending specimens is to determine the accuracy of the modeling techniques under bending loading. Three-point bending tests were done to examine the bending behavior.
The third specimen is the eccentric specimen. The goal for the eccentric specimen is validation of the mathematical modeling approach under an eccentric loading case, which consists of combined tensile and bending loads.

4.1 Designing and Manufacturing Parts with Continuous Filament Fabrication

As discussed in Chapter 2, CFF is one way of manufacturing composite parts with AM. Markforged is one of the pioneers of this technology globally, and some companies in Turkey offer Markforged products such as filaments and printers. Hence, Markforged printers are selected to manufacture parts because they are easy to access. Moreover, for the matrix material White Nylon, and the reinforcement material Carbon Fiber is selected since those materials were researched primarily in the literature and are available in filament supplier companies.

4.2 Design and Fabrication of Tensile Specimen

As discussed previously, to validate the mathematical model under tensile loading, tensile specimens must be manufactured and tested. The specimen dimensions are selected according to Type IV specimen sizes given in standard ASTM D 638 - Standard Test Method for Tensile Properties of Plastics [47]. Since there is no specific tensile testing standard for AM, this standard is followed. ASTM D638 suggests tailoring the length and width of the gripping section of the specimen to guarantee enough friction between the part and the specimen to hold the parts in the gripper without any slipping concern. Moreover, as shown in Figure 4.1, the pre-defined dimensions for tensile specimens do not allow a proper fiber reinforcement with two rings.

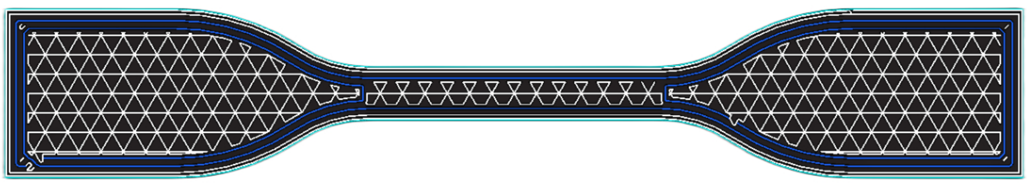

Figure 4.1: Reinforcement with original dimensions

Hence, the width of the specimen is enlarged by 3 mm than defined in the standard. In Figure 4.2, original dimensions in mm as length unit are defined in ASTM D638 standard are given, and in Figure 4.3 tailored dimensions are shown.

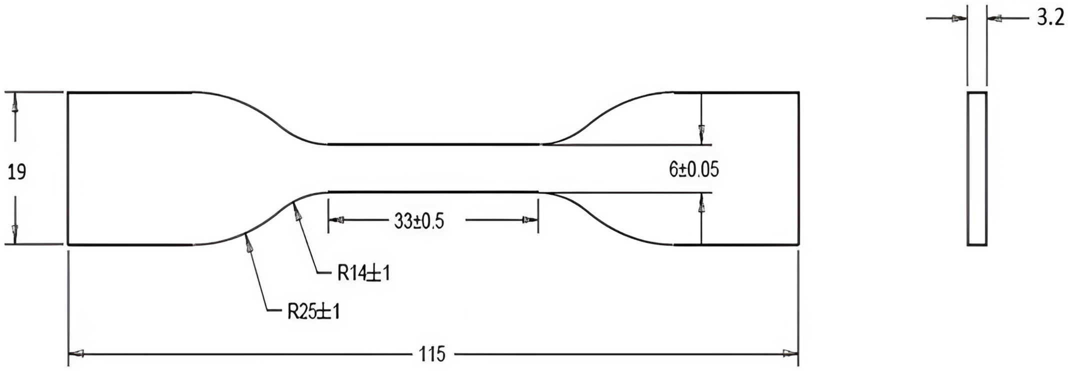

Figure 4.2: Original dimensions of ASTM D638 Type IV specimen [47]

Figure 4.3: Tailored dimensions of ASTM D638 Type IV specimen

Then, an STL file is created in SpaceClaim, a CAD software embedded in ANSYS. The STL file is uploaded to the online slicer software for Markforged printers (eiger.io) to arrange the design, such as creating infill, concentric reinforcement, assigning material, and slicing the specimen in order to make the specimen ready for manufacturing.

Slicer suggests a maximum infill of 55 % to obtain better dimensional accuracy and a better union of infill and reinforcement. A triangular infill pattern is selected for simplicity. The number of the roof and top layers, which are made of White Nylon, is chosen as four, which is a suggestion of the slicer in order to ensure bonding to the build plate during manufacturing and separation from the building plate after the manufacturing is over. Moreover, the number of walls made by White Nylon shell is selected as two, having a total thickness of 0.8 mm, to unite the outer shell White Nylon wall to Carbon Fiber reinforcement.

Overall, after the slicing is done, the specimen is ready to print with a total of 26 layers, each with a thickness of 0.125 mm, and 22 of them (layers between 3-24) are reinforced with concentric Carbon Fiber rings, while first and last two layers are the roof and top layers. Two cross-sectional views of the specimen, one is for the roof and top, and the other includes reinforcement, are given in Figure 4.4

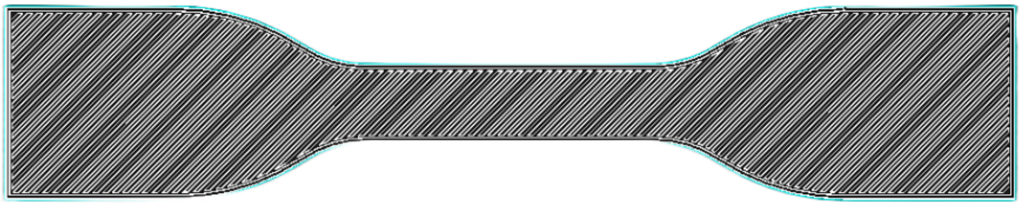

(a) Roof and top layers

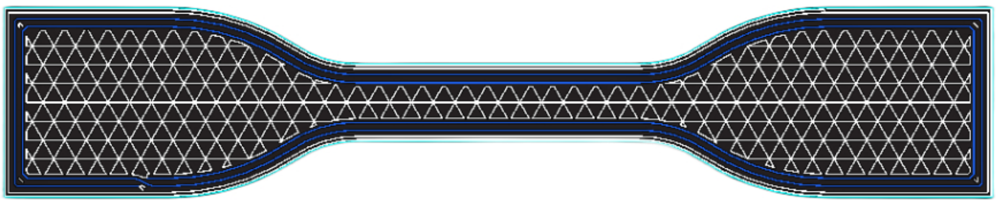

(b) Reinforcement layer

Figure 4.4: Cross sectional view of tensile specimen

Since there are no overhangs in the design, no support structures are needed with the selected printing direction given in Figure 4.5

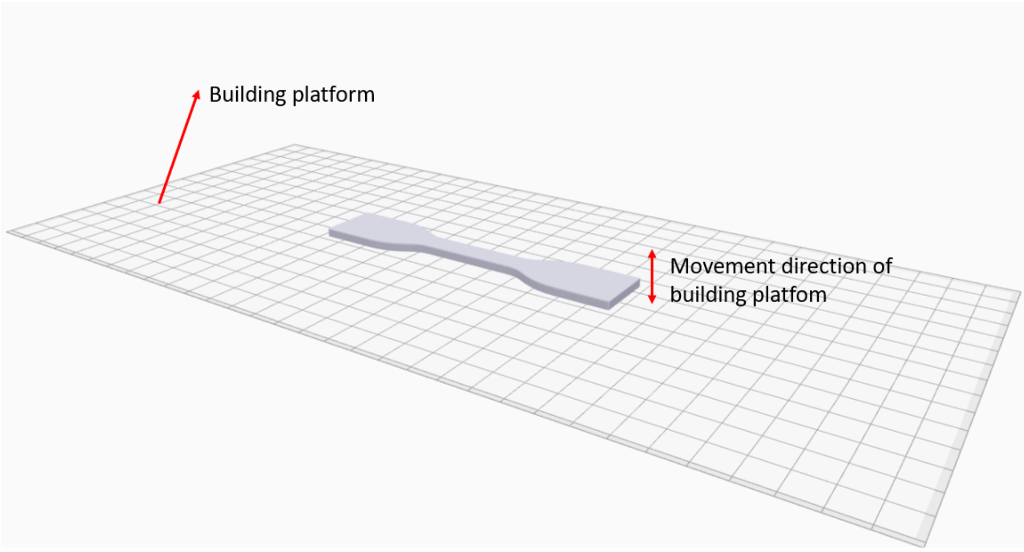

Figure 4.5: Tensile specimen building direction

All the settings that the slicer allows to change for the printing process are also given in Figure 4.6

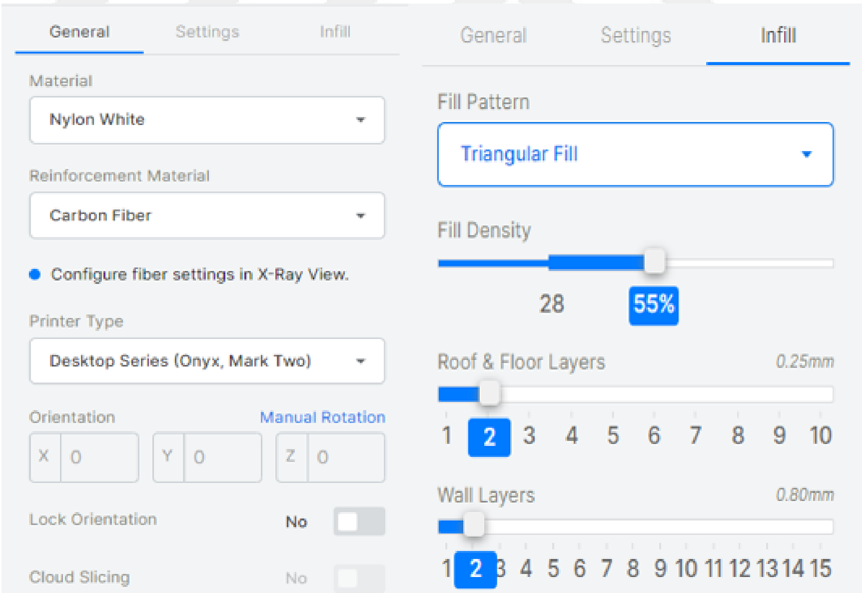

Figure 4.6: Tensile specimen printing parameters

According to the slicer, the total time of printing a specimen is 1 hour and 1 minute, which exactly matches the actual production time, excluding the heating and cooling time of nozzles. A specimen contains 0.95 cm^3 of Carbon Fiber, and White Nylon has a volume of 4.22 cm^3 where the overall mass of a specimen is 5.44 grams. The cost of material to produce a single specimen is 3.75 USD, according to Markforged [25]. Three specimens with the same dimensions, interior geometry, and printing parameters are manufactured to be tested.

4.3 Design and Fabrication of Bending Specimen

To verify the mathematical model under flexural loading, a 3-point bending test was performed. A test specimen having similar but not the exact dimensions as the specimen given in the related test standard ASTM-D-790-Standard Test Methods for Flexural Properties of Unreinforced and Reinforced Plastics and Electrical Insulating Materials [48] is designed and manufactured from White Nylon (matrix) and Carbon Fiber (reinforcement) materials. The reason for not using the same specimen geometry depicted in the standard is that the test's purpose is not to measure the flexural properties but to validate the numerical model. Hence, a smaller, which is reinforced by two concentric Carbon Fiber shells, specimen having dimensions of 160 mm x 10 mm x 8 mm, is decided to be manufactured. Moreover, having a smaller specimen has many advantages, such as reducing material consumption and manufacturing time and cost. The dimensions of the specimen are given in Figure 4.7.

Then, a procedure similar to the tensile specimen is followed to manufacture the bending specimen. First, geometry is converted into an STL file in SpaceClaim in order to slice the parts into layers in slicer software. The STL file is uploaded to slicer software to set the required design inputs, such as infill pattern and ratio, material assignment, and reinforcement.
Again, the slicer suggests a maximum infill ratio of 55 % for better dimensional accuracy and better bonding of infill and reinforcement. Triangular infill pattern is used to be consistent with the tensile part. Obeying the slicer's suggestion, two roof and top layers are assigned to ensure bonding to build the plate without any distortion. As used in tensile specimens, the number of shell walls from White Nylon material is selected as two, having a thickness of 0.8 mm to bond the outer White Nylon shell to the reinforcement.

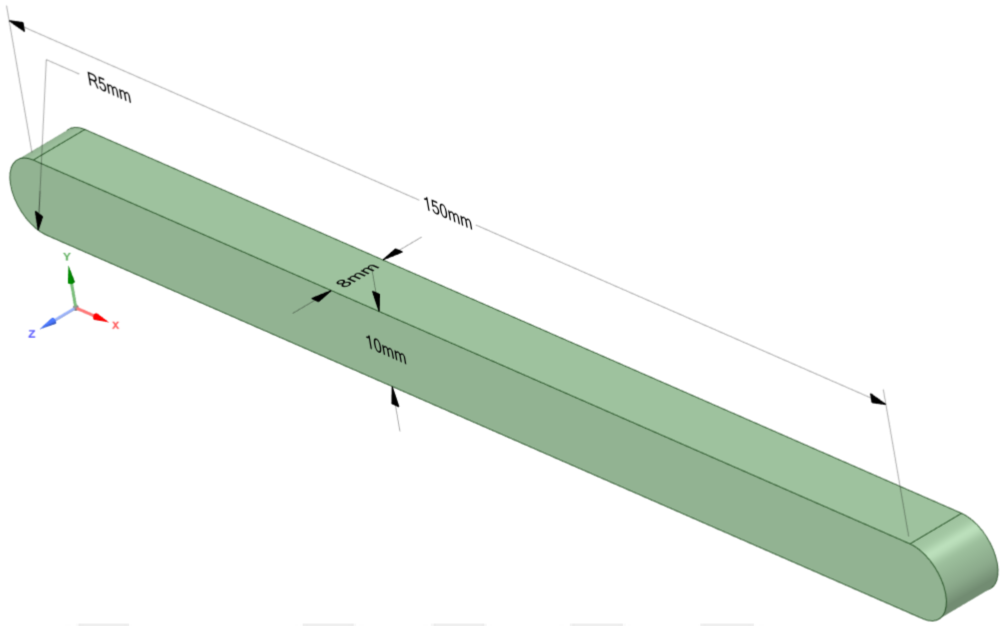

Figure 4.7: Dimensions of 3 point bending specimen

In short, after the slicing is done, the specimen is ready to print with a total of 64 layers, each with a thickness of 0.125 mm, and 60 of them (layers between 3-62) are reinforced with concentric Carbon Fiber rings while first and last two layers are roof and top layers. Two cross-sectional views of the specimen, one is for the roof and top, and the other is for reinforcement, given in Figure 4.8.

For the selected printing orientation given in Figure 4.9, no support structures are needed.

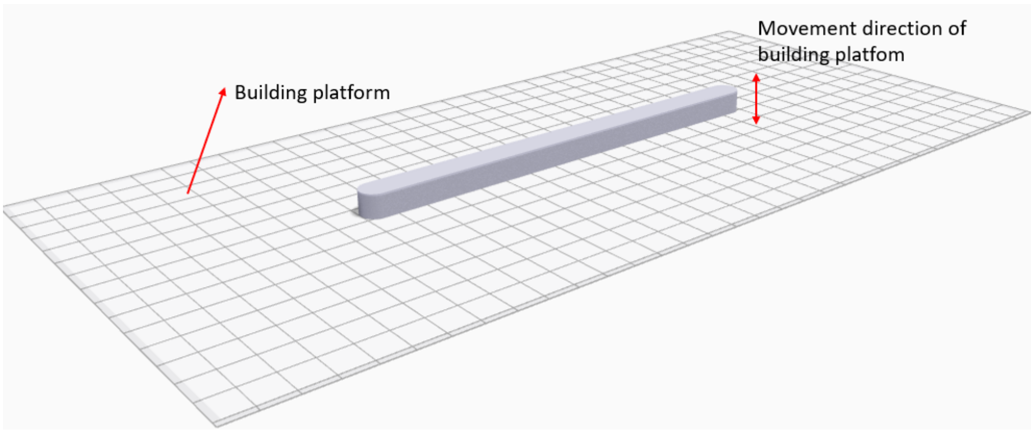

Figure 4.9: Bending specimen building direction

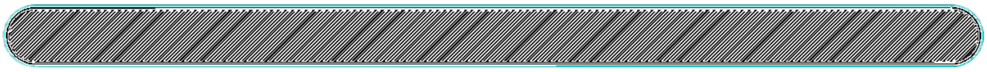

(a) Roof and top layers

(b) Reinforcement layer

Figure 4.8: Cross sectional view of bending specimen

Printing parameters for manufacturing the bending specimen are selected the same as the ones for the tensile specimen, as given in Figure 4.10

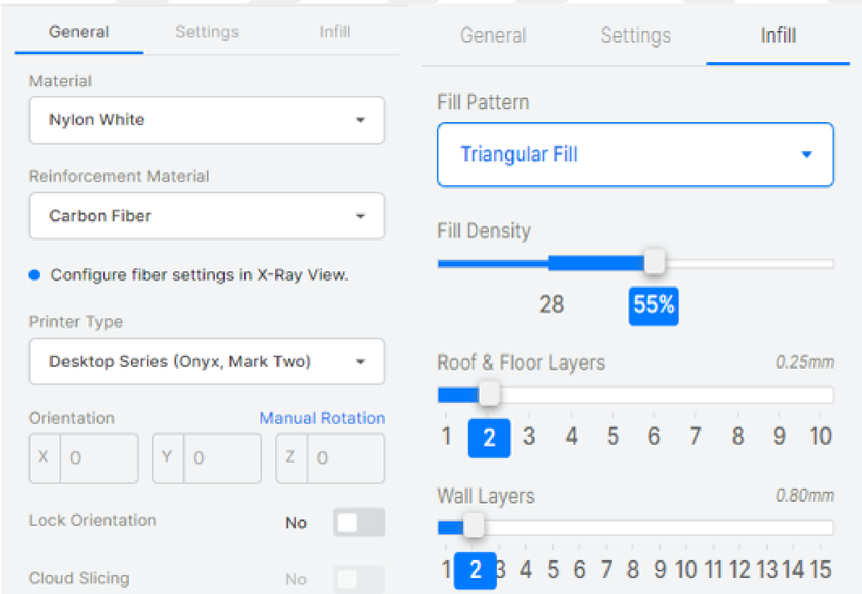

Figure 4.10: Bending specimen printing parameters

According to the slicer, the total time of printing a specimen is 1 hour and 54 minutes, which exactly matches the actual production time, excluding the heating and cooling time of nozzles. A specimen contains 2.68 cm^3 of Carbon Fiber, and White Nylon has a volume of 6.61 cm^3 where the overall mass of a specimen is 10.18 grams. The cost of material to produce a single specimen is 9.43 USD, according to Markforged [25]. Three specimens with the same dimensions, interior geometry, and printing parameters are manufactured to be tested.

4.4 Design and Fabrication of Eccentric Specimen

An eccentric specimen is designed to prove the model works accurately under combination of different loading types, such as normal and bending loads. To load the specimen eccentrically while keeping the design, manufacturing, cost, and production efforts minimal, a two-force member given in the book of Beer et al. [49] is designed. Load conditions and free body diagram of the member are shown in Figure 4.11.

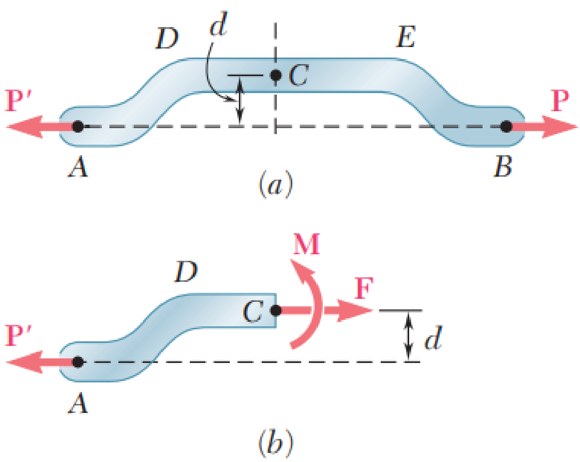

Figure 4.11: Eccentric specimen geometry (a) and free body diagram (b) [49]

Dimensions of the specimen are chosen so that two reinforcement rings will fit. All dimensions are tailored to minimize material consumption and printing time. In Figure 4.12, dimensions of the specimen are provided.

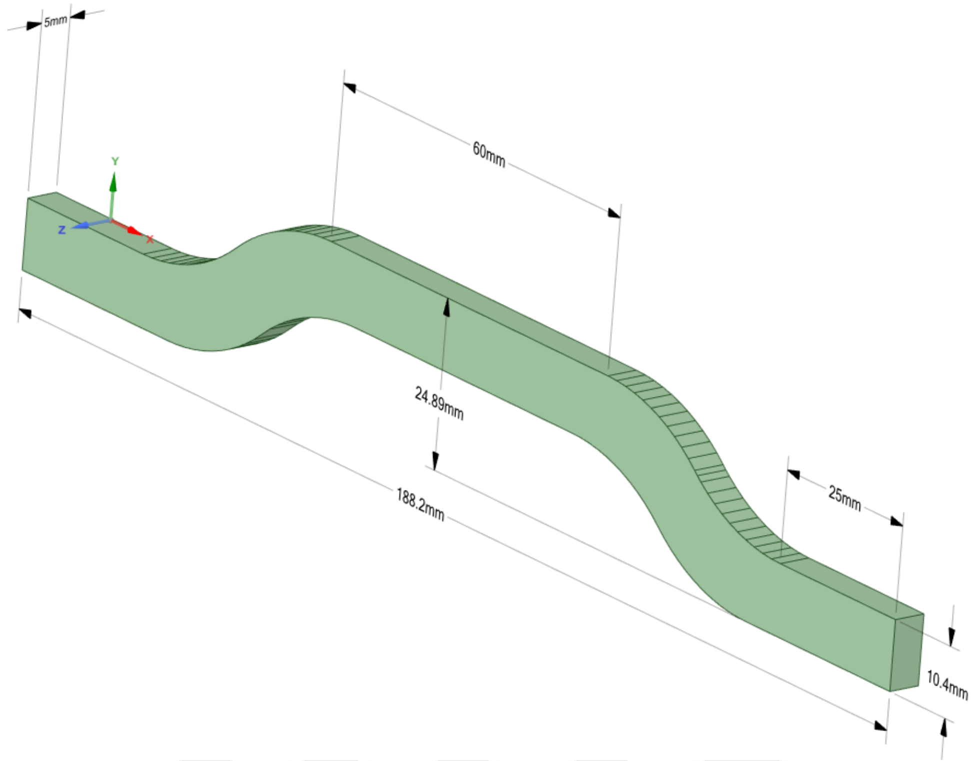

Figure 4.12: Dimensions of eccentric specimen

After the design is ready, the same manufacturing procedure for tensile and bending specimen's is followed. First, an STL file is created in SpaceClaim in order to slice the parts into layers in slicer software. The STL file is uploaded to slicer software to arrange the required design inputs, such as infill pattern and ratio, material assignment, and reinforcement.

In the interior design stage, slicing software suggests a maximum infill ratio of 55 % to obtain dimensional accuracy and better bonding of infill and reinforcement. Triangular infill pattern is selected to be consistent with tensile and bending specimens. A number of roof and top layers are selected as five to guarantee bonding the part to build the plate without any distortion. A number of shell walls are chosen as two with 0.8 mm thickness, just like the tensile and bending specimens, to bond the outer White Nylon shell to the reinforcement.

In brief, the part is sliced into 40 layers, each one having a thickness of 0.125 mm. 36 of the layers (layers between 3-38) are reinforced concentrically with carbon fiber rings, and the rest (first and last two layers) are roof and top layers. Hence, they are made of White Nylon only. Cross-sectional views of the eccentric specimen, one for roof and top and the other for reinforcement, are given in Figure 4.13.

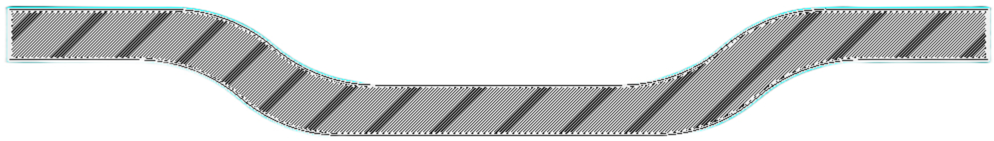

(a) Roof and top layers

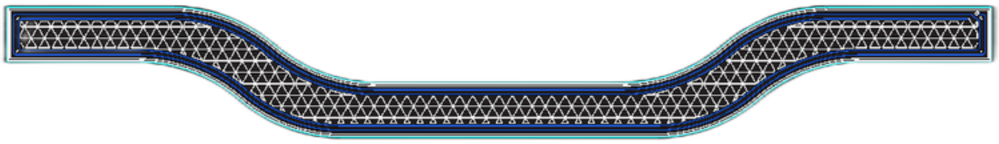

(b) Reinforcement layer

Figure 4.13: Cross sectional view of eccentric specimen

Printing orientation is selected in order not to need any support structures, as given in Figure 4.14

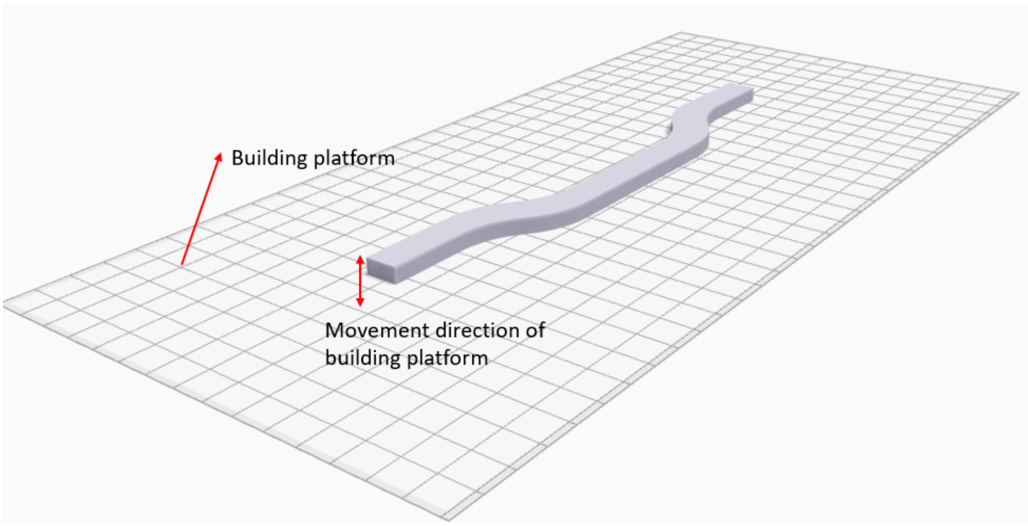

Figure 4.14: Eccentric specimen building direction

The same printing parameters used for tensile and bending specimens are selected, as provided in Figure 4.15

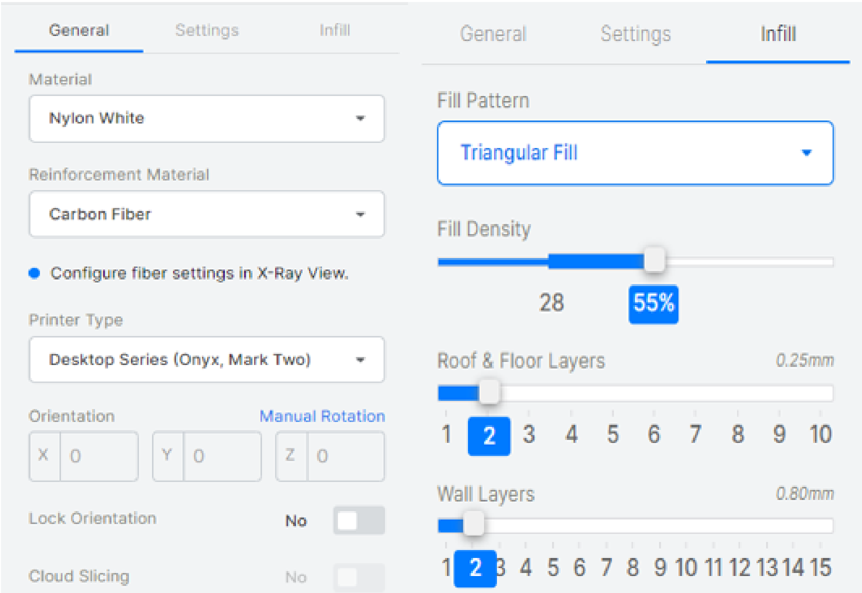

Figure 4.15: Eccentric specimen printing parameters

According to the slicer, the total time of printing a specimen is 1 hour and 1 minute, which exactly matches the actual production time, excluding the heating and cooling time of nozzles. A specimen contains 0.95 cm^3 of Carbon Fiber, and White Nylon has a volume of 4.22 cm^3 where the overall mass of a specimen is 5.44 grams. The cost of material to produce a single specimen is 3.75 USD, according to Markforged [25]. Three specimens with the same dimensions, interior geometry, and printing parameters are manufactured to be tested.

4.5 Closure

In this Chapter, the design and manufacturing of three specimens are explained. The design consideration for specimens is the reduction of material consumption, manufacturing time, and cost. All specimens are made of White Nylon matrix and Carbon Fiber as reinforcement material, and the dimensions for the specimens are arranged to have two concentric carbon fiber reinforcement rings.

CHAPTER 5

NUMERICAL MODELLING APPROACH FOR CONTINUOUS FILAMENT FABRICATED PARTS

In this Chapter, Finite Element modeling of CFF parts will be discussed. First, the numerical modeling technique will be explained in detail, and then the FEA of three different loading cases, namely tensile, bending, and eccentric, will be discussed.

As discussed in Chapter 2, no well-accepted techniques exist to model CFF parts. There are discrepancies between tests and simulation results, and the techniques are part-specific. In order to find a solution to this situation, a new FEA methodology is developed.
In general, an FE analysis includes seven main steps to obtain a numerical model from a geometry file. These steps:

- Importing geometry file to analysis environment
- Creating the material card
- Assigning material to geometry
- Creating contacts, joints, etc. between parts
- Meshing parts to discretize geometry
- Creating boundary conditions, assigning loads
- Solution and post-processing

For the CFF parts, an STL file is created in CAD software, which will later be used in the slicer to print the part. This file only includes vertexes of the outer shell of the part; it does not include any information about the infill or interior of the part. Hence, one should create an infill structure after importing the STL file into the analysis software. In order to reflect the printed geometry to the numerical model, manually modeled infill structures in analysis software should be as same as possible as the infill generated by the slicer. For this purpose, one can measure the infill lengths in an actual structure or from the preview of the slicer. The former is preferred in this work. Since all the specimens are made of equilateral triangles, the measurement of one triangle's dimensions is enough. After deciding the dimension of one side of a triangle, a pattern is created as shown in Figure 5.1.

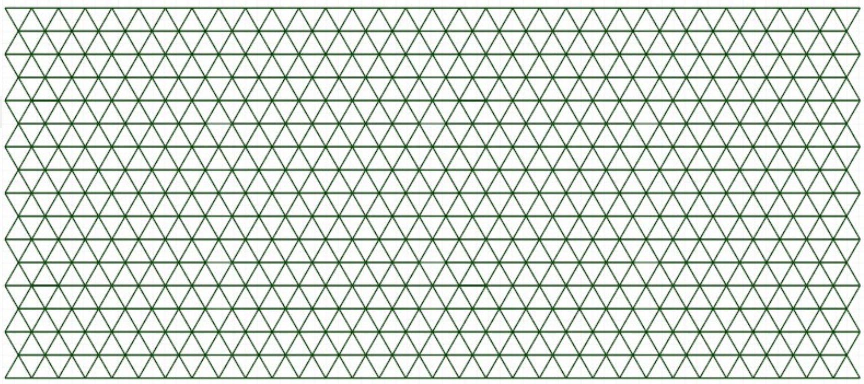

Figure 5.1: Infill geometry generation

Then, the outer boundaries of the part and generated infill intersect, and the infill staying at the outer boundary of the part is deleted. Figure 5.2 provides a representative infill generation for a rectangular specimen.

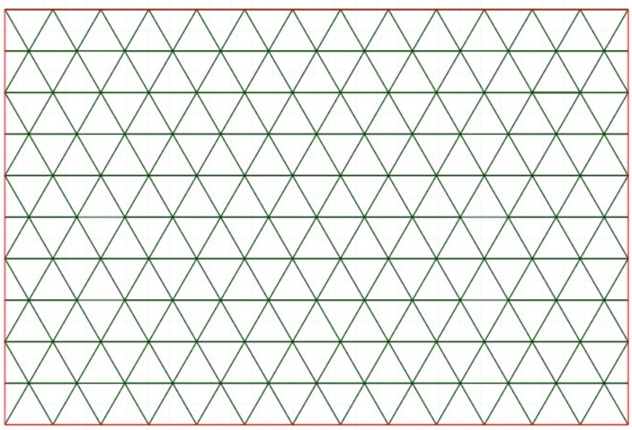

Figure 5.2: Infill geometry generation for a representative geometry

Creation of 2D sketch finishes these steps explained in Figure 5.1 and 5.2. Then, surface bodies are generated by pulling these curves. The creation of surface bodies from 2D sketches is shown in Figure 5.3. After this operation, all the infill elements and the outer shell become distinct surface bodies.

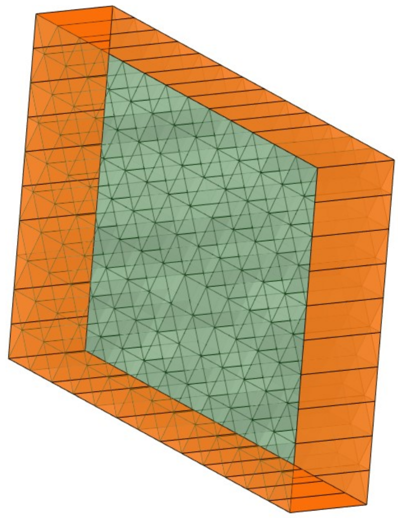

Figure 5.3: Surface body generation for a representative geometry

In FEA, a relation should be given between bodies in contact to constrain their movement. Joints, beams, and contacts generally provide these relations. Joints and beams are used to simulate the mechanical linking via machine elements such as fasteners, screws, or bolts. Contacts are used to constrain the bodies that touch each other. In this work, neither contacts nor joints or beams are used to define the relation between bodies since these types of connections link bodies more rigid than they actually are. Instead, Ansys Spaceclaim has an option called shared topology. This option creates a conformal mesh at the interface between bodies and constrains the displacement of bodies in contact so that they have the same displacements. Bodies in contact share nodes at the interface, and the displacement of the nodes is the same for all the bodies touching each other. This connection provides less rigidity to the model than bonded contacts or joints, since, in bonded contacts, bodies are connected at all nodes within a specific tolerance, while shared topology connects bodies through common nodes only. In Figure 5.4, the result of the shared topology option is provided. The red lines show the shared nodes common for four surfaces, and those surfaces are constrained to have the same displacements.

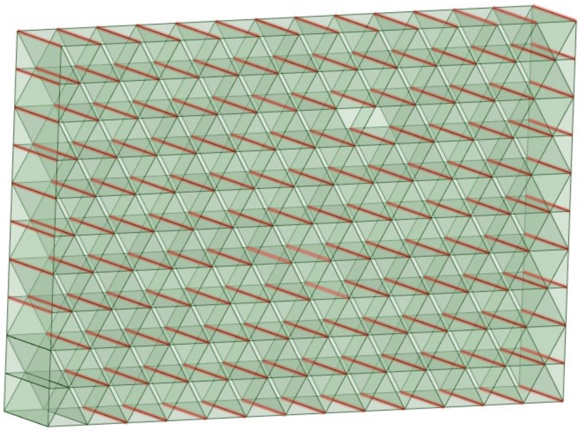

Figure 5.4: Shared topology illustration for a representative geometry

At this step, the geometry creation and constraining of the bodies are done. Now, one should assign the required material properties to bodies. One can create its own specific material with desired mechanical properties or use the pre-defined materials in Ansys's material library. Then, the material assignment is done using the Ansys Mechanical interface. In Figure 5.5, the creation of new material cards is represented.

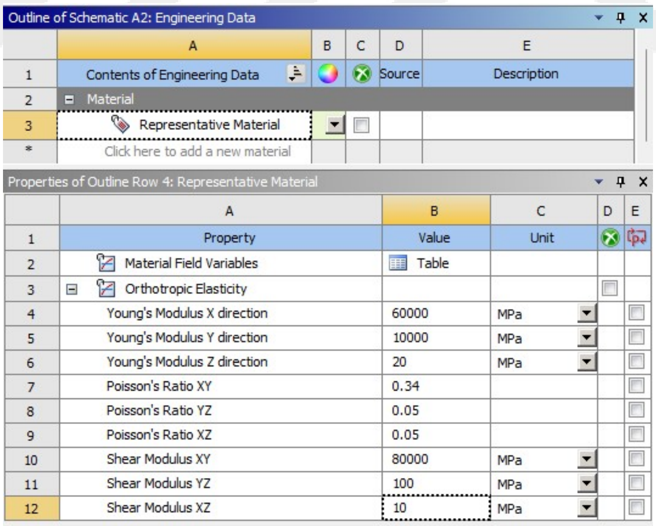

Outline of Schematic A2: Engineering Data

	A	B	C	D	E
1	Contents of Engineering Data			Source	Description
2	Material				
3	Representative Material				
*	Click here to add a new material				

Properties of Outline Row 4: Representative Material

	A	B	C	D	E
1	Property	Value	Unit		
2	Material Field Variables	Table			
3	Orthotropic Elasticity				
4	Young's Modulus X direction	60000	MPa		
5	Young's Modulus Y direction	10000	MPa		
6	Young's Modulus Z direction	20	MPa		
7	Poisson's Ratio XY	0.34			
8	Poisson's Ratio YZ	0.05			
9	Poisson's Ratio XZ	0.05			
10	Shear Modulus XY	80000	MPa		
11	Shear Modulus YZ	100	MPa		
12	Shear Modulus XZ	10	MPa		

Figure 5.5: Creating a material card in Ansys Mechanical

As shown in Figure 5.5, material properties of three directions are taken as inputs for numerical analysis. One can perform material characterization tests to obtain out-of-plane material properties if a 3D stress state is under investigation. However, the

scope of this thesis is to model 2D load cases; hence, only in-plane material properties are obtained via tests, as discussed in Chapter 3. Out-of-plane material properties are not of interest, and dummy properties are assigned to them.
While assigning the materials to the parts, one should be careful about the coordinate system. The software, Ansys Mechanical, assigns material directions according to a global coordinate system, which is defined by the software. In other words, E_1 is assigned as E_x, where the x direction corresponds to the global coordinate system's x direction. If the material directions described in Figure 3.1 are not compatible with the default global coordinate system, one should create a new coordinate system for assigning correct material directions or rotate the geometry accordingly.

Although the software requires material properties in three material directions, since FE analysis will be run with surface elements in the horizontal plane, 2D material properties are needed and sufficient, i.e., the definition of material properties in out-of-plane direction will not required for 2D analysis. The directions specified in material creation are the directions of the global coordinate system of Ansys Mechanical. One can assign a different coordinate system to arrange the material directions if needed.

In Ansys Mechanical, one should assign the thickness of the surface bodies. For the AM parts, the thickness of the surface body should be the same as the nozzle diameter. After the surface thickness is assigned, proper materials should be assigned to all bodies. The geometric model, which includes material assignment and surface thickness, is ready at this point. The next step is meshing, which is discretization of the geometry into finite elements, in order to describe the body with matrices. Generally, a mesh dependency study is conducted for the real parts to select the correct size for the mesh elements in order to make the results independent of the mesh size. Mesh dependency work is not done for the representative geometry, but it is done for three specimens that will be mentioned later in this chapter. After meshing the part, one can visually understand the shared topology type of connection between bodies by checking the shared nodes between bodies. In Figure 5.6, four shared nodes between bodies are shown with green indicators. Shared topology provides a "softer" connection between bodies than the contacts. While contact elements have infinite stiffness and rigidly connect the bodies with many nodes, shared elements do not provide that unrealistic rigidity; they constrain the relative motion between parts with shared nodes. Moreover, contacts should be defined for all the bodies that touch each other, one by one; however, shared topology does not require any extra effort.

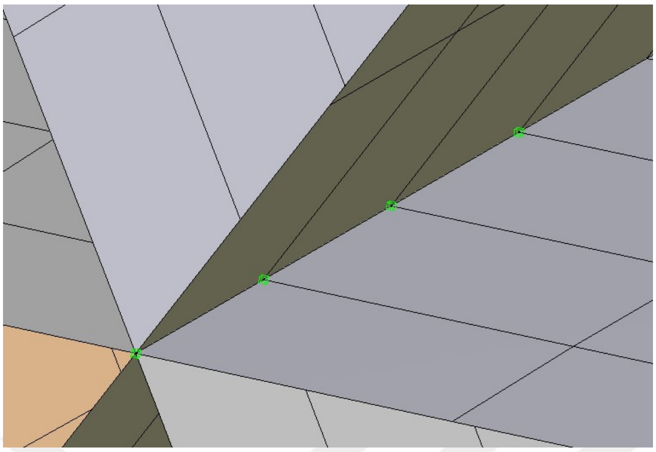

Figure 5.6: Illustration of shared nodes

The next step is to define loads and boundary conditions. Loads and boundary conditions should reflect the actual case. For this representation, fixed support is defined as the boundary condition, and 5 N of lateral load is defined, as shown in Figure 5.7.

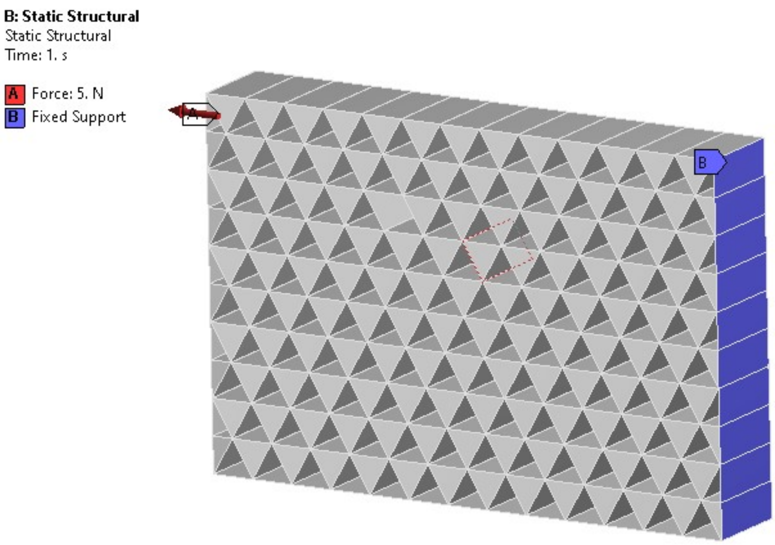

Figure 5.7: Boundary condition and loading of representative model

At the final step, one should post-process the solution and obtain the required outputs such as deformations, stresses, strains, etc. The deformation results for this example are given in Figure 5.8.

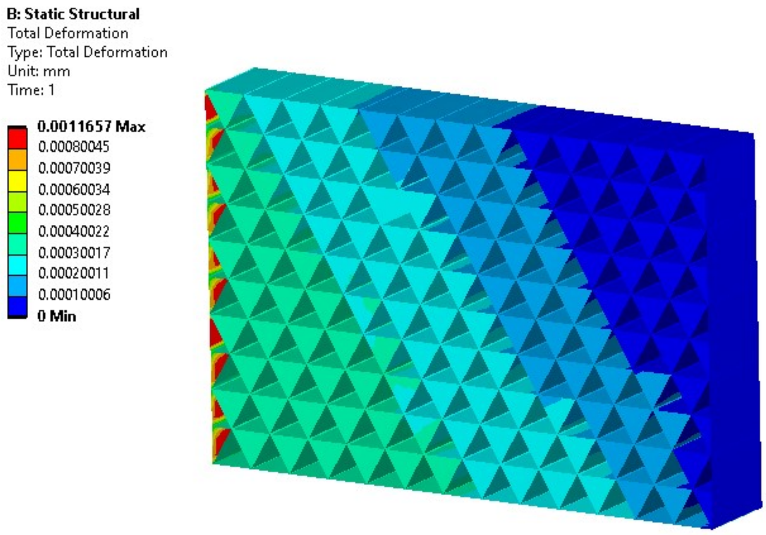

Figure 5.8: Displacement result of representative model

5.1 Numerical Modelling of Tensile Test Specimen

This section will discuss numerical modeling details such as geometry creation, meshing, mesh dependency study, boundary conditions, and numerical analysis results for tensile specimens.

At the beginning of this chapter, the road map for FEA of CFF parts is mentioned. The same methodology is followed for the numerical modeling of tensile specimens. The first step is creating surface bodies and infill geometry. For this purpose, the STL file used in the manufacturing is imported into Spaceclaim software. Since STL files split bodies into triangles, first triangles are converted into a solid body, and the specimen's silhouette is obtained to create surface bodies and fill them with triangular infill later. as given in Figure 5.9.

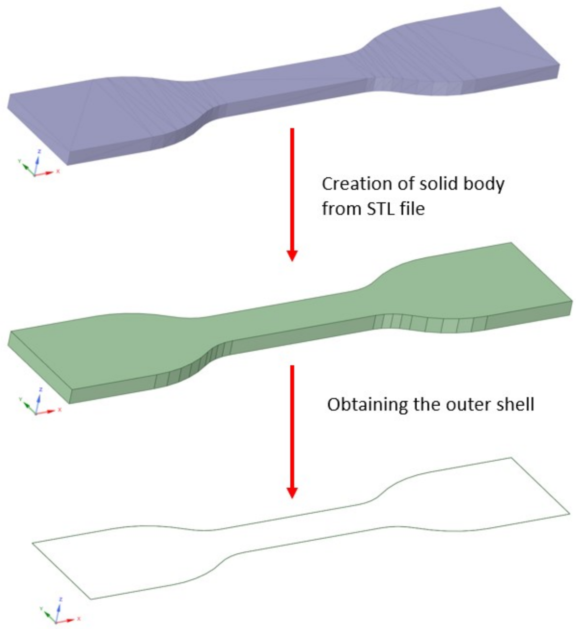

Figure 5.9: Obtaining silhouette of the tensile specimen from STL file

Then, the infill structure consisting of equilateral triangles with a side length of 2.194 mm is created. In Figure 5.10, infill provided by the slicer and created infill for FEA simulations are given.

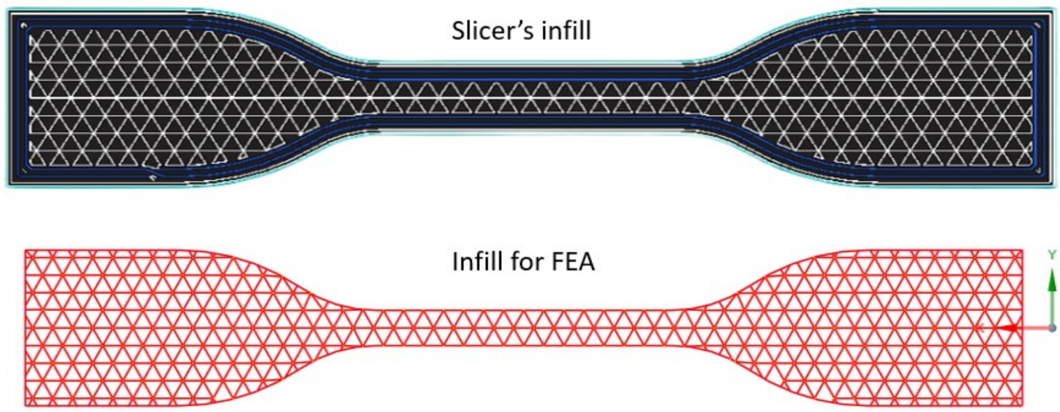

Figure 5.10: Comparison of infill provided by slicer and created for FEA simulations

After the geometry is prepared for the numerical analysis, White Nylon and Carbon Fiber material cards are created, with the material properties given in Table 5.1. As decided before, Carbon Fiber is modeled as an orthotropic material. All the infill bodies' material is assigned as White Nylon, and the material for the outer shell is selected as Carbon Fiber to reflect the concentric reinforcement.

Table 5.1: Summary of Material Properties Used in FEA

Material	**Property**	**Value**
White Nylon	$E_{\text{White Nylon}}$	$960\,\text{MPa}$
	$\nu_{\text{White Nylon}}$	0.41
Continuous Carbon Fiber	E_1	$49.1\,\text{GPa}$
	E_2	$2.17\,\text{GPa}$
	G_{12}	$1.36\,\text{GPa}$
	ν_{12}	0.34

The next step is meshing the part. For the meshing of the part, as mentioned before shell elements are used. The shape of the elements are set as "Program Controlled" since the mesher automatically meshes the part to obtain the best element quality. In order to capture curvatures triangular and quadrilateral elements are preferred. Moreover, to obtain better results, second order (quadratic) type of elements are utilized instead of first order (linear) elements. In Figure 5.11, (a) and (b) represents triangular elements, while (c) and (d) are quadrilateral ones. As seen, (b) and (d) have nodes in the middle of the edges, which makes these elements second order, while (a) and (c) do not have any middle nodes. ANSYS Mechanical meshes the part to obtain the best element quality, while keeping mesh connections (node merging). Hence, mostly, the parts consist of quadrilateral elements, however, for node merge purposes, rarely triangular elements are used. In general, for all three load cases, infill structures are made of quadrilateral elements. Moreover, outer shell is meshed with quadrilateral elements, however, in order to satisfy the node merge requirements, the shape of the elements of outer shells are worse than infill structures. Because, the edges of the infills are imprinted on the outer surface by software, in order to specify the infill pattern. After, these edges are meshed with the common nodes of the infill edges. And these elements are shown as randomness in the geometry.

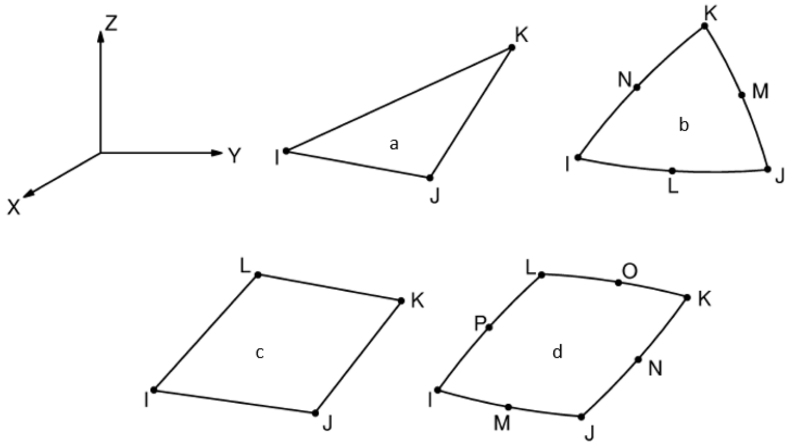

Figure 5.11: Types of elements used in FEA

Ansys Mechanical suggests an element size of 0.5 mm for this geometry to capture the part's geometric details. Figure 5.12 shows the created mesh with the default element size 0.5 mm.

Figure 5.12: 0.5 mm mesh of tensile specimen

Later, a mesh dependency study is conducted, and results are shared. Since the numerical analysis aims to simulate the tensile test, boundary conditions and loading are applied in the same way as defined in the tests. The universal testing machine takes displacement input and measures the reaction forces; hence, in the numerical analysis, the load is defined as displacement at one tip of the specimen gripped into the testing machine, and the other tip is fixed. Figure 5.13 shows boundary conditions and loading.

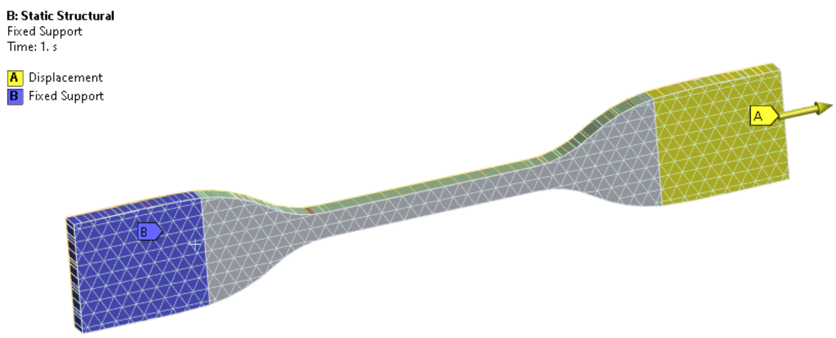

Figure 5.13: Boundary condition and loading for tensile specimen

As mentioned before, the testing machine measures the axial load at the gripped end with the load cell. Hence, the reaction force at the fixed end is taken as the analysis output to compare with test results. Since no non-linearities are defined in the linear numeric model, such as material non-linearity, variable loading, geometric non-linearities or contacts containing non-linearities like friction, the model works linearly, i.e., doubling displacement inputs doubles the force output. For a unit displacement of 1 mm, a reaction force of 1304 N is obtained from numerical analysis. The deformed shape of the tensile specimen is given in Figure 5.14, and the reaction force vs axial displacement output of the numeric model is given in Figure 5.16.

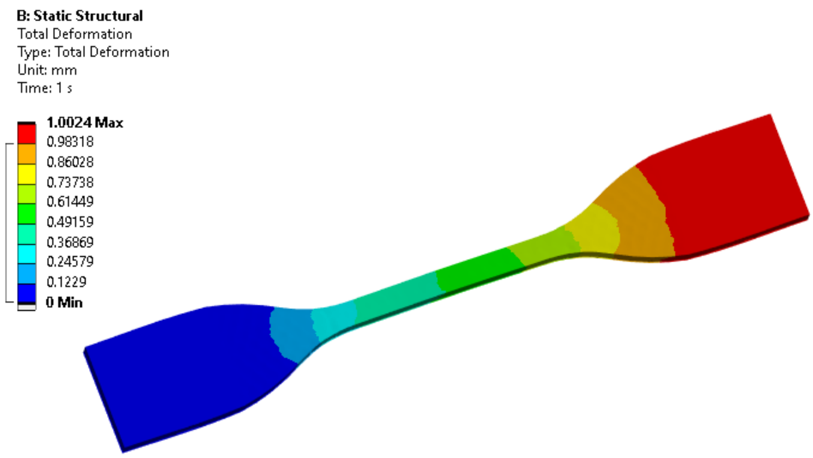

Figure 5.14: Deformation of tensile specimen under 1 mm axial loading

Equivalent von Mises stress distrubition of the tensile specimen is provided in Figure 5.15. In CFF composites, there is currently no accepted stress criterion defined in the literature. Instead, researchers commonly rely on equivalent von Mises stress results to illustrate the load distribution and identify regions where high stresses occur. This approach provides insights into the stress patterns and potential failure points within the composite material, offering a practical means of evaluating its performance under various loading conditions.

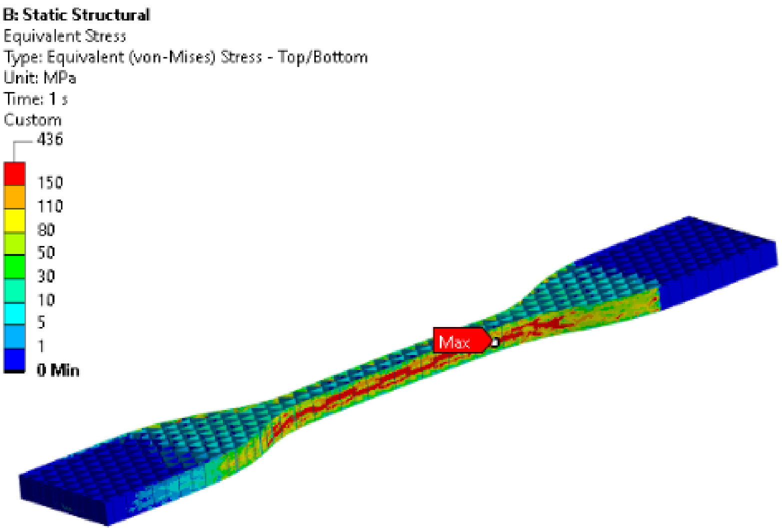

Figure 5.15: von Mises stress of tensile specimen

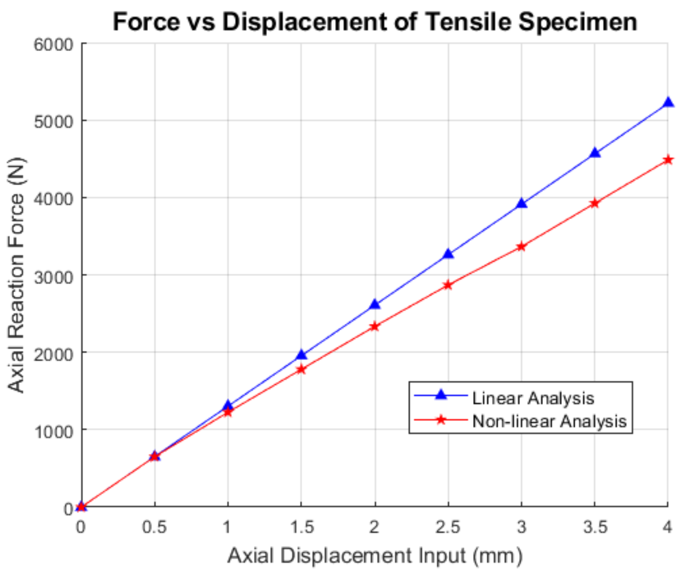

Figure 5.16: Results of numerical analysis of tensile specimen

After the result with the default element size is obtained, a mesh dependency study is conducted. The change in reaction force vs mesh size graph is given in Figure 5.17, and the summary of the mesh dependency study is given in Table 5.2

In order to refine the FEA model of tensile test, non-linear model is prepared. In this model, both material (non-linear stress-strain curve) and geometric (large deformations) non-linearities are included. Including non-linearities into FEA analysis make the problem more complex, however results show better correlation with tests, as mentioned in Chapter 6.

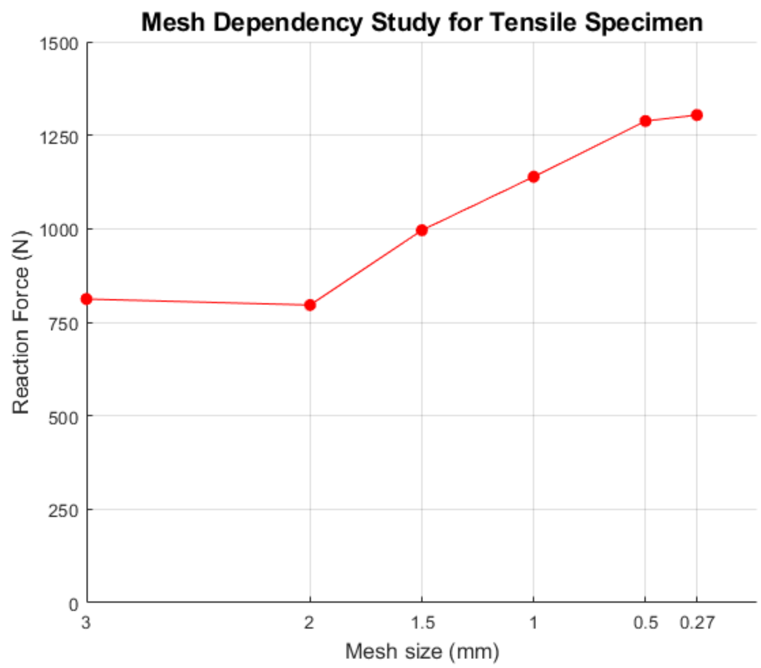

Figure 5.17: Mesh dependency study for tensile specimen

Table 5.2: Summary of Mesh Dependency Study for Tensile Specimen

Element Size (mm)	Number of Elements	Reaction Force (N)	Solution Time
3.0	2981	812	1m28s
2.0	4283	796	1m27s
1.5	8140	996	1m36s
1.0	12004	1139	1m37s
0.5	46716	1288	1m48s
0.27	160656	1304	2m19s

5.2 Numerical Modelling of Bending Test Specimen

This section explains the numerical modeling details, such as geometry creation, meshing, mesh dependency study, boundary conditions, and numerical analysis results for bending specimens.
At the beginning of this chapter, the road map for FEA of CFF parts is mentioned. The same methodology is followed for the numerical modeling of bending specimens. The first step is creating surface bodies and infill geometry. For this purpose, the STL file used in the manufacturing is imported into Spaceclaim software. Since STL files split bodies into triangles, first triangles are converted into a solid body, and the specimen's silhouette is obtained to create surface bodies and fill them with triangular infill later. as given in Figure 5.18.

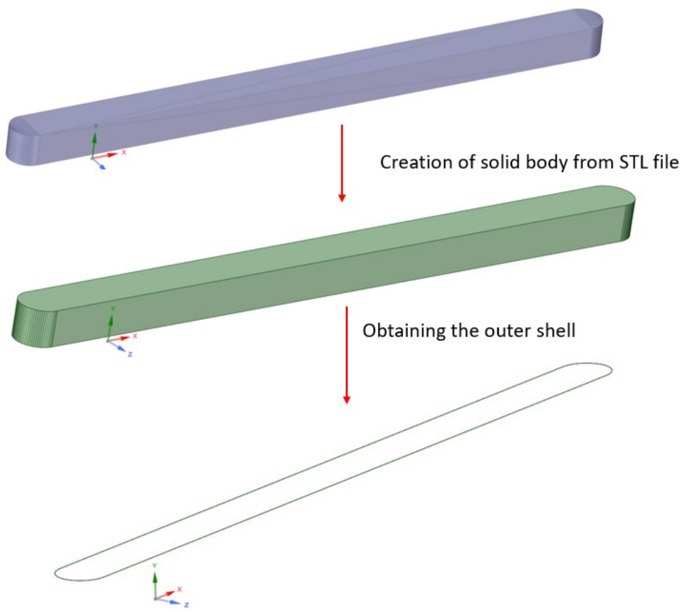

Figure 5.18: Obtaining silhouette of the bending specimen from STL file

Then, the infill structure consisting of equilateral triangles with a side length of 2.771 mm is created. In Figure 5.19, infill provided by the slicer and created infill for FEA simulations are given.

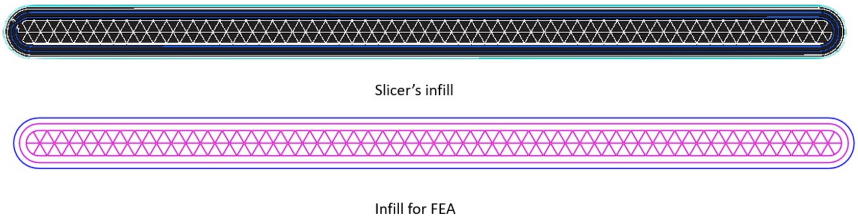

Figure 5.19: Comparison of infill provided by slicer and created for FEA simulations

In addition to the bending specimen, the three-point bending test includes three rigid supports. Hence, three rigid supports with 10 mm of diameter are modeled from solid cylinders and placed on geometry as shown in Figure 5.20.

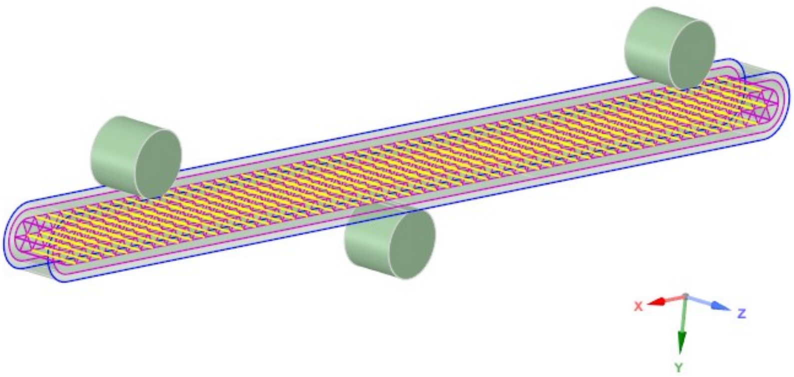

Figure 5.20: Three-point bending test configuration

After the simulation geometry is prepared for the numerical analysis, the same material cards for White Nylon and Carbon Fiber are assigned. The outer shell of the specimen (concentric reinforcement) is modeled from Carbon Fiber material, the infill structure's material is assigned as White Nylon, and for the rigid cylinders, structural steel material is chosen.

The following step is meshing the part. For the meshing of the part, as mentioned before shell elements are used. The shape of the elements are set as "Program Controlled" since the mesher automatically meshes the part to obtain the best element quality. In order to capture curvatures triangular and quadrilateral elements are preferred. Moreover, to obtain better results, second order (quadratic) type of elements are utilized instead of first order (linear) elements. In Figure 5.11, (a) and (b) represents triangular elements, while (c) and (d) are quadrilateral ones. As seen, (b) and (d) have nodes in the middle of the edges, which makes these elements second order, while (a) and (c) do not have any middle nodes. ANSYS Mechanical meshes the part to obtain the best element quality, while keeping mesh connections (node merging). Hence, mostly, the parts consist of quadrilateral elements, however, for node merge purposes, rarely triangular elements are used. In general, for all three load cases, infill structures are made of quadrilateral elements. Moreover, outer shell is meshed with quadrilateral elements, however, in order to satisfy the node merge requirements, the shape of the elements of outer shells are worse than infill structures. Because, the edges of the infills are imprinted on the outer surface by software, in order to specify the infill pattern. After, these edges are meshed with the common nodes of the infill edges. And these elements are shown as randomness in the geometry. Ansys Mechanical suggests an element size of 0.5 mm for this geometry to capture the part's geometric details. Figure 5.21 shows the created mesh with the default element size 0.5 mm.

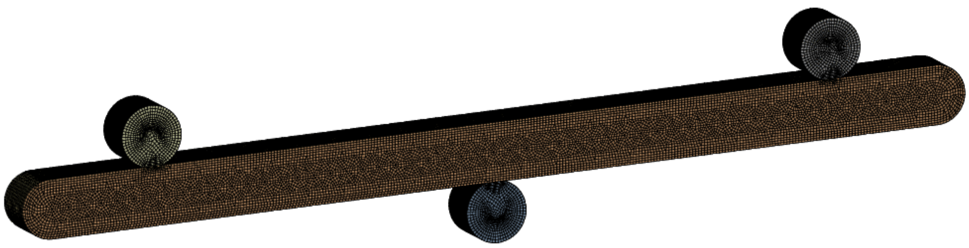

Figure 5.21: 0.5 mm mesh of bending specimen

In order to reflect the actual test conditions in simulation, contacts between rigid supports and the bending specimen are defined as frictionless contact in Ansys Mechanical. This type of contact allows the slipping of the defined faces relative to each other, with zero friction coefficient. Frictionless contact definition is shown in Figure 5.22.

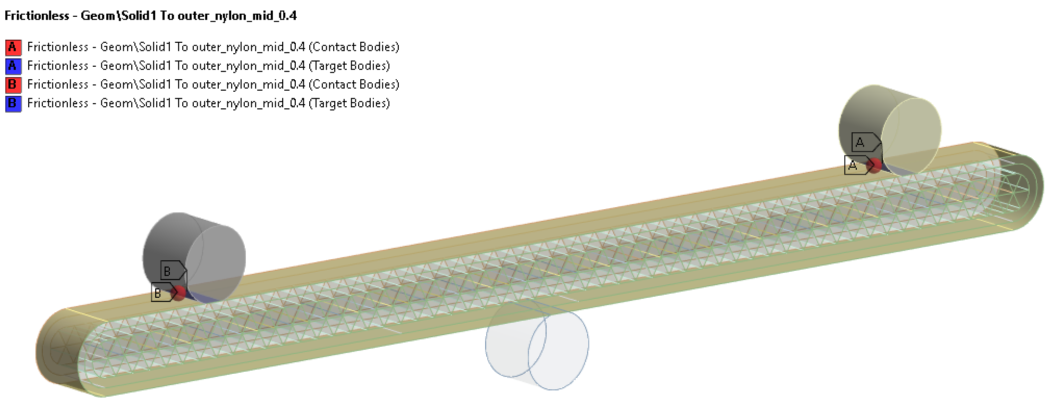

Figure 5.22: Definition of frictionless contact

To satisfy convergence conditions, 0.2 mm of face meshing is used in contact surfaces. The meshing of these surfaces is given in Figure 5.23.

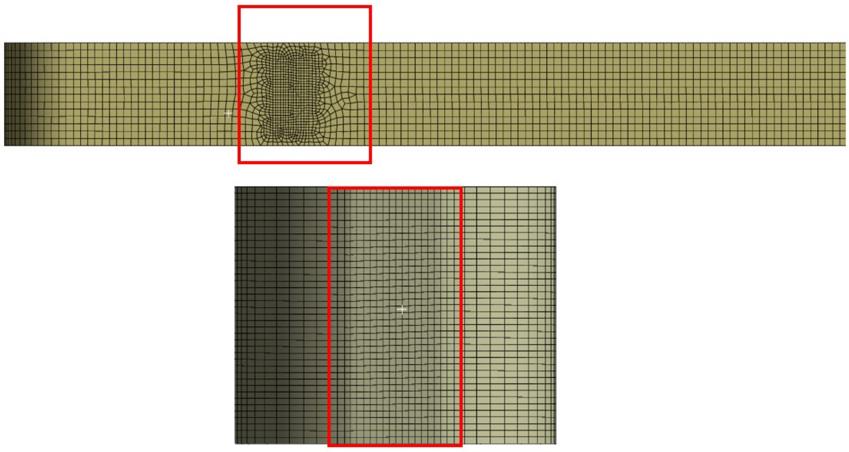

Figure 5.23: Face meshing of contact surfaces

Later, a mesh dependency study is conducted for the bending test simulation, and the results are shared. Since the numerical analysis aims to simulate the three-point bending test, boundary conditions and loading are applied similarly to those defined in the tests. The universal testing machine takes displacement input and measures the reaction forces; hence, in the numerical analysis, the load is defined as the displacement of two rigid cylinders, and the cylinder on the bottom is constrained to be fixed. Moreover, the rotation degree of freedom of the support cylinders on top of the specimen is given. Figure 5.24 shows boundary conditions and loading.

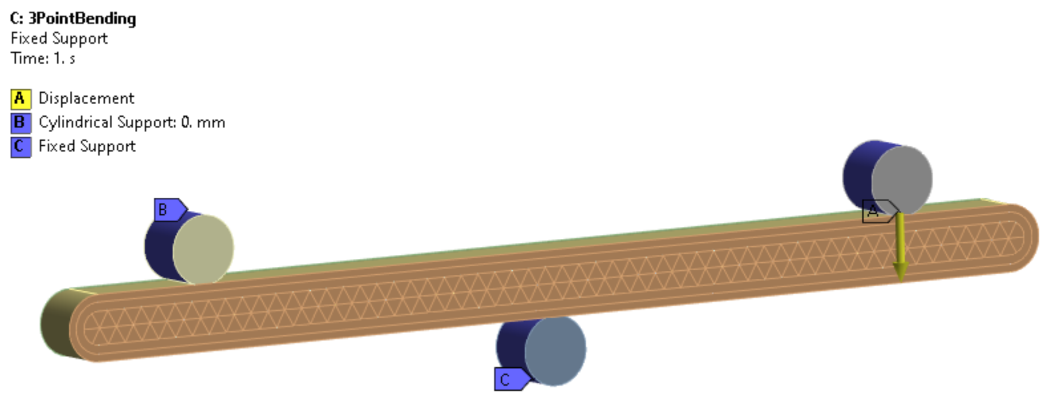

Figure 5.24: Boundary condition and loading for bending specimen

As mentioned, the testing machine measures the axial load at the gripped end with the load cell. For the three point bending test, the gripped end is considered as two rigid cylinders placed on top of the part. Hence, the reaction force at the fixed end is taken as the analysis output to compare with test results. Since no non-linearities are defined in the numeric model, such as material non-linearity, variable loading, or contacts containing non-linearities like friction, the model works linearly, i.e., doubling displacement inputs doubles the force output. For a unit displacement of 1 mm, a reaction force of 296 N is obtained from numerical analysis, solved with 0.5 mm mesh size. The deformed shape of the tensile specimen is given in Figure 5.25 and the reaction force vs axial displacement output of the numeric model is given in Figure 5.27.

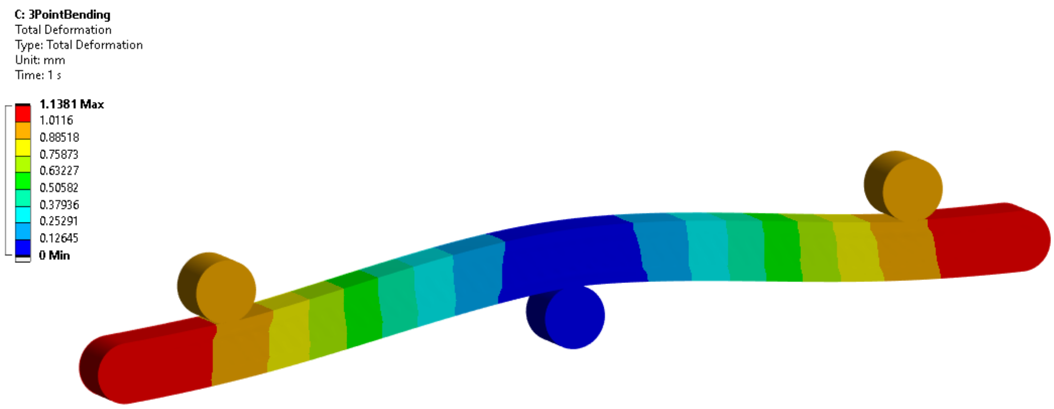

Figure 5.25: Deformation of bending specimen under 1 mm loading

Equivalent von Mises stress distribution of the bending specimen is provided in Figure 5.26. In CFF composites, there is currently no accepted stress criterion defined in the literature. Instead, researchers commonly rely on equivalent von Mises stress results to illustrate the load distribution and identify regions where high stresses occur. This approach provides insights into the stress patterns and potential failure points within the composite material, offering a practical means of evaluating its performance under various loading conditions.

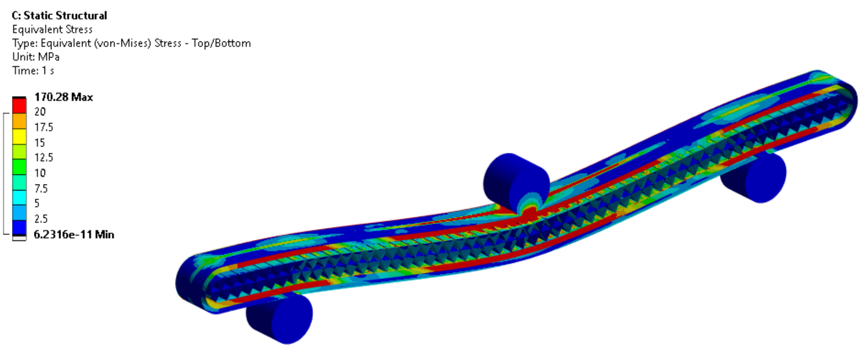

Figure 5.26: von Mises stress of bending specimen

After the result with the default element size is obtained, a mesh dependency study is conducted. The change in reaction force vs mesh size graph is given in Figure 5.28, and the summary of the mesh dependency study is given in Table 5.3

In order to refine the FEA model of bending test, non-linear model is prepared. In this model, both material (non-linear stress-strain curve) and geometric (large de-

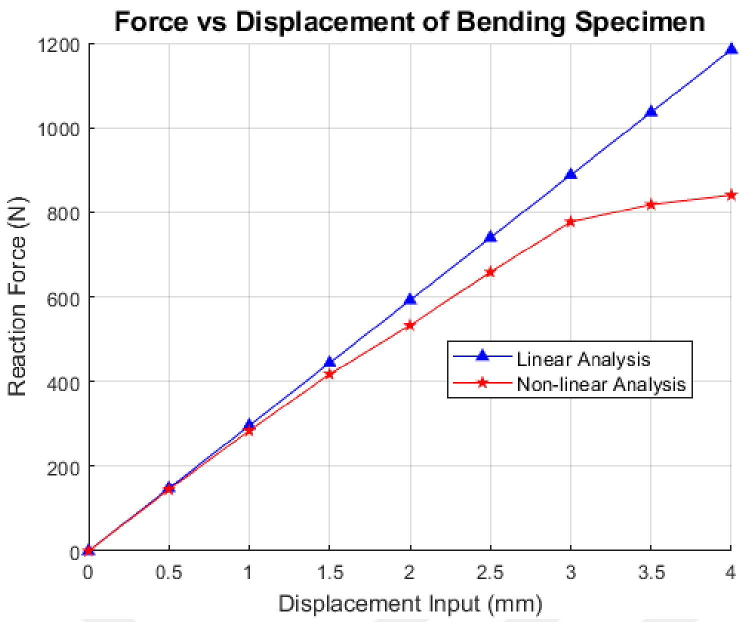

Figure 5.27: Results of numerical analysis of bending specimen

formations) non-linearities are included. Including non-linearities into FEA analysis make the problem more complex, however results show better correlation with tests, as mentioned in Chapter 6.

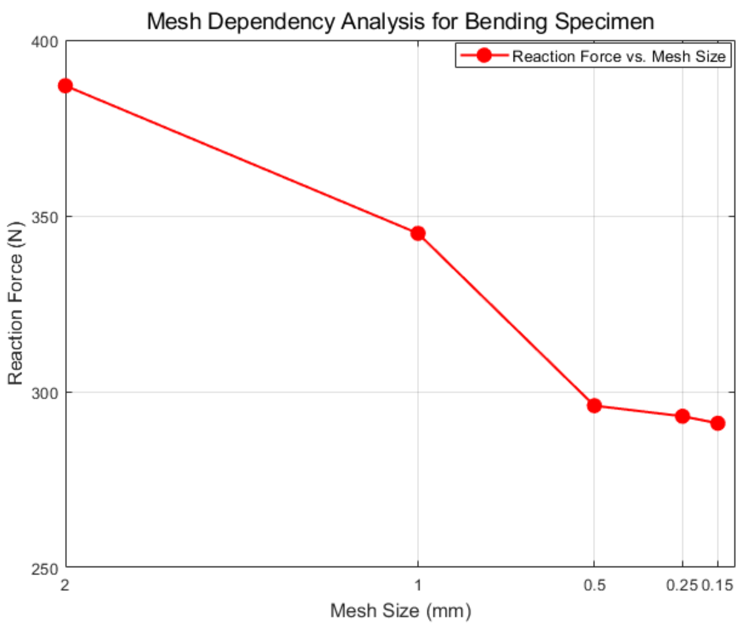

Figure 5.28: Mesh dependency study for bending specimen

In order to refine the FEA model of bending test, non-linear model is prepared. In this model, both material (non-linear stress-strain curve) and geometric (large deformations) non-linearities are included. Including non-linearities into FEA analysis makes the problem more complex, however results show better correlation with tests, as mentioned in Chapter 6.

Table 5.3: Summary of Mesh Dependency Study for Bending Specimen

Element Size (mm)	Number of Elements	Reaction Force (N)	Solution Time
2.0	33541	387	1m43s
1.0	55060	345	1m15s
0.5	160034	296	2m7s
0.25	572110	293	8m19s
0.15	1684996	291	19m13s

5.3 Numerical Modelling of Eccentric Test Specimen

This section explains the numerical modeling details, such as geometry creation, meshing, mesh dependency study, boundary conditions, and numerical analysis results for eccentric specimens.
At the beginning of this chapter, the road map for FEA of CFF parts is mentioned. The same methodology is followed for the numerical modeling of eccentric specimens. The first step is creating surface bodies and infill geometry. For this purpose, the STL file used in the manufacturing is imported into Spaceclaim software. Since STL files split bodies into triangles, first triangles are converted into a solid body, and the specimen's silhouette is obtained to create surface bodies and fill them with triangular infill later as given in Figure 5.29.

Then, the infill structure consisting of equilateral triangles with a side length of 2.6 mm is created. In Figure 5.30, infill provided by the slicer and created infill for FEA simulations are given.

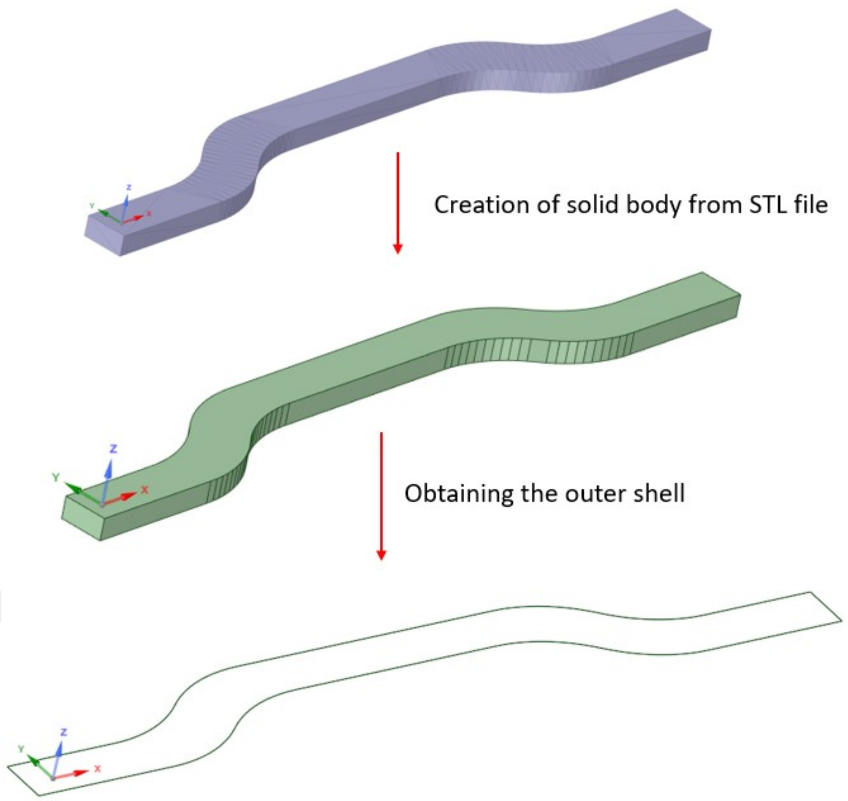

Figure 5.29: Obtaining silhouette of the eccentric specimen from STL file

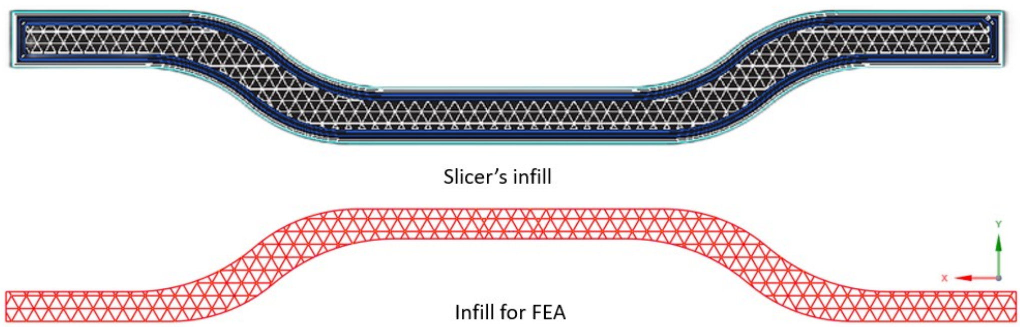

Figure 5.30: Comparison of infill provided by slicer and created for FEA simulations

After the simulation geometry is prepared for the numerical analysis, the same material cards for White Nylon and Carbon Fiber are assigned. The outer shell of the specimen (concentric reinforcement) is modeled from Carbon Fiber material, while the infill structure's material is assigned as White Nylon.

The next step is meshing the part. For the meshing of the part, as mentioned before shell elements are used. The shape of the elements are set as “Program Controlled” since the mesher automatically meshes the part to obtain the best element quality. In order to capture curvatures triangular and quadrilateral elements are preferred. Moreover, to obtain better results, second order (quadratic) type of elements are utilized instead of first order (linear) elements. In Figure 5.11, (a) and (b) represents triangular elements, while (c) and (d) are quadrilateral ones. As seen, (b) and (d) have nodes in the middle of the edges, which makes these elements second order, while (a) and (c) do not have any middle nodes. ANSYS Mechanical meshes the part to obtain the best element quality, while keeping mesh connections (node merging). Hence, mostly, the parts consist of quadrilateral elements, however, for node merge purposes, rarely triangular elements are used. In general, for all three load cases, infill structures are made of quadrilateral elements. Moreover, outer shell is meshed with quadrilateral elements, however, in order to satisfy the node merge requirements, the shape of the elements of outer shells are worse than infill structures. Because, the edges of the infills are imprinted on the outer surface by software, in order to specify the infill pattern. After, these edges are meshed with the common nodes of the infill edges. And these elements are shown as randomness in the geometry. Ansys Mechanical suggests an element size of about 0.4 mm for this geometry to capture the part’s geometric details. Figure 5.31 shows the created mesh with the default element size 0.4 mm.

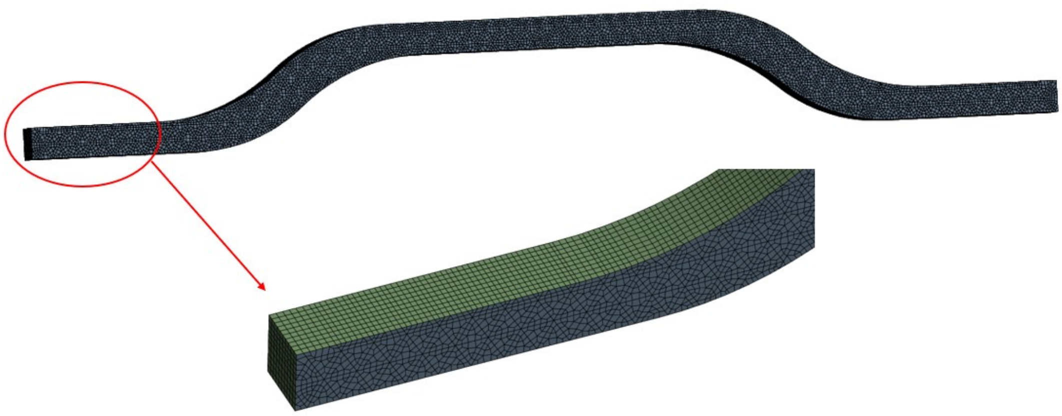

Figure 5.31: 0.4 mm mesh of eccentric specimen

Later, a mesh dependency study is conducted, and results are shared. Since the numerical analysis aims to simulate the axial loading of the eccentric specimen, boundary conditions and loading are applied in the same way as defined in the tests. The universal testing machine takes displacement input and measures the reaction forces; hence, in the numerical analysis, the load is defined as displacement at one tip of the specimen gripped into the testing machine, and the other tip is fixed. Figure 5.32 shows boundary conditions and loading.

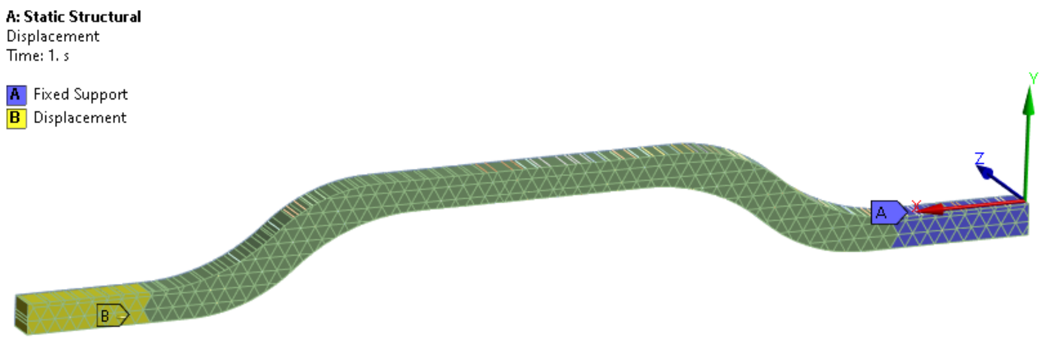

Figure 5.32: Boundary condition and loading for eccentric specimen

As mentioned before, the testing machine measures the axial load at the gripped end with the load cell. Hence, the reaction force at the fixed end is taken as the analysis output to compare with test results. Unlike the tensile test, displacement of the midsection of the eccentric is also measured with a mechanical strain gauge with a gauge length of 25 mm. This gauge is used to measure the extension derived from both tensile and bending loading in the axial direction. In FE analysis, two nodes in the middle section having a distance of 25 mm are selected, and the relative displacement of those nodes is considered and compared with the extension of the strain gauge. In Figure 5.33, nodes representing the legs of the strain gauge are shown.

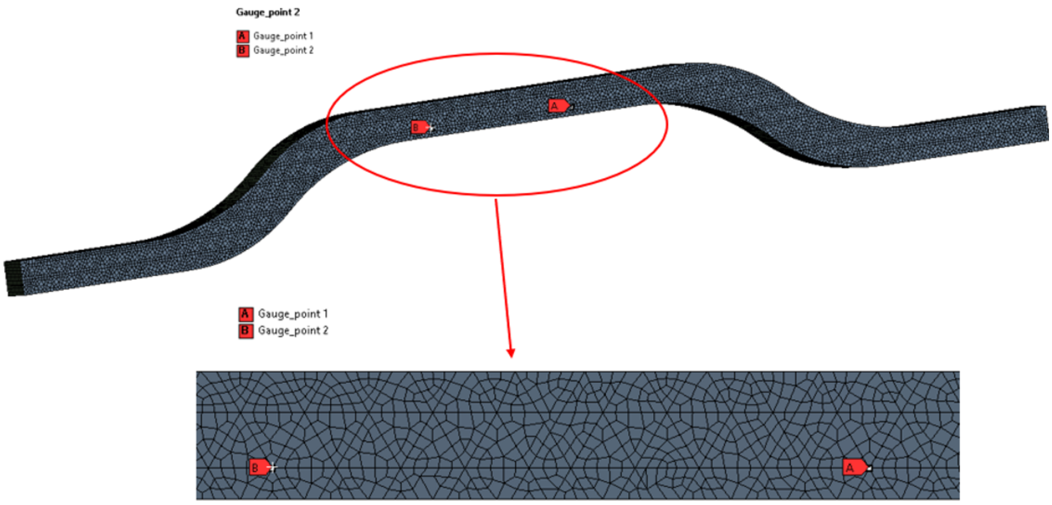

Figure 5.33: Nodes representing the legs of strain gauge

Since no non-linearities are defined in the numeric model, such as material non-linearity, variable loading, or contacts containing non-linearities like friction, the model works linearly, i.e., doubling of displacement inputs doubles the force output. A unit displacement of 1 mm at the tip results in a reaction force of 273 N, and a 0.013 mm extension between gauge nodes is obtained from numerical analysis with a 0.4 mm mesh size. The axial deformation shape of the eccentric specimen is given in Figure 5.34 since the strain gauge is only capable of measuring the extension in the axial direction, and the numerical result for reaction force vs extension between legs of the strain gauge is given in Figure 5.34.

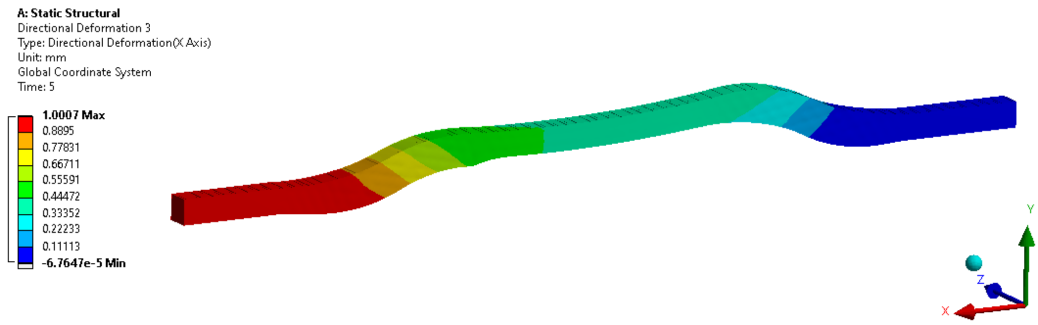

Figure 5.34: Axial deformation of eccentric specimen under 1 mm axial loading

Equivalent von Mises stress distribution of the bending specimen is provided in Figure 5.35. In CFF composites, there is currently no accepted stress criterion defined in the literature. Instead, researchers commonly rely on equivalent von Mises stress results to illustrate the load distribution and identify regions where high stresses occur. This approach provides insights into the stress patterns and potential failure points within the composite material, offering a practical means of evaluating its performance under various loading conditions.

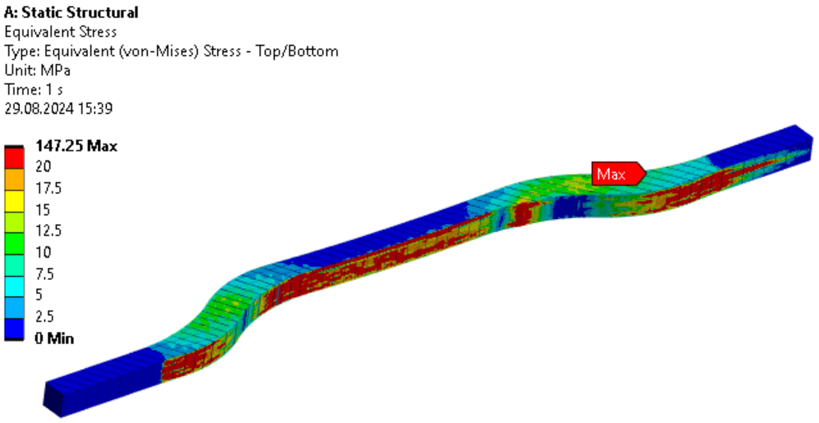

Figure 5.35: von Mises stress of eccentric specimen

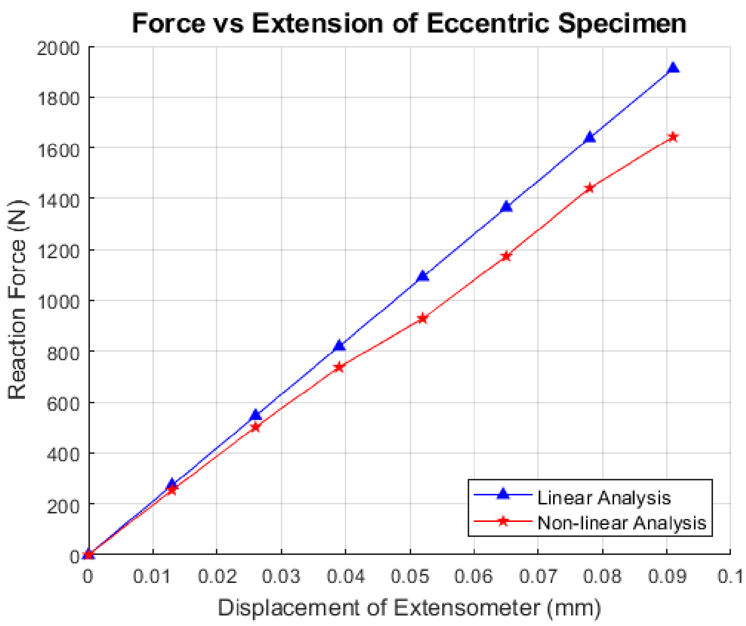

Figure 5.36: Results of numerical analysis of eccentric specimen

After the result with the default element size is obtained, a mesh dependency study is conducted. The change in reaction force vs mesh size graph is given in Figure 5.37, and the summary of the mesh dependency study is given in Table 5.4

In order to refine the FEA model of eccentric test, non-linear model is prepared. In this model, both material (non-linear stress-strain curve) and geometric (large deformations) non-linearities are included. Including non-linearities into FEA analysis make the problem more complex, however results show better correlation with tests, as mentioned in Chapter 6.

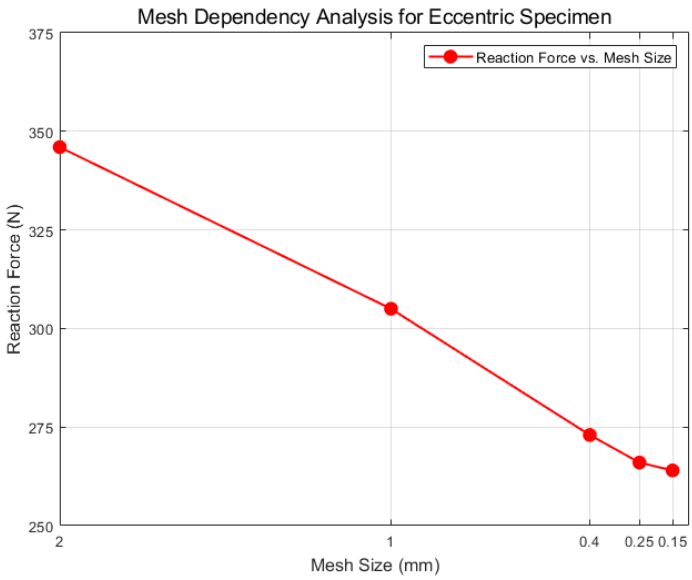

Figure 5.37: Mesh dependency study for eccentric specimen

Table 5.4: Mesh Dependency Study for Eccentric Specimen

Element Size (mm)	Number of Elements	Reaction Force (N)	Solution Time
2.0	5174	346	52s
1.0	14535	288	1m2s
0.4	46116	273	1m14s
0.25	177910	266	3m0s
0.15	569831	264	8m11s

5.4 Closure

In this Chapter, the numerical analysis procedure and results for CFF parts, especially for three specimens with distinct loading cases are explained. Surface elements (shells) are used with shared topology options to constrain nodes and enhance the accuracy of FEA results. Then, loading and boundary conditions of the models are provided for each test specimen. Moreover, mesh dependency analysis is performed to ensure the mesh resolution is sufficient to capture the results accurately. Force-displacement data are obtained as outputs of analysis in order to compare and validate the analysis results with tests, which are explained in the next chapter.

CHAPTER 6

TEST OF CONTINUOUS FILAMENT FABRICATED SPECIMENS

This chapter illustrates the testing purpose, the test infrastructure, and measurement details. Then, test details of three specimens, namely tensile, bending, and eccentric specimens, are explained. Finally, the results of tests and numerical analysis are

The goal of testing is developing and validating the numerical analysis approach. In Chapter 5, loading and boundary conditions for the numerical analysis are shared. Loading and boundary conditions of the numerical analysis are defined according to the testing of the specimens to compare the results.

For the tests, the BESMAK BMT-E Series Universal Testing Machine, which has a load cell capable of measuring a maximum of 200 kN axial load, a built-in displacement controller, and one axis strain gauge, is used. The photo of the testing machine and mechanical strain gauge is provided in Figure 6.1. The machine works with displacement input, and all the tests are done with a testing speed of 1 mm/min. Moreover, the sampling rate for displacement input and force output is selected as 50 Hz in order to obtain the testing data accurately while avoiding noises in the results.

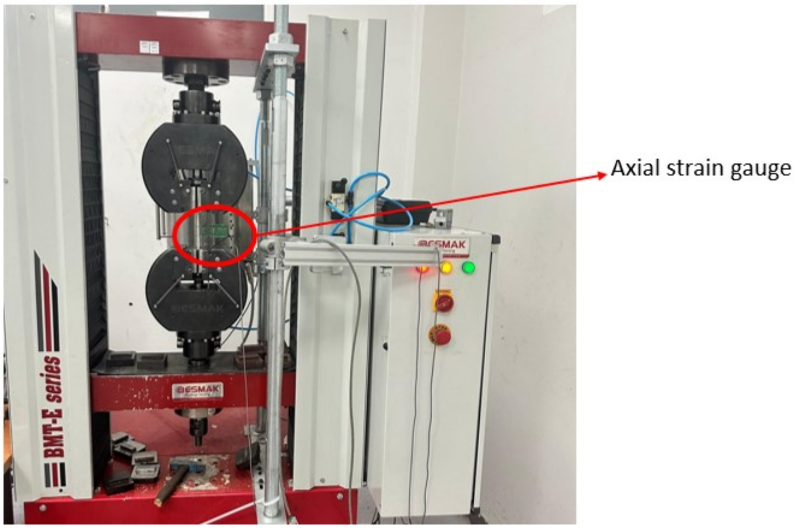

Figure 6.1: Testing machine and the strain gauge

6.1 Testing of Tensile Specimen

As mentioned in Chapter 4, three tensile specimens are manufactured to be tested. For all specimens, testing conditions, such as gripped areas, are the same, and an illustration of the tensile test is provided in Figure 6.2. The displacement of the gripper and the reaction force to displacement are measured simultaneously.

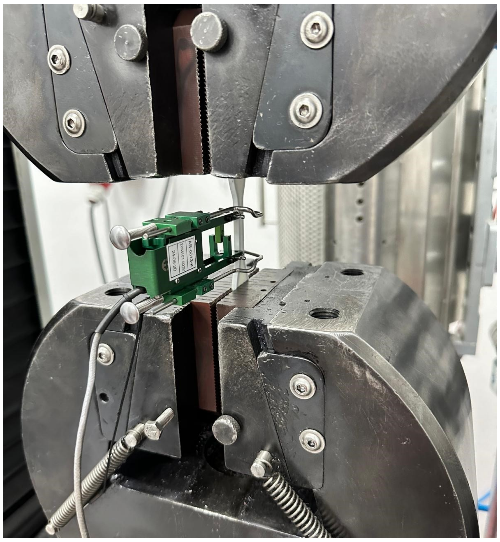

Figure 6.2: Tensile testing

The tensile test results for three specimens are given in Figure6.3. The results show that specimens are ruptured about 4 mm of axial displacement. Moreover, there is a bump in all three tests. During the tests, local cracks are occurred in the infill structure. While performing the test, when the axial displacement is about 0.6 mm, sounds of local cracks are heard. These local cracks change the load distribution along the part and the force-displacement curve shifted. Also, in Figure 6.4 tested tensile specimen is provided.

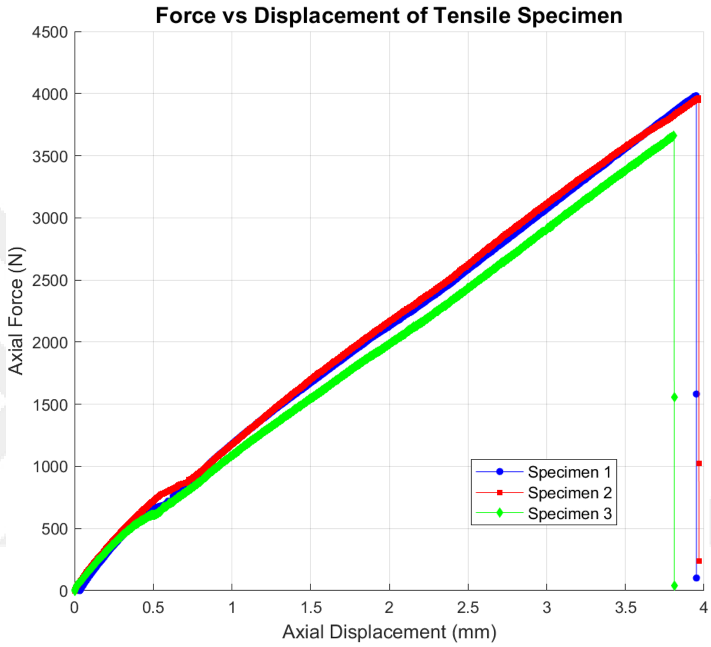

Figure 6.3: Results of tensile tests

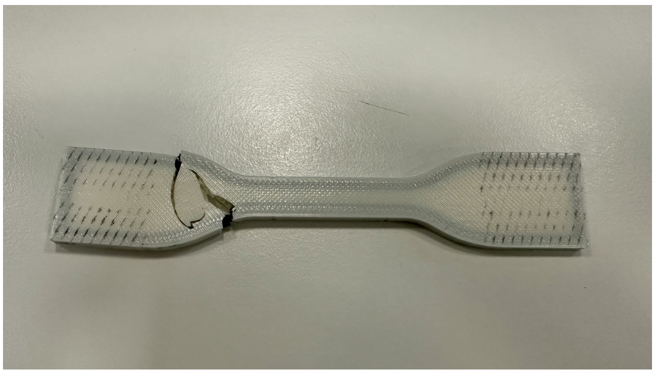
Figure 6.4: Tested tensile specimen

6.2 Testing of Bending Specimen

As mentioned in Chapter 4, three bending specimens are manufactured to be tested. Testing conditions, such as the location of cylindrical supports, the distance between the two upper supports responsible for loading, and the alignment between the bottom support and center of the test specimens, are arranged to be the same as for the three specimens using a test fixture. An illustration of the bending test is provided in Figure 6.5. The displacement of the gripper and the reaction force to displacement are measured simultaneously.

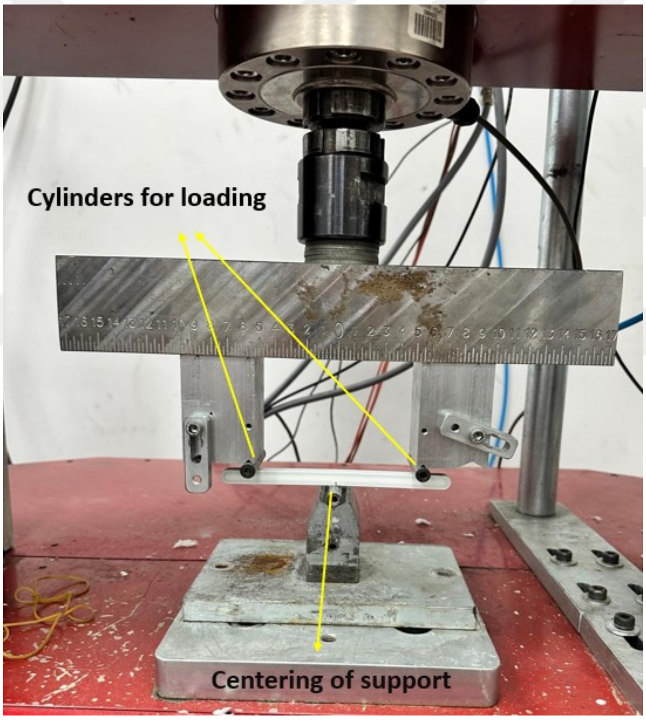

Figure 6.5: Three point bending testing

The results of bending tests for three specimens are given in Figure6.6. The results show that displacements greater than 3.5 mm, specimens do not respond to the load anymore, and local deformations are observed after the tests. During the test of Specimen 3, the test is ended manually since similar behavior is expected.

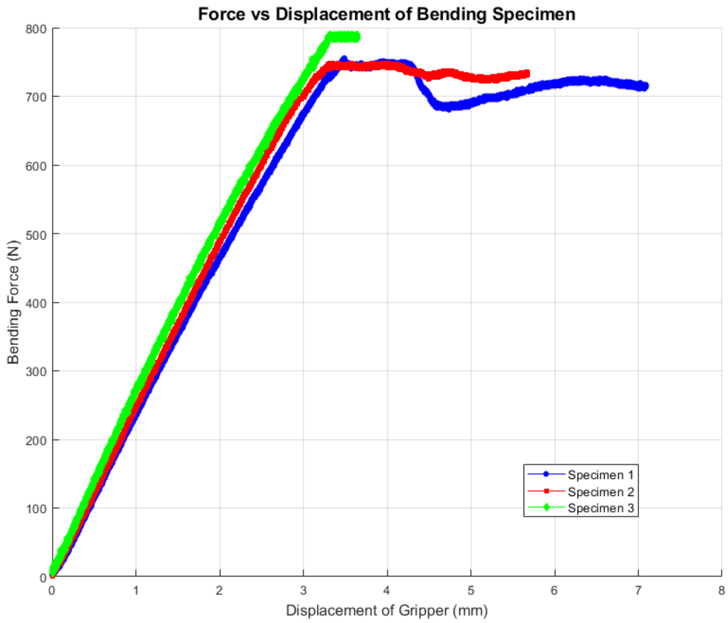

Figure 6.6: Results of three-point bending tests

In Figure 6.7 tested bending specimen is provided.

Figure 6.7: Tested bending specimen

6.3 Testing of Eccentric Test Specimen

As mentioned in Chapter 4, three eccentric specimens are manufactured to be tested. For all three specimens, testing conditions, such as gripped areas and placement of the strain gauge, are the same, and an illustration of the eccentric test is provided in Figure 6.8. The purpose of the testing is to measure the deformation of the middle section of the eccentric specimen so that one can observe the combined effects of axial force and bending moment. Hence, unlike tensile and bending specimens, the extension of the strain gauge is considered instead of the movement of the gripper.

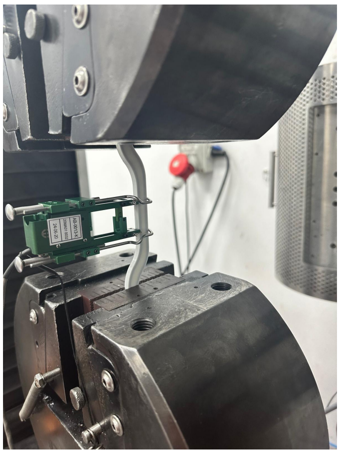

Figure 6.8: Eccentric specimen testing

The eccentric test results for three specimens are given in Figure6.9. The initial distance between the legs of the gauge is 25 mm and can not be altered. As seen in the 6.9, the force-displacement behavior of the specimens is not completely linear. This could be a result of a more complicated loading, the combination of axial and bending forces, or the misalignment of the specimens.

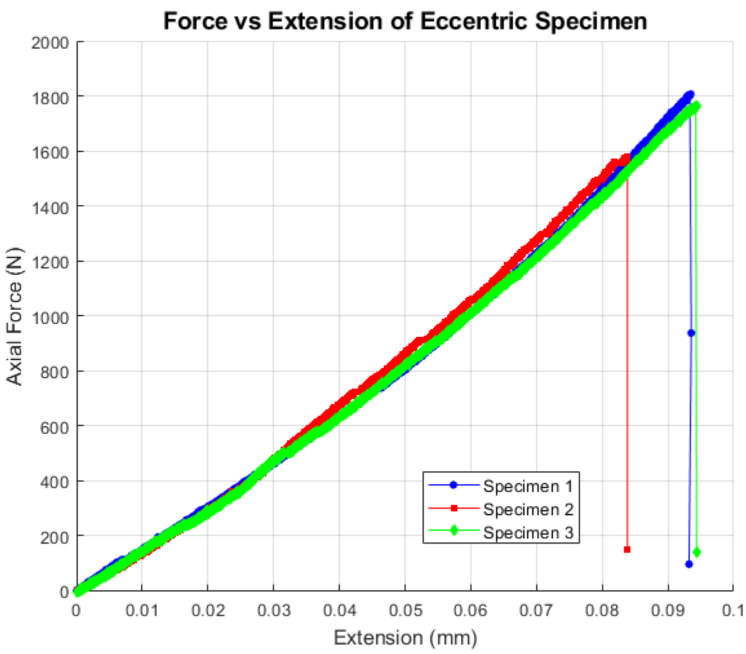

Figure 6.9: Results of eccentric tests

In Figure 6.10 tested eccentric specimen is provided.

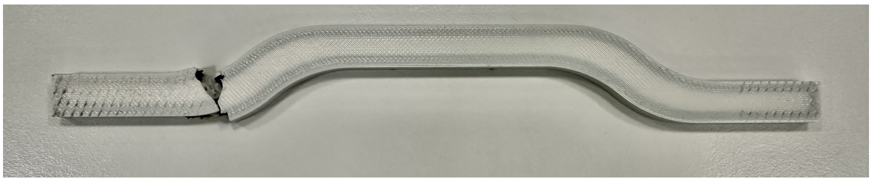

Figure 6.10: Tested eccentric specimen

6.4 Comparison of Test and Numerical Analysis Results

As stated before, the purpose of the testing is to investigate the numerical modeling approach. Hence, in this section comparison of tests and numerical results is discussed.

The details of FE modeling and testing of tensile specimens are discussed previously. In Figure 6.11, axial displacement vs reaction force curves were measured during the test, and numerical analysis results are provided. Results of tests and analysis are in good agreement, up to about 1.5 mm of axial displacement. However, after this point, the linear numerical model behaves stiffer than the tests, as given in Table 6.1. The reasons for this phenomenon are explained in section 6.5. In order to obtain more realistic results, nonlinear analysis is also run. In non-linear analysis, model behaves softer and results are closer to the averaged tests results.

Table 6.1: Comparison of Numerical Results with Test Results for Tensile Specimen

Displacement (mm)	Force of Linear FEA (N)	Force of Non-Linear FEA (N)	Measured Test Force (N)
0.5	652	651	658
1	1304	1225	1150
1.5	1956	1779	1638
2	2608	2334	2092
2.5	3260	2868	2548
3	3912	3364	3031
3.5	4564	3925	3502

The details of FE modeling and testing of bending specimens are discussed previously. In Figure 6.12, axial displacement vs reaction force curves were measured during the test, and numerical analysis results are provided. Results of tests and anal-

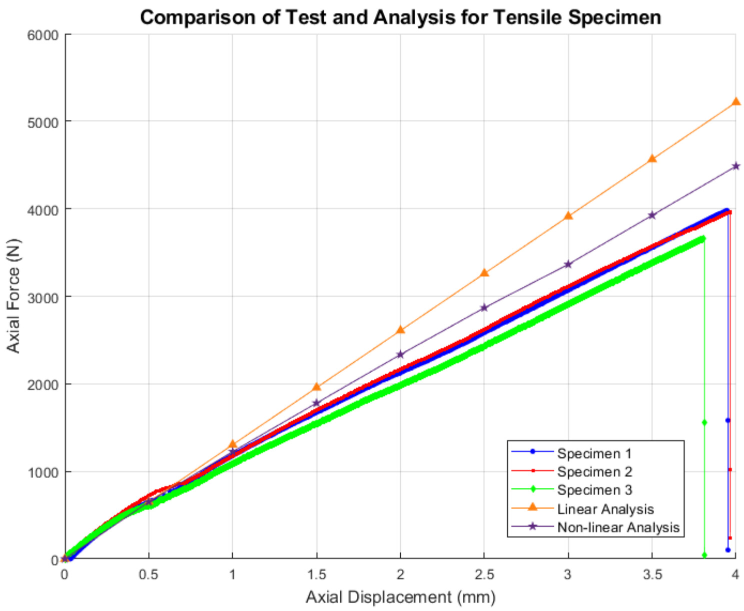

Figure 6.11: Comparison of results of FEA and test for tensile specimen

ysis are in good agreement, up to about 1.5 mm of displacement. However, after this point, the numerical model behaves more rigidly than the tests, as given in Table 6.2. The reasons for this phenomenon are explained in section 6.5. In order to obtain more realistic results, nonlinear analysis is also run. In non-linear analysis, model behaves softer and results are closer to the averaged tests results.

Table 6.2: Comparison of Numerical Results with Test Results for Bending Specimen

Displacement (mm)	Force of Linear FEA (N)	Force of Non-Linear FEA (N)	Measured Test Force (N)
0.5	148	145	125
1	296	284	251
1.5	444	417	371
2	592	533	488
2.5	740	659	597
3	888	777	698
3.5	1036	818	761
4	1184	841	748

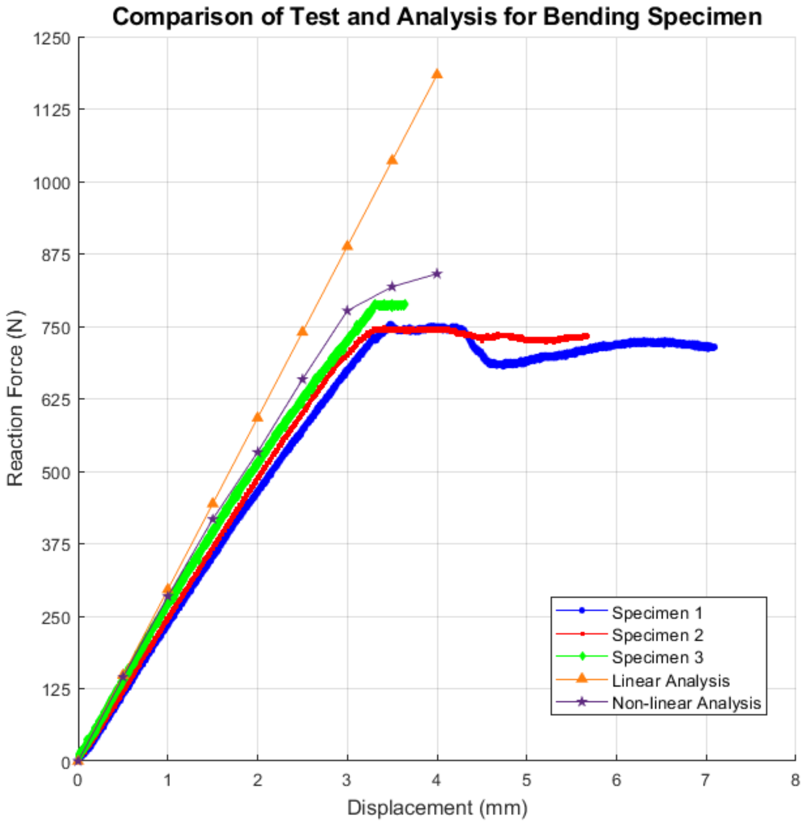

Figure 6.12: Comparison of results of FEA and test for bending specimen

The details of FE modeling and testing of eccentric specimens are discussed previously. In Figure 6.13 extension vs reaction force curves measured during the test, and the numerical analysis result are provided. The results of the tests and analysis agree with the overall extension values. In general, the numerical model behaves much stiffer than the tests because the numerical model assumes linear behavior, while test results diverge quadratically. Nevertheless, as the force reactions of the test increase, the absolute errors (the difference between the numerical and measured values) remain relatively constant or do not increase as rapidly, as given in Table 6.3. The reasons for possible discrepancies are explained in section 6.5. In order to obtain more realistic results, nonlinear analysis is also run. In non-linear analysis, model behaves softer and results are closer to the averaged tests results.

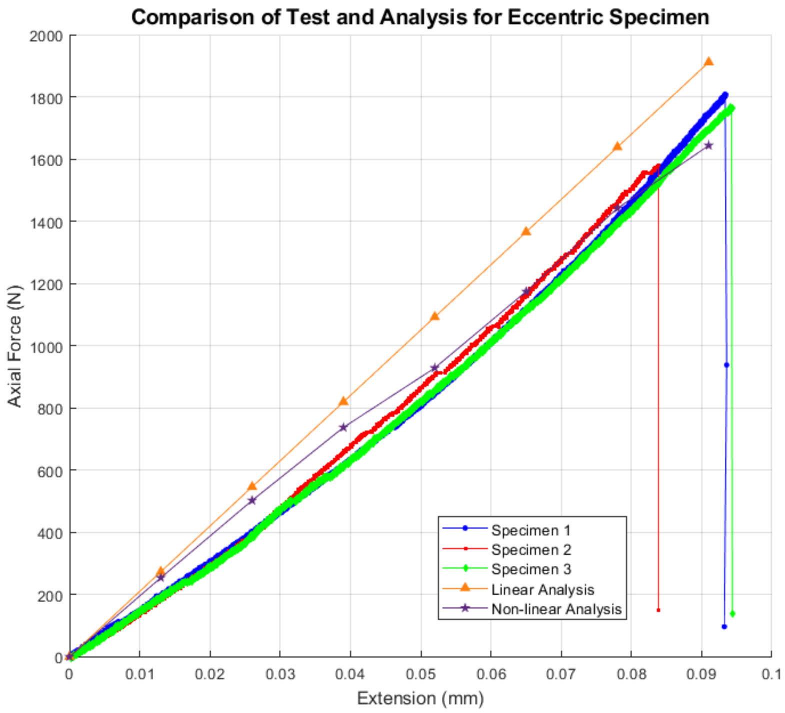

Figure 6.13: Comparison of results of FEA and test for eccentric specimen

Table 6.3: Comparison of Numerical Results with Test Results for Eccentric Specimen

Displacement (mm)	Force of Linear FEA (N)	Force of Non-Linear FEA (N)	Measured Test Force (N)
0.5	273	254	199
1	546	502	408
1.5	819	737	635
2	1092	928	879
2.5	1365	1174	1138
3	1638	1441	1428
3.5	1911	1643	1726

6.5 Causes of Discrepancies Between Experimental and FEA Results

FEA results often include errors when they are compared with the test results. Assumptions and simplifications are made during the modeling phase in order to describe the real-life scenarios mathematically and obtain computationally feasible models. Hence, in order to enhance the modeling approach, one should be aware of the roots of inaccuracies between tests and FEA results. For this research, sources of inaccuracies are listed below.

- Both Carbon Fiber and White Nylon are modeled as linear elastic materials. However, their actual behavior is non-linear, especially for higher strains.

- White Nylon is modeled as an isotropic material for simplicity because its stiffness is relatively lower compared to carbon fiber. Although modeling White Nylon as an orthotropic material would offer a more accurate representation and slightly enhance the numerical model's results, it would necessitate additional material characterization tests.

- In non-linear analyses, both geometric and material non-linearities are incorporated, enhancing the accuracy of numerical results and improving their convergence to experimental data.

- Although the created infill structure represents the real geometry of the specimen mostly, it has minor differences compared to the real specimen.

- During the tests, local cracks and rapture occur in the infill structure. This affects the overall load distribution inside the specimen; even carbon fiber carries most of the load, and the specimen behaves still almost linear and elastic.

- Localized regions with gaps or no (or partial) bonding to the previous layers exist. This originates from manufacturing and could not be modeled in FEA. In Figure 6.14, computational tomography (CT) results of the tensile specimens are provided. As seen, there are gaps and unbonded parts in the micro-scale.

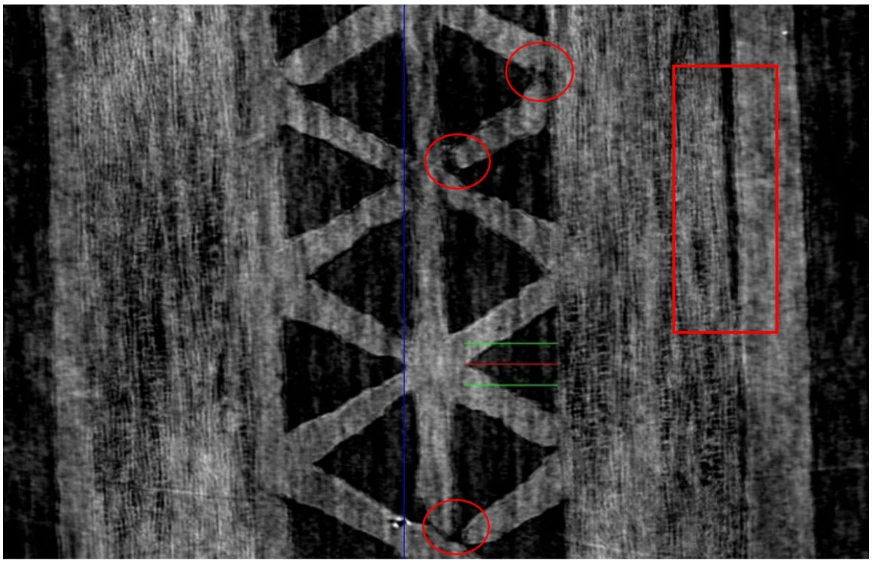

Figure 6.14: CT results

- There may be some issues related to tests, such as errors in measurements and slipping of the gripping section.
- Mesh dependency is studied as much as the hardware allows. For finer mesh, the change in results is assumed insignificant.

CHAPTER 7

DISCUSSION AND CONCLUSION

In this thesis, a numerical method approach is studied and validated with tests for a new AM method called CFF. Since CFF is a new technology, there are still questions about numerical simulation techniques to be used for the parts manufactured by the CFF method. This method is trendy, and many manufacturing companies are working to develop the CFF technology since it enables the design of parts with high strength and low weight. Although there are many studies in the literature regarding numerical simulations for CFF parts, there is no novel and widely accepted methodology. Hence, there is a gap in the literature on this topic.

In this work, Carbon Fiber is used as the reinforcement material and White Nylon as the matrix material for composite manufacturing to develop a numerical modeling approach since they are relatively cheap and reachable. For this purpose, material characterization tests are first decided and performed for Carbon Fiber and White Nylon to be used as input in numerical simulations. Then, three load cases are designed to investigate the validity of the modeling approach. Three specimens per each loading case are designed and manufactured to be tested later. Numerical models are prepared, and FE analyses are solved. Finally, tests are executed to compare the results of the numerical model and tests.

Although comparisons between numerical models and tests are often based on stresses or strains, identifying and realizing the occurrence of a failure of a part filled with infill structure is not possible since very localized failures in the highly stress-concentrated infill regions are encountered mostly, even if the whole part behaves in the elastic regime. Moreover, measuring the stresses to detect the failure inside the part is impossible. Hence, in this work, the comparison method is decided to be based on deformation and forces, which are also indicators of overall part stiffness. As discussed in Chapter 5, there are some discrepancies between numerical results and tests. These inaccuracies are addressed in Section 6.5.

The behavior of the specimens for all load cases is stiffer in numerical analyses than in the tests. For the same displacement inputs, the reaction force obtained from FE analysis is greater than that obtained from the tests. The main reason for this is the inherent characteristics of the CFF method. In numerical analysis, both the bonding between layers and the bonding within the infill structure are modeled as if they were perfectly bonded; gaps or internal errors in dimensions are disregarded. However, this is not the case in actual specimens. Moreover, the FEA models do not include residual strains due to high nozzle temperatures during manufacturing.

Considering the eccentric specimen, FEA results seem valid for a limited region. First, the measurement technique used in the test brings some errors. FEA result agrees with test results for small extensions, but numerical results are stiffer for higher displacements. All the reasons stated in the previous paragraph are valid also for the eccentric specimens to explain the stiffer behavior in high displacements. In addition to them, some non-linearities may arise from the combined load complexity and some testing errors. The bending moment depends on the alignment of the part to the gripper because even a small eccentricity mismatch directly affects the applied moment on the part. Despite meticulous efforts to ensure alignment during the tests, the lack of a suitable fixture for precise alignment may have introduced errors. In contrast, the Finite Element Analysis (FEA) assumes perfect alignment of the part. Therefore, the discrepancy between the test results and the analysis may be attributed not only to potential errors in the FEA but also to inaccuracies in the test alignment. In summary, this work presents a novel numerical approach for the FE analysis of CFF parts. The proposed analysis technique has been rigorously validated through a series of simulations involving various loading scenarios, ensuring its robustness across different conditions. Additionally, comprehensive experimental studies were conducted to validate the simulation results and compare them with the test data. Finally, a thorough examination of potential sources of discrepancies between the numerical predictions and experimental findings is provided, offering insights into the factors contributing to any observed variations.

7.1 Future Works

This thesis develops an FE approach to model CFF parts. In the scope of this work, only 2D loading cases are applied, and corresponding numerical models are discussed. However, as a future work, one should consider obtaining 3D material properties and performing 3D analysis to enhance the extent of the numerical modeling approach in order to evaluate the design of real machine elements. Moreover, as mentioned before, only linear and elastic material models are utilized for Carbon Fiber and White Nylon. However, elastoplastic and more complex material models will better reflect the actual stress-strain behavior of these materials. Also, White Nylon is assumed to be an isotropic material since the overall stiffness of the parts generally relies on the stiffness of the Carbon Fiber. However, in real life, White Nylon also has similar behavior to Carbon Fiber; it should be modeled as an orthotopic material, just like Carbon Fiber, but this will require extra material characterization tests. Additionally, the comparison between numerical models and tests is done for the elastic regime; the comparison is based on force and displacement values.To enhance the accuracy of the numerical models, future work should also involve utilizing advanced measurement techniques like Digital Image Correlation (DIC) or strain gauges to capture detailed strain and stress data during experiments. This data can be compared with FE model predictions to assess and improve simulation accuracy. Nonlinear calibration of FE models using experimental data could further refine material parameters, reducing discrepancies between simulated and measured results.

REFERENCES

[1] J. Beaman, D. L. Bourell, C. Seepersad, and D. Kovar, "Additive manufacturing review: Early past to current practice," *Journal of Manufacturing Science and Engineering*, vol. 142, no. 11, p. 110812, 2020.

[2] J. Zhang, "Cybersecurity risks and mitigation strategies in additive manufacturing," *Progress in Additive Manufacturing*, vol. 3, 06 2018.

[3] A. Patel and M. Taufik, "Extrusion-based technology in additive manufacturing: a comprehensive review," *Arabian Journal for Science and Engineering*, vol. 49, no. 2, pp. 1309–1342, 2024.

[4] *UNE-EN ISO/ASTM 52900:2017: Additive Manufacturing, General Principles, Terminology (ISO/ASTM 52900:2015).* AENOR, 2017.

[5] R. B. Kristiawan, F. Imaduddin, D. Ariawan, Ubaidillah, and Z. Arifin, "A review on the fused deposition modeling (fdm) 3d printing: Filament processing, materials, and printing parameters," *Open Engineering*, vol. 11, no. 1, pp. 639–649, 2021.

[6] I. Gibson, D. Rosen, B. Stucker, and M. Khorasani, *Material Extrusion*, pp. 171–201. Cham: Springer International Publishing, 2021.

[7] R. Hsissou, R. Seghiri, Z. Benzekri, M. Hilali, M. Rafik, and A. Elharfi, "Polymer composite materials: A comprehensive review," *Composite structures*, vol. 262, p. 113640, 2021.

[8] M. Yakout and M. Elbestawi, "Additive manufacturing of composite materials: an overview," in *Proceedings of the 6th International Conference on Virtual Machining Process Technology (VMPT), Montréal, QC, Canada*, vol. 29, 2017.

[9] Y. Wang, Y. Zhou, L. Lin, J. Corker, and M. Fan, "Overview of 3d additive manufacturing (am) and corresponding am composites," *Composites Part A: Applied Science and Manufacturing*, vol. 139, p. 106114, 2020.

[10] W. Abd-Elaziem, M. Khedr, A.-E. Abd-Elaziem, M. M. A. Allah, A. A. Mousa, H. M. Yehia, W. M. Daoush, and M. A. A. El-Baky, "Particle-reinforced polymer matrix composites (pmc) fabricated by 3d printing," *Journal of Inorganic and Organometallic Polymers and Materials*, vol. 33, no. 12, pp. 3732–3749, 2023.

[11] K. Palanikumar, "Analyzing surface quality in machined composites," in *Machining technology for composite materials*, pp. 154–182, Elsevier, 2012.

[12] H. Chung and S. Das, "Processing and properties of glass bead particulate-filled functionally graded nylon-11 composites produced by selective laser sintering," *Materials Science and Engineering: A*, vol. 437, no. 2, pp. 226–234, 2006.

[13] U. Kalsoom, A. Peristyy, P. N. Nesterenko, and B. Paull, "A 3d printable diamond polymer composite: a novel material for fabrication of low cost thermally conducting devices," *RSC Adv.*, vol. 6, pp. 38140–38147, 2016.

[14] S. Hwang, E. I. Reyes, K.-s. Moon, R. C. Rumpf, and N. S. Kim, "Thermo-mechanical characterization of metal/polymer composite filaments and printing parameter study for fused deposition modeling in the 3d printing process," *Journal of Electronic Materials*, vol. 44, pp. 771–777, 2015.

[15] D. R. Paul and L. M. Robeson, "Polymer nanotechnology: nanocomposites," *Polymer*, vol. 49, no. 15, pp. 3187–3204, 2008.

[16] Y. Li, Z. Feng, L. Huang, K. Essa, E. Bilotti, H. Zhang, T. Peijs, and L. Hao, "Additive manufacturing high performance graphene-based composites: A review," *Composites Part A: Applied Science and Manufacturing*, vol. 124, p. 105483, 2019.

[17] S. Meng, H. He, Y. Jia, P. Yu, B. Huang, and J. Chen, "Effect of nanoparticles on the mechanical properties of acrylonitrile–butadiene–styrene specimens fabricated by fused deposition modeling," *Journal of Applied Polymer Science*, vol. 134, no. 7, 2017.

[18] A. Nadernezhad, S. Unal, N. Khani, and B. Koc, "Material extrusion-based additive manufacturing of structurally controlled poly (lactic acid)/carbon nanotube

nanocomposites," *The International Journal of Advanced Manufacturing Technology*, vol. 102, pp. 2119–2132, 2019.

[19] A. Plymill, R. Minneci, D. A. Greeley, and J. Gritton, "Graphene and carbon nanotube pla composite feedstock development for fused deposition modeling," 2016.

[20] J. Bai, R. D. Goodridge, R. J. Hague, M. Song, and M. Okamoto, "Influence of carbon nanotubes on the rheology and dynamic mechanical properties of polyamide-12 for laser sintering," *Polymer Testing*, vol. 36, pp. 95–100, 2014.

[21] X. Wang, M. Jiang, Z. Zhou, J. Gou, and D. Hui, "3d printing of polymer matrix composites: A review and prospective," *Composites Part B: Engineering*, vol. 110, pp. 442–458, 2017.

[22] S. F. Kabir, K. Mathur, and A.-F. M. Seyam, "A critical review on 3d printed continuous fiber-reinforced composites: History, mechanism, materials and properties," *Composite Structures*, vol. 232, p. 111476, 2020.

[23] C. Yang, X. Tian, T. Liu, Y. Cao, and D. Li, "3d printing for continuous fiber reinforced thermoplastic composites: mechanism and performance," *Rapid Prototyping Journal*, vol. 23, no. 1, pp. 209–215, 2017.

[24] H. Mei, Z. Ali, Y. Yan, I. Ali, and L. Cheng, "Influence of mixed isotropic fiber angles and hot press on the mechanical properties of 3d printed composites," *Additive Manufacturing*, vol. 27, pp. 150–158, 2019.

[25] Markforged, "Planning and 3d printing a composite part."

[26] G. W. Melenka, B. K. Cheung, J. S. Schofield, M. R. Dawson, and J. P. Carey, "Evaluation and prediction of the tensile properties of continuous fiber-reinforced 3d printed structures," *Composite Structures*, vol. 153, pp. 866–875, 2016.

[27]

[28] Markforged, "Material storage." `https://support.markforged.com/portal/s/article/Material-Storage`, 2024. Accessed: 2024-06-18.

[29] F. Ning, W. Cong, Y. Hu, and H. Wang, "Additive manufacturing of carbon fiber-reinforced plastic composites using fused deposition modeling: Effects of process parameters on tensile properties," *Journal of composite materials*, vol. 51, no. 4, pp. 451–462, 2017.

[30] M. T. Birosz, D. Ledenyak, and M. Ando, "Effect of fdm infill patterns on mechanical properties," *Polymer Testing*, vol. 113, p. 107654, 2022.

[31] S. Atatreh, M. S. Alyammahi, H. Vasilyan, T. Alkindi, and R. A. Susantyoko, "Evaluation of the infill design on the tensile properties of metal parts produced by fused filament fabrication," *Results in Engineering*, vol. 17, p. 100954, 2023.

[32] H. Mei, Z. Ali, I. Ali, and L. Cheng, "Tailoring strength and modulus by 3d printing different continuous fibers and filled structures into composites," *Advanced Composites and Hybrid Materials*, vol. 2, pp. 312–319, 2019.

[33] J. Naranjo-Lozada, H. Ahuett-Garza, P. Orta-Castañón, W. M. Verbeeten, and D. Sáiz-González, "Tensile properties and failure behavior of chopped and continuous carbon fiber composites produced by additive manufacturing," *Additive Manufacturing*, vol. 26, pp. 227–241, 2019.

[34] J. M. Chacón, M. A. Caminero, E. García-Plaza, and P. J. Núnez, "Additive manufacturing of pla structures using fused deposition modelling: Effect of process parameters on mechanical properties and their optimal selection," *Materials & Design*, vol. 124, pp. 143–157, 2017.

[35] Eiger.io, "Markforged slicer." `https://www.eiger.io`, 2024. Accessed: 2024-06-18.

[36] M. Galati, M. Viccica, and P. Minetola, "A finite element approach for the prediction of the mechanical behaviour of layered composites produced by Continuous Filament Fabrication (CFF)," *Polymer testing*, vol. 98, p. 107181, 6 2021.

[37] F. Van Der Klift, Y. Koga, A. Todoroki, M. Ueda, Y. Hirano, and R. Matsuzaki, "3d printing of continuous carbon fibre reinforced thermo-plastic (cfrtp) tensile test specimens," *Open Journal of Composite Materials*, vol. 6, no. 1, pp. 18–27, 2015.

[38] H. Al Abadi, H.-T. Thai, V. Paton-Cole, and V. Patel, "Elastic properties of 3d printed fibre-reinforced structures," *Composite Structures*, vol. 193, pp. 8–18, 2018.

[39] V. A. Martin, R. H. Kraft, T. H. Hannah, and S. Ellis, "An energy-based study of the embedded element method for explicit dynamics," *Advanced Modeling and Simulation in Engineering Sciences*, vol. 9, no. 1, p. 12, 2022.

[40] A. Avanzini, D. Battini, and L. Giorleo, "Finite element modelling of 3d printed continuous carbon fiber composites: Embedded elements technique and experimental validation," *Composite Structures*, vol. 292, p. 115631, 2022.

[41] Dassault Systems, "Abaqus user's guide." https://www.3ds.com/support/documentation/user-guides, 2024. Accessed: 2024-07-07.

[42] M. Žmindák, P. Novak, J. Soukup, D. Milosavljevic, and M. Kaco, "Finite element simulation of tensile test of composite materials manufactured by 3d printing," in *IOP Conference Series: Materials Science and Engineering*, vol. 776, p. 012082, IOP Publishing, 2020.

[43] F. Ghebretinsae, O. Mikkelsen, and A. D. Akessa, "Strength analysis of 3d printed carbon fibre reinforced thermoplastic using experimental and numerical methods," in *IOP conference series: materials science and engineering*, vol. 700, p. 012024, IOP Publishing, 2019.

[44] Markforged, "3D Printing Carbon Fiber and Other Composites — markforged.com." https://markforged.com/resources/learn/design-for-additive-manufacturing-plastics-composites/understanding-3d-printing-strength/3d-printing-carbon-fiber-and-other-composites. [Accessed 08-04-2024].

[45] M. Forged, "Carbon fiber 3d printing," 2024.

[46] S. Kellas, J. Morton, and K. Jackson, "An evaluation of the$\pm$45 tensile test for the determination of the in-plane shear strength of composite materials," in *Proceedings*, SAMPE, Ovina, CA, 1991.

[47] A. S. D. . on Mechanical Properties, “Standard test method for tensile properties of plastics,” American Society for Testing and Materials, 1998.

[48] A. S. D. . on Mechanical Properties, “Standard test methods for flexural properties of unreinforced and reinforced plastics and electrical insulating materials,” American Society for Testing and Materials, 2017.

[49] F. P. Beer, E. R. Johnston, J. T. DeWolf, and D. F. Mazurek, *Mechanics of Materials*. McGraw-Hill Education, 2015.